1-1-2016

Oxygen Transport, Shear Stress, And Metabolism In Perfused Hepatocyte-Seeded Scaffolds With Radial Pore Architecture: Experimental And Computational Analyses

Chijioke Mbanu
Wayne State University,

OXYGEN TRANSPORT, SHEAR STRESS, AND METABOLISM IN PERFUSED HEPATOCYTE-SEEDED SCAFFOLDS WITH RADIAL PORE ARCHITECTURE: EXPERIMENTAL AND COMPUTATIONAL ANALYSES

by

CHIJIOKE ANAELE MBANU

DISSERTATION

Submitted to the Graduate School

of Wayne State University,

Detroit, Michigan

in partial fulfillment of the requirements

for the degree of

DOCTOR OF PHILOSOPHY

2016

MAJOR: BIOMEDICAL ENGINEERING

Approved by:

_____

Advisor Date

_____

_____

_____

_____

DEDICATION

Dedicated to my beautiful wife and three children (Jennifer, Adrianna, Adanna and Akagha)

Also to my Mother, Father, Brother and Sister

ACKNOWLEDGEMENTS

To Jennifer - my wife and queen. With you nothing is impossible. Without you I am nothing. To my three beautiful children Adrianna, Adanna and Akagha. A father could not be more proud of his children than I am. Words cannot describe the love that I have for all of you. Know that it is unwavering, unconditional and infinite.

A very special thanks goes to Gloria Nkechi and Bartholomew Emeshiama Mbanu, my mother and father. Thank you for never giving up on me and for the continuous words of encouragement and inspiration. Both of you have molded me into the person I am today. You've taught me how to be a man, how to love, care, respect others and most importantly respect myself. From my childhood to this very day, your words "Keep pushing, keep moving forward – Mbanu's never give up" motivates me to work hard for everything that I have and never forget to give back to my people. To my loving sister Nkechi (Ms. Fat Chops) who's been by my side through all my trials and tribulations. One could not have a better confidant than you. Lastly, to my older brother Dr. Ibeawuchi Mbanu who's been my protector, mentor, friend and the bar to which I measure myself. Without words you've made me realize that my potential is limitless and that with hard work and perseverance, all goals are achievable.

I would like to express my special appreciation and thanks to my advisor Dr. Howard W.T. Matthew. You've been a tremendous mentor to me. I would like to thank you for encouraging my research, teaching me how to think like a scientist and challenging me to do better. Without your patience, wisdom, tutelage and kind heart this degree would not be possible. I would also like to thank Dr. Pamela VandeVord, Dr. Michelle Grimm and Dr. Harini Sundararaghavan for serving as my committee members.

Finally, thank you to all of the friends that I've made along this journey. There are too many of you to mention but you know who you are – Much love and respect. Last but certainly

not least, I want extend a massive thank you to Dr. Therese Bou-Akl for extensive mentoring and invaluable guidance.

TABLE OF CONTENTS

Dedication ii

Acknowledgements iii

List of Figures ix

List of Tables xiv

CHAPTER ONE: INTRODUCTION 1

CHAPTER TWO: LITERATURE REVIEW 6

2.1 Liver Anatomy, Physiology and Pathogenesis 6

2.2 Hepatic Extracellular Matrix (ECM) 6

2.3 Hepatocytes 7

2.4 Hepatocyte Cell Junctions 9

2.5 Liver Oxygen Tensions 10

2.6 Modes of Liver Failure 10

2.7 Treatment of Acute Liver Failure 11

2.7.1 Surgical Based Approaches 11

2.7.2 Non-Biological Approach 12

2.7.3 Cell-Based Therapies 14

2.7.4 Tissue Engineered/Regenerative Medicine Constructs 17

2.8 Hepatocyte – 2D Cell Culture to 3D Bioreactor Studies 18

2.8.1 2D Hepatocyte Cultures 18

2.8.2 3D Implantable Porous Scaffolds and Perfusion Cultures 19

2.9 Chitosan as a Biomaterial for Tissue Engineering Constructs 22

2.10 Computational Fluid Dynamics (CFD) and Bioreactor Cultures 23

CHAPTER THREE: PERFUSION BIOREACTOR OPTIMIZATION, AND THE TANDEM EFFECTS OF DIRECTED AND CONVECTIVE OXYGENATION ON HEPATIC FUNCTION ____ 26

3.1 Introduction ____ 26

3.2 Materials and Methods ____ 28

3.2.1 Sources of Materials and Reagents ____ 28

3.2.2 Scaffold Fabrication ____ 28

3.2.3 Hepatocyte Isolation ____ 30

3.2.4 Culture Conditions ____ 31

3.2.5 Metabolic Output Measurements ____ 33

3.2.6 Histological Analysis ____ 34

3.2.7 Statistical Analysis ____ 34

3.3 Results ____ 35

3.3.1 Scaffold Characterization ____ 35

3.3.2 Bioreactor Design/Optimization and the Effects on 3D Chitosan Scaffolds with Direct and Convective Oxygenation on Hepatocyte Phenotypic Expression ____ 36

3.3.2(a) First Generation Bioreactor Design and Results ____ 37

3.3.2(b) Second Generation Bioreactor Design and Results ____ 42

3.3.2(c) Third Generation Bioreactor Design and Results ____ 47

3.4 Discussion ____ 55

3.5 Conclusion and Future Works ____ 61

CHAPTER FOUR: COMPUTATIONAL FLUID DYNAMIC ASSESSMENT OF HOW MASS FLOW RATES EFFECTS FLUID FLOW PROFILES, SHEAR STRESS AND OXYGEN CONSUMPTION IN A CELL-INFUSED MICROENVIRONMENT ____ 62

4.1 Introduction ____ 62

4.2 Materials and Methods ____ 65

4.2.1 Computational Model of Hepatocyte Infused Porous Scaffold ____ 65

4.2.2 Modeling Fluid Flow _____ 68

4.2.3 Modeling Species (Oxygen) Transport and Consumption _____ 69

4.4.4 CFD Simulation Workflow _____ 72

4.3 Results _____ 73

4.3.1 Computational Fluid Dynamics Results for Fluid Flow and Vector Profile _____ 73

4.3.2 Computational Fluid Dynamics Results for Wall Shear Stress ____ 78

4.3.3 Computational Fluid Dynamics Results for Oxygen Consumption _ 84

4.4 Discussion _____ 91

4.5 Conclusion and Future Work _____ 96

CHAPTER FIVE: EVALUATION OF HOW SHEAR STRESS AND MASS TRANSFER AFFECT HEPATOCELLULAR-FUNCTIONALITY, MORPHOLOGY AND VIABILITY EMPIRICAL ASSESSMENT OF CFD SIMULATIONS _____ 98

5.1 Introduction _____ 98

5.2 Materials and Methods _____ 100

5.2.1 Sources of Materials and Reagents _____ 100

5.2.2 Scaffold Fabrication _____ 100

5.2.3 Hepatocyte Isolation _____ 100

5.2.4 Culture Conditions _____ 101

5.2.5 Metabolic Output Measurements _____ 102

5.2.6 Histological Analysis _____ 102

5.2.7 Statistical Analysis _____ 103

5.3 Results _____ 103

5.3.1 Effects of Direct Oxygenation (Static Bioreactor Culture) _____ 103

5.3.2 Effects of Direct Oxygenation and Convective Transport at 5 ml/min_ _____ 107

5.3.3 Effects of Direct Oxygenation and Convective Transport at 15 ml/min _

112

5.3.4 Effects of Direct Oxygenation and Convective Transport at 20 ml/min 117

5.3.5 Effects of Direct Oxygenation and Convective Transport at 25 ml/min 122

5.4 Discussion 132

5.5 Conclusion and Future Work 134

CHAPTER SIX: EVALUATION OF HOW THE REDUCTION IN SCAFFOLD DIMENSIONS AND INCREASED CELLULAR COMPACTNESS INFLUENCE LIVER PHENOTYPIC EXPRESSION AND AGGREGATE FORMATION 136

6.1 Introduction 136

6.2 Materials and Methods 137

6.2.1 Sources of Materials and Reagents 137

6.2.2 Scaffold Fabrication 138

6.2.3 Hepatocyte Isolation 138

6.2.4 Culture Conditions 138

6.2.5 Metabolic Output Measurements 139

6.2.6 Histological Analysis 139

6.2.7 Statistical Analysis 139

6.3 Results 140

6.3.1 Effects of 14% Reduction in Scaffold Diameter 140

6.3.2 Effects of 30% Reduction in Scaffold Diameter 144

6.4 Discussion 153

6.5 Conclusion and Future Work 155

References 157

Abstract 185

Autobiographical Statement 187

LIST OF FIGURES

Figure 1: Chemical structure of chitosan structure _____ 22

Figure 2: Schematic and 3D rendering of chitosan scaffold embedded with gas permeable silicone tubing _____ 30

Figure 3: Top, front and angled view of chitosan scaffold embedded with gas permeable tubing _____ 30

Figure 4: Scanning Electron Micrograph images of 3-dimensional chitosan scaffold. Scaffold pore structure at central port and periphery. Cross section cut to show tapered radial orientation of pore structure _____ 36

Figure 5: Schematic of first generation perfusion bioreactor system with seeded scaffold and flow perfusion circuit _____ 38

Figure 6: Rate of albumin synthesis for first iteration perfusion bioreactor at 10 ml/min flow rate _____ 39

Figure 7: Rate of Ureagenesis synthesis for first iteration perfusion bioreactor at 10 ml/min flow rate _____ 40

Figure 8: Histological H&E stain of hepatocyte-seeded chitosan scaffold for first iteration perfusion bioreactor at 10 ml/min flow rate _____ 41

Figure 9: Schematic of second generation perfusion bioreactor system with seeded scaffold and flow perfusion circuit _____ 43

Figure 10: Rate of albumin synthesis for second iteration perfusion bioreactor at 10 ml/min flow rate _____ 44

Figure 11: Rate of Ureagenesis synthesis for second iteration perfusion bioreactor at 10 ml/min flow rate _____ 45

Figure 12: Histological H&E stain of hepatocyte-seeded chitosan scaffold for second iteration perfusion bioreactor at 10 ml/min flow rate _____ 46

Figure 13: Schematic of third generation perfusion bioreactor system with seeded scaffold and flow perfusion circuit _____ 48

Figure 14: Bioreactor culture setup showing cell seeded scaffold medium reservoir and oxygenator _____ 49

Figure 15: Rate of albumin synthesis for third iteration perfusion bioreactor at 10 ml/min flow rate and pH 7.2 _____ 50

Figure 16: Rate of Ureagenesis synthesis for third iteration perfusion bioreactor at 10 ml/min flow rate and pH 7.2 _____ 51

Figure 17: Histological H&E stain of hepatocyte-seeded chitosan scaffold for third iteration perfusion bioreactor at 10 ml/min flow rate and pH 7.2 _____ 52

Figure 18: Rate of albumin synthesis for the comparison of the first, second and third generation perfusion bioreactors at 10 ml/min flow rate _____ 54

Figure 19: Rate of Ureagenesis synthesis for the comparison of the first, second and third iteration perfusion bioreactors at 10 ml/min flow rate _____ 54

Figure 20: Rationale, workflow and final rendering for cell-infused pore structure for CFD model and subsequent simulations _____ 67

Figure 21: Velocity vector distribution and fluid flow profile from computational fluid dynamics simulation at 3.36 x10^{-6} g/s (5 ml/min) _____ 75

Figure 22: Velocity vector distribution and fluid flow profile from computational fluid dynamics simulation at 6.737 x10^{-6} g/s (10 ml/min) _____ 76

Figure 23: Velocity vector distribution and fluid flow profile from computational fluid dynamics simulation at 1.01 x10^{-5} g/s (15 ml/min) _____ 77

Figure 24: Contours of shear stress distribution from computational fluid dynamics simulation at 3.36 x10^{-6} g/s (5 ml/min) _____ 79

Figure 25: Contours of shear stress distribution from computational fluid dynamics simulation at 6.737 x10^{-6} g/s (10 ml/min) _____ 80

Figure 26: Contours of shear stress distribution from computational fluid dynamics simulation at 1.01 x10^{-5} g/s (15 ml/min) _____ 81

Figure 27: Wall shear stress vs. Scaffold position (cm) from computational fluid dynamics simulation at 1.47x10^{-5} g/s (20 ml/min) _____ 83

Figure 28: Wall shear stress vs. Scaffold position (cm) from computational fluid dynamics simulation at 1.84x10^{-5}g/s (25 ml/min) _____ 83

Figure 29: Contours of oxygen concentration distribution from computational fluid dynamics simulation at 3.36 x10^{-6} g/s (5 ml/min) _____ 86

Figure 30: Oxygen concentration profile vs. scaffold length (cm) from computation fluid dynamics simulations at 3.36 x10^{-6} g/s (5 ml/min) _____ 87

Figure 31: Contours of oxygen concentration distribution from computational fluid dynamics simulation at 6.737 x10^{-6} g/s (10 ml/min) _____ 88

Figure 32: Oxygen concentration profile vs. scaffold length (cm) from computation fluid dynamics simulations at 6.737 x10^{-6} g/s (10 ml/min) _____ 89

Figure 33: Contours of oxygen concentration distribution from computational fluid dynamics simulation at 1.10 x10^{-5} g/s (15 ml/min) _____ 90

Figure 34: Oxygen concentration profile vs. scaffold length (cm) from computation fluid dynamics simulations at 1.10 x10^{-5} g/s (15 ml/min) _____ 91

Figure 35: Schematic of third iteration perfusion bioreactor system with seeded scaffold and flow perfusion circuit _____ 102

Figure 36: Rate of albumin synthesis for static culture vs. double layer collagen gel (control) _____ 104

Figure 37: Rate of ureagenesis synthesis for static culture vs. double layer collagen gel (control) _____ 104

Figure 38: Histological montage (H&E stain) of hepatocyte-seeded scaffold, under static flow conditions with only direct oxygenation _____ 106

Figure 39: Enlarged images of H&E stained hepatocyte-seeded scaffold, under static flow conditions with only direct oxygenation _____ 107

Figure 40: Rate of albumin synthesis for 5 ml/min perfusion culture vs. double layer collagen gel (control) _____ 109

Figure 41: Rate of ureagenesis synthesis for 5 ml/min perfusion culture vs. double layer collagen gel (control) _____ 109

Figure 42: Histological montage (H&E stain) of hepatocyte-seeded scaffold, under 5 ml/min perfusion conditions with direct oxygenation _____ 111

Figure 43: Enlarged images of H&E stained hepatocyte-seeded scaffold, under 5 ml/min flow conditions with direct oxygenation _____ 112

Figure 44: Rate of albumin synthesis for 15 ml/min perfusion culture vs. double layer collagen gel (control) _____ 114

Figure 45: Rate of ureagenesis synthesis for 15 ml/min perfusion culture vs. double layer collagen gel (control) _____ 114

Figure 46: Histological montage (H&E stain) of hepatocyte-seeded scaffold, under 15 ml/min perfusion conditions with direct oxygenation _____ 116

Figure 47: Enlarged images of H&E stained hepatocyte-seeded scaffold, under 15 ml/min flow conditions with direct oxygenation _____ 117

Figure 48: Rate of albumin synthesis for 20 ml/min perfusion culture vs. double layer collagen gel (control) _____ 119

Figure 49: Rate of ureagenesis synthesis for 20 ml/min perfusion culture vs. double layer collagen gel (control) _____ 119

Figure 50: Histological montage (H&E stain) of hepatocyte-seeded scaffold, under 20 ml/min perfusion conditions with direct oxygenation _____ 121

Figure 51: Enlarged images of H&E stained hepatocyte-seeded scaffold, under 20 ml/min flow conditions with direct oxygenation _____ 122

Figure 52: Rate of albumin synthesis for 25 ml/min perfusion culture vs. double layer collagen gel (control) _____ 124

Figure 53: Rate of ureagenesis synthesis for 25 ml/min perfusion culture vs. double layer collagen gel (control) _____ 124

Figure 54: Histological montage (H&E stain) of hepatocyte-seeded scaffold, under 25 ml/min perfusion conditions with direct oxygenation _____ 126

Figure 55: Enlarged images of H&E stained hepatocyte-seeded scaffold, under 25 ml/min flow conditions with direct oxygenation _____ 127

Figure 56: Flow rate comparison (static to 25 ml/min) for rate of albumin protein synthesis _____ 129

Figure 57: Flow rate comparison (static to 25 ml/min) for rate of ureagenesis synthesis _129

Figure 58: Flow rates (static to 25 ml/min) vs. cell aggregate area (μm^2) _____ 130

Figure 59: Schematic of 14% (1.29 cm) and 30% (1.05 cm) reduced diameters chitosan scaffolds with embedded gas permeable tubing _____ 138

Figure 60: Rate of albumin protein synthesis for 14% (1.29 cm) reduced diameter scaffold culture at 15 ml/min perfusion vs. double layer collagen gel (control) _____ 141

Figure 61: Rate of ureagenesis synthesis for 14% (1.29 cm) reduced diameter scaffold culture at 15 ml/min perfusion vs. double layer collagen gel (control) _____ 142

Figure 62: Histological montage (H&E stain) of 14% (1.29 cm) reduced diameter, hepatocyte-seeded scaffold, under 15 ml/min perfusion with direct oxygenation _____ 143

Figure 63: Enlarged images of H&E stained 14% (1.29 cm) reduced diameter, hepatocyte-seeded scaffold, under 15 ml/min perfusion with direct oxygenation _____ 144

Figure 64: Rate of albumin protein synthesis for 30% (1.05 cm) reduced diameter scaffold culture at 15 ml/min flow rate vs. double layer collagen gel (control) _____ 146

Figure 65: Rate of ureagenesis synthesis for 30% (1.05 cm) reduced diameter scaffold culture at 15 ml/min perfusion vs. double layer collagen gel (control) _____ 146

Figure 66: Histological montage (H&E stain) of 30% (1.05 cm) reduced diameter, hepatocyte-seeded scaffold, under 15 ml/min flow rate with direct oxygenation _____ 148

Figure 67: Enlarged images of H&E stained 30% (1.05 cm) reduced diameter, hepatocyte-seeded scaffold, under 15 ml/min flow rate with direct oxygenation _____ 149

Figure 68: Rate of albumin protein synthesis for scaffold size comparison (1.05 cm to 1.5 cm) at 15 ml/min flow rate _____ 151

Figure 69: Rate of ureagenesis synthesis for scaffold size comparison (1.05 cm to 1.5 cm) at 15 ml/min flow rate _____ 152

LIST OF TABLES

Table 1: Parameters for computational fluid dynamics (CFD) model at 37℃_____ 71

Table 2: Mesh element parameters for the number of cells and cell aggregates per pore segment_____ 72

Table 3: Concentration flux (gradient) across the length of cell aggregate(s) per sequential segment._____ 87

Table 4: Percent change in oxygen consumption per successive aggregate(s) containing segment._____ 89

Table 5: paired t-test (equal variance, $p<0.05$) results that establish significance or insignificance between the effects of varying flow rates on albumin protein synthesis_____ 130

Table 6: paired t-test (equal variance, $p<0.05$) results that establish significance or insignificance between the effects of varying flow rates on urea secretion___ 131

CHAPTER ONE: INTRODUCTION

The pathogenesis and uncertain heterogeneous etiology of liver disease and subsequent failure have led to increased patient morbidity/mortality rates and still represent a steadfast socio-economic burden in most developed and underdeveloped countries. Liver failure presents itself in many ways (i.e. chronic failure, acute failure, acute-to-chronic etc.) and is estimated to cause 9.4 deaths per 100, 000 US citizens annually. Going forward, acute liver/hepatic failure will be given precedence in this segment because the need for transplantation is of the essence and failure rates post-transplantation are considerably lower than chronic or acute-to-chronic incidences [1].

Acute hepatic failure (AHF) is an aggressive, unpredictable clinical syndrome that is hallmarked by the loss of homeostatic functionality when the rate of hepatic death supersedes that of hepatic regeneration [2] not the inability to regenerate hepatocytes [3]. AHF provokes hepatic necrosis, apoptosis or necrapoptisis [4] which leads to catastrophic conditions such as coagulopathy, circulation dysfunction, encephalopathy, cerebral edema, coma and possible death via multi-organ failure [5]. It is estimated that AHF will affect more than 2800 and 500 in the United States and United Kingdom respectively. In the adult community, AHF is manifested by viral hepatitis or drug induced hepatotoxicity [6]. The issue is more critical in the neonatal and pediatric age group, where hepatic decomposition is attributed to prenatal infections, hypotension/shock, hematological malignancies, infectious hepatitis, immune disregulation and inborn metabolic disorders [7]. Although prognosis varies with etiology, in terms of mortality, 90% is noted for adults [8], 74% for children [9] and 70% for neonates [7].

Absent a pre-existing pathosis, recovery is attainable in acute hepatic failure if: (a) functionality is sufficiently replaced; (b) the liver's regenerative competency is preserved; (c) and the pathogenic factor is abated or rendered quiescent [10]. Unfortunately, resolution for

end-stage hepatic failure patients lies solely in orthotopic liver transplantation. In the United States more than 14,110 adults and 2,490 children await a suitable transplant organs [11], with numbers compounding at rates of 20% to 30% annually [12]. The dilemma of organ shortages is also aggravated by the fact that cadaver organ availability has only increased by 2% to 3% per year [12]. This is exacerbated by pre-transplant concerns such as “small-for-size” or “large-for-size” syndrome [13] and post-transplant complications like acute graft rejection, liver abscesses, adrenal gland hemorrhage, lymphoproliferative disorders[14] and chronic immuno-suppression therapy, which can heighten liver and kidney damage and lead to increased susceptibility to viral infections in the pediatric age group [15].

In spite of the significant advances in medicinal therapies, donor pool expansion techniques and extracorporeal support systems, a viable cure for acute failure still plagues the scientific community. To combat this shortfall, concerted research efforts have focused on the field of tissue engineering. It is believed that in its fruition, the field will yield an “off the shelf”, reliable modality or at best a countermeasure that will retard the progression of the hepatic pathosis. To this end, it is imperative that the future focus shifts to how the independent and synergistic function of parenchymal and nonparenchymal cells, in conjunction with how external and internal environmental stimuli influence their interactions and downstream cellular processes.

The lack of an effective therapy for liver diseases in conjunction with the need for healthy donor livers and reliable donor pool expansion techniques has fueled the race for transplantable tissue engineered analogues. The actualization of a neo-organ fashioned from isolated liver cells (hepatocytes) would have positive medicinal ramifications for patients suffering from acute liver failure (ALF), acute-to-chronic liver failure and inborn enzyme and metabolic diseases. This realization would also increase the off-shelf availability of transplantable organs in concert with creating a definitive donor pool expansion technique.

However the fruition of a functional hepatic tissue engineered modality is hampered by deficient long-term endogenous phenotypic expression and cell viability. More specifically, major limitations are seen in the areas of transport (e.g. oxygen supply and tension, nutrient and waste exchange) and the accurate characterization of the fluid dynamic micro-environment within hepatocyte impregnated three dimensional scaffolds.

The **primary hypothesis** of this body of work is that direct and sustained physiological oxygenation in conjunction with a perfused aqueous oxygen supply within a three dimensional milieu will ensure short-to-medium term cell viability while encouraging suitable liver specific functionality. In order to investigate this hypothesis chitosan scaffolds were fabricated as a cylindrical, three dimensional tube with embedded gas-permeable silicone tubing to simulate in vivo capillary gas exchange. The metrics employed to evaluate the efficacy of this model were nuclear viability staining, albumin production and ureagenesis.

We utilized a computational fluid dynamic (CFD) model to accurately characterize and understand the shear stresses that were imposed on the hepatocytes within the micro-porous scaffold environment. This CFD model was used to identify which culture medium flow rates imposed the least amount of damage caused by hydrodynamic forces, while still allowing for adequate convective flow throughout the scaffold's spatial geometry. The flow rates used in the CFD model were also investigated using an in-vitro perfusion bioreactor system in conjunction with our three dimensional, hepatocyte-seeded scaffold.

Lastly, we investigated the effects of altering the scaffold's geometry in an attempt to increase the hepatocyte packing density and encourage cellular aggregation. **We hypothesize that** by creating a micro-environment that promotes cellular aggregation we would see enhanced cell-to-cell and cell-to-substratum contact throughout the scaffold interior, thus positively modulating hepatic functionality and restoring the cells to their phenotypic differentiated state.

The **specific aims** for this study were:

1) Design and assemble a perfusion bioreactor system with integrated direct oxygenation capabilities suitable for maintaining *in vitro* hepatocyte single cell and spheroid cultures.
2) Compare the effects that aqueous oxygenation versus aqueous+direct oxygenation have on hepatocyte metabolism and differentiated state.
3) Develop a computer-generated computational fluid dynamics (CFD) model to understand the internal scaffold flow characteristics and the micro shear environment at various flow rates. We would also use this model to assess how these flow rates affect hepatocyte oxygen uptake kinetics along the length of the scaffold.
4) Validate the aforementioned flow rates mentioned in specific aim three with our perfusion bioreactor system to assess which rates corresponded best with the CFD data and positively influenced hepatic differentiated activities.
5) Evaluate the effects of reducing the scaffold's volume and increasing seeding densities have on albumin production, ureagenesis, viability and aggregate morphology. .

The remainder of the dissertation is organized as follows: Chapter two reviews the background and significance of the liver's anatomy, physiology and pathogenesis. It also explains the importance of hepatocytes and the role they play in maintaining homeostasis, the modes of hepatic failure and the various in-use and exploratory methods that are being employed to restore function after it has been compromised. Chapter three reports the effects that aqueous plus direct oxygenation have on hepatic differentiated functionality in a three dimensional chitosan scaffold perfusion bioreactor model. These results are also compared to a perfusion bioreactor model that utilizes the same model less direct oxygenation. Additionally, we looked at how this three dimensional perfusion model

modulated albumin protein expression, ureagenesis, aggregate morphology and viability.

Chapter four reports the results of our computational fluid dynamic (CFD) model that investigated the hydrodynamic forces imposed on the hepatocytes imbedded in our chitosan scaffold at various flow rates. The CFD model also aided in elucidating the fluid flow and oxygen uptake characteristics within the cell-seeded scaffold environment. Chapter five is devoted to validating the flow rates used in the CFD model (chapter four) and assessing the effects of these rates on hepatic function. In addition to functionality, we also examined how these flow rates affected hepatocyte viability. Chapter six looks at how changing the spatial geometry of the scaffold modulated functionality, hepatocyte morphology and viability. Each chapter provides a background for the research objectives, explains the methodology and material utilized to conduct the experiments, describes results and summarizes these results in a discussion segment.

CHAPTER TWO: LITERATURE REVIEW

2.1 Liver Anatomy, Physiology and Pathogenesis

The liver is a complex, highly vascularized bio-ecological system. It achieves homeostasis through the harmonious orchestration of multiple metabolic interactions, numerous cytokine networks and the co-interplay of its cellular constituents and matrix components [16, 17]. Situated under the diaphragm, the liver consists of two major lobes that are further segregated into smaller units. The strategic position (i.e. between the gastrointestinal tract and systemic circulation) of the liver allows receivership of venous blood from multiple sources. Therefore the liver is able to regulate the concentration of incoming hormones, toxins and lipophilic and hydrophilic nutrients in the terminal hepatic venules through various endocrine functions. By this it is able to efficiently function as an effector and sensor organ [18] table 1. In addition to its endocrine activity, the liver also exhibits exocrine functionality.

The intricate spatial orientation of the liver's cellular architecture is considered a histological homogenous structure; however this notion is contrasted by its morphometric and histochemical heterogeneity. This heterogeneity stems from the zonal (periportal and centrolobular) and regional (septal and portal) variances in subcellular structural features, metabolic capacities of the cellular elements, substrate concentrations and hormone levels [19]. Cellular heterogeneity is also facilitated by varying cell receptors and their corresponding densities and dynamic gradients (oxygen, biomatrix etc.) that are established between the upstream and downstream segments of the hepatic sinusoid [18].

2.2 Hepatic Extracellular Matrix (ECM)

The hepatic extracellular matrices (ECM) are insoluble structures that constitute the reticulin framework of the liver. Restricted to the portal tracts, sinusoid walls and the central

veins the hepatic ECM composition encompasses three distinct classes of macromolecules: collagens, non-collagenous glycoproteins and proteoglycans [20]. In addition the liver ECM is composed of water, electrolytes and trace flow-through elements which constitute its minor constituents [21]. Its architecture is distinct from other epithelial organs in that it lacks extensive areas of connective tissue and a cell separating basement membrane. Moreover it carries a strategic location and function: It acts as a reduced permeability demarcation between the portal blood plasma and the parenchyma; and aids in the bidirectional exchange of macromolecules between hepatocytes and circulating blood [22].

The main functions of the hepatic ECM are similar to its epithelial organ counterparts in that it allows intercellular communication, cohesiveness between cells and provides a structural framework [23, 24]. More specifically through positional, locomotive, growth, and differentiation-promoting signals, the hepatic ECM is able to regulate parenchymal and non-parenchymal function, gene expression, differentiation, proliferation, cell polarity and apoptosis [25]. Moreover the insolubility of the hepatic ECM allows it to exert influences over cellular activities at short range and in tight spatially controlled fashions [26]. Furthermore, the dynamic aspects of matrix degradation (via Metalloproteinases) and zonal gradients formed by its macromolecular components also contribute to the modulation of hepatic function [18, 27, 28].

2.3 Hepatocytes

Hepatocytes are large polyhedral epithelial intermediate cells that spawn from endodermal foregut precursor cells [29]. Analogous to other epithelial cells, hepatoctyes are highly polarized; and accounts for 60% of the cell population and 80% of the organ volume [30]. Structurally, hepatocytes are between 30 to 40μm in diameter, organized in unicellular muralium that bifurcate and anastomose to form an intricate network with limiting plates at the capsule and portal regions [31].

Anatomically, the hepatocyte contains three main domains: Basolateral domain, Apical or Cannicular and the Laterl domain which account for 70%, 15% and 15% of the total cell surface area respectively [32] . The cytoskeleton of the hepatocyte and the maintenance of its overall integrity are paramount to hepatic-specific functionality. The cytoskeleton is composed of many different proteins that assist in overall cell health, however the major components that are germane to this effort are microfilaments, microtubules and intermediate filaments [33]. Briefly Microfilaments are responsible for cell membrane motility, endocytosis, exocytosis and vesicle transfer. Microtubules are mainly involved with the secretion of vital liver-specific functional products such as albumin, fibrinogen and numerous glycoproteins [31]. Lastly are intermediate filaments (cytokeratins) act as intracellular scaffolds in areas where mechanical stress is prevalent. Furthermore they are associate with maintaining structural polarity within the hepatocyte and providing a framework for actin distribution endocytotic vesicles along the plasma membrane [34]. When assessed independently these structures are chemically and functionally distinct, however when working in conjunction, they are responsible for the modulation and functional demands of the hepatocyte in response to various external and intercellular stimuli.

The complexity of the liver also stems from the thousands of vital homeostatic operations performed by its main parenchymal functional unit. As the workhorse of the liver, hepatocytes are responsible for a myriad of metabolic processes, xenobiotic biotransformation, bile production and liver transcriptome (i.e. genes expressed as measured by mRNA) [30]. Such activities are influenced by the hepatocytes high rate of oxygen consumption and its ability to produce and regulate its energy reserves.

Zonation or compartmentalization of gene expression, morphology and function exist within the hepatic acinus. Hepatic zonation is determined by oxygen, substrate/extracellular matrix protein distribution and hormone gradients between the periportal and perivenous

areas [35]. Hepatocellular zonation results in parenchymal heterogeneity with respect to infrastructure, ultrastructure and protein activity. This complex aspect is exacerbated by the fact that zonal heterogeneity is dynamic and is subject to change based on the level of hepatic pathos or its current metabolic status [19].

2.4 Hepatocyte Cell Junctions

The hepatocytes ability to remain in a homeostatic state is overwhelming modulated by its ability to maintain vital interactions with its adjacent environment. Such interactions, which are mediated by both nonjunctional and junctional mechanisms, include cell-to-cell and cell-to-extracellular matrix contacts. The presence and adequate maintenance of these junctional mediated interactions that are critical for hepatic-specific functions including albumin secretion, ammonia detoxification, glycogenolysis and bile secretion [36]. Gap junctions are a specialized group of intracellular channels that provide a pathway for intracellular communication between adjacent hepatoytes, participates in all aspects of the cell cycle and aids in hepatic homeostasis [37]. Tight junctions specialize in sealing adjacent epithelial cells together, but also form a much regulated tissue space divide that contributes to the maintenance of tissue integrity. Tight junctions are also known to play a critical role in cellular interaction and intra-actions (i.e. signal transduction, transcriptional regulation and cell cycle [38]), communication and modulate the movement of selective paracellular solutes across the epithelium [39]. The in-vivo cellular plate architecture of the liver relies tremendously on these junctions as they maintain polarity by demarcating the hepatic apical surface from the basolateral surface which in turn ensures adequate bile secretion and the removal of xenobiotic agents [40]. Integrins are a class of adhesion molecules in which hepatocytes utilize to adhere to their ECM or basement membranes. The adhesion receptors/ECM interactions help to maintain basal-apical polarity, tissue integrity and cellular architecture [41]. In vivo, the type of integrin expression is dependant on the constituents of

the basement membrane and parenchyma zonal location [42]. However in vitro integrin expression levels are strictly controlled by the type of cell-ECM interactions [43]. Integrins activate intracellular signaling pathways or cascades in response to various extacellular environmental cues. Intracellular proteins such as FAK and Erk aid in regulating migration, and differentiation proliferation, and Rho in morphology [44, 45]. Additionally MAPK and Akt once activated by FAK are responsible for the suppression of receptor/ECM detachment based apoptosis (Anoikis) [46].

2.5 Liver Oxygen Tensions

As the metabolic epicenter for the human body, the liver is responsible for regulating numerous functions. Such functions include but are not limited to carbohydrate, amino acid and fatty acid metabolism, bile secretion and detoxification, which are orchestrated by the hepatic parenchymal cells [47]. Because of such a heavy physiological burden, adequate oxygen consumption under strict hepatic zonal pO_2 is critical to maintaining the liver microenvironment. The hepatocyte relies on over 1500 mitochondria for energy production and consumes oxygen at a rate of .3 to .9nmol/sec/10^6 cells [48]. As mentioned earlier the liver is zonal is nature with regulated oxygen tension for each zone. The zones and corresponding oxygen tension ranges are as follows: periportal – 60 to 65 mmHg (84 – 91 µmol/L), perivenous – 30 to 35 mmHg (42 – 49 µmol/L) [49].

2.6 Modes of Liver Failure

Several factors have been identified that trigger the intrinsic and or extrinsic pathways that contribute to cellular death. Such factors include hypoxia, reactive oxygen species, toxins and various immune processes. Cellular death can be categorized by either apoptosis or necrosis. Necrosis, also known as oncotic necrosis or oncosis, is considered a passive form of cell death that is a consequence of some form of acute metabolic perturbation or acute drug induced hepatotoxicity. It leads to oxygen deprivation and subsequent ROS

generation and mitochondrial dysfunction [50]. Apoptosis, conversely, is programmed cell death that initiated by intrinsic mechanisms that are regulated by various signaling pathways. This mode of death leads to cellular resorption which mitigates inflammatory responses and leakage of cellular constituents into the extracellular space [51]. Autophagy is lysosomal catabolic pathway that is characterized by the degradation of cytosolic proteins and organelles. It is induced during starvation and promotes survival by providing amino acids and participating in glucose metabolism. However in cases of prolonged starvation acute liver insufficiencies occur which triggers autohpagic cell death [52].

2.7 Treatment of Acute Liver Failure

2.7.1 Surgical Based Approaches

Split Liver Transplantation

As previously stated orthotopic liver transplantation is the gold standard of treatment. However suitable organs for transplantation are the limiting common denominator. Due to this shortening of cadaveric organs, donor pool expansion techniques such as split liver transplantation have been employed. The protocol has reported results similar to whole liver transplantation. However the procedure many be complicated by complicated by anatomical variations. Furthermore, lack of availability has led to the use of marginal to sub-par quality organs [53].

Living Donor Transplantation

Comparable to split liver transplantation, living donor transplantation has also been used with the intent of ameliorating the organ shortage crisis. Living donor transplantation takes advantage of the right lobe in the case of adult patients and the left for adolescents. Due to the complexity associated with a lobectomy procedure, donors are predisposed to great health risks. Again, the lack of availability has compromised selection criteria, allowing ailing and elderly individuals to become candidates [54].

2.7.2 Non-Biological Approach

Hemofiltration/Hemodialysis

Hemodialysis was introduced with the intent of efficient hepato-toxin removal by way of diffusion, but offered little in this way as an effective filtering measure of small water soluble molecules with molecular weights less than 5000. Driven by convection, hemofiltration offered a higher competence for filtration as it extracted middle molecular weight compounds ranging from 5000 to 10000 [55]. In addition to hemofiltration's inability to eradicate lipophilic or protein bond substances [56], it also lacks specificity in its abstraction of low and medium molecular weight substances. Both methods used concomitantly, coined hemodiafiltration, demonstrated improved biochemical parameters and neurological status, but had little effect on patient survival rates [57]. Dialysis circuits are also known to induce a range of biological effects such as production of endogenous monocytic pyrogens [58], heightened levels of superoxides, IL-6, IL-1, TNF-α and C3a/C5a via complement cascade activation. However, little is known of the effects that dialysis has on the mitogens EGF and HGF [59].

Hemoperfusion

Hemoperfusion describes the aggressive removal of protein bound toxic molecules via blood circulation over sorbent materials such as activated charcoals, anion exchange resins or synthetic neutral resins. In addition to the decline in fibrinogen levels, deleterious effects stemmed from the bio-incompatibility between blood and the extracorporeal circuit, resulting in leukopaenia, removal of coagulation factors and activation of the complement cascade [60].

Despite countermeasures used to mitigate foreign body reactions such as biocompatible polymer coatings [61] and encapsulants, the nonspecific targeting of molecules of varying molecular weights and chemical characteristics remained a challenge. During hemoperfusion charcoal absorbents exhibited complete removal of hormones and growth

factors [62-65] critical to hepatic regeneration whereas platelet and leucocyte counts were diminished with resins [60]. When coupled with albumin dialysis (Hemodiabsorbtion), cytokines IL-6 and TNF-α [60], in addition to substances with high albumin affinity were abated [62]. The elucidation of the effect that this technology has on the removal of mitogens EGF and HGF is still unclear.

Plasma Exchange

Plasma exchange essentially is a technique of separating plasma from the patient's cellular blood component via plasmapheresis and exchanging it with an equivalent volume of fresh frozen plasma from a healthy donor. The method's aim is to suppress symptoms of hepatic failure by removal of circulating toxins and waste products to promote an environment that is conducive to liver recovery or regeneration. Although this method has shown improvement in hemodynamic stability [66], coagulation profiles and cerebral function, adverse effects such as coagulation imbalance, citrate load [67, 68], toxic effect, infection and pulmonary and neurological complications are noted [59]. Other faults experienced by this therapy is the non-selective manner in which it abates or reduces potentially helpful substances that could contribute to hepatic convalescence[69] and its ineffectiveness in decreasing the large intracellular pool of hepatoxins that accumulate during liver failure. These factors in conjunction with the need for high volumes of replacement plasma and cost have restricted its use.

Albumin Dialysis

Considered the most proficient non-biological modality, albumin dialysis combines the detoxification of water-soluble and protein-bound toxins in a recirculating closed-loop albumin circuit. To date, Molecular Adsorbents Recirculating System (MARS) is the most comprehensively assessed dialysis system. MARS incorporates a two-fold passive transport sequence allowing a down-stream diffusion of toxins from the plasma to the free binding sites

of the membrane and secondly, from the membrane to the free binding sites of the dialysate. The dialysate is filtered via anion exchange chromatography, charcoal filtration and sequential dialysis. The system likewise allows non-albumin bound, low molecular weight, water soluble molecules to transgress the membrane [70].

2.7.3 Cell-Based Therapies

The complexity of the liver combined with the detoxificational, bio-transformational and metabolic ineptness of current non-biological support systems have galvanized the efforts towards the use of viable hepatocytes as a means of perpetuating and regulating liver specific functions. The ideology behind hybrid bioartificial liver support systems is that liver-specific functions can be re-established by hepatocytes in an exogenous milieu. To this, implantation techniques, systems and extracorporeal devices have been developed to cultivate this ideal.

Extracorporeal Whole Liver Perfusion (ECLP)

This method involves perfusing a patient's blood through a xenogeneic or allogeneic liver. ECLP has been proven to support ALF patients for several days [71], however it is considered impractical due its association with xenogenic immuno-complexes. Nonetheless transgenic porcine livers (TPL) have been used in attempts to overcome the potential immunological barriers posed by its predecessors. Clinically, patients treated via ECLP-TPL showed no symptoms of porcine endogenous retrovirus (PERV) infection [72]. Moreover, preclinical baboon and ex-vivo xeno-perfusion models have garnered promise, showing reduced complement activation and superior histology [73-75]. Still more clinical trials are needed to explicate the potential for high xeno-protein influx and transferal of other zoonosis.

Cellular Implantation

Cellular implantation attained favor because it is simpler, less invasive, cost-effective and fewer cells are needed to sustain life. The intrinsic micro-environment of the liver was sought as the primary site to foster engraftment and functionality. However this led to severe

hypertension and hepatic necrosis due to aggregate formation and thrombi in distal portal branches, sinusoids and central veins [76, 77]. Various ectopic sites have also been explored e.g. peritoneum, lungs, fat pads, pancreas, mesenteric leaves, under the kidney capsule and subcutaneous tissues [78-80] but only the spleen has shown potential [81]. In addition, a liver-specific architecture, basement substratum and venous supply that encompasses the mechanical and biochemical environment of the hepatic sinusoid was lacking [82].

To enhance functionality, advanced systems using microcarrier beads, spheroid aggregates and biodegradable polymeric immobilization substances have been employed. In addition angiogenic agents have been employed with success to pre-transplant sites, but have been deemed beneficial only for metabolic disorders not ALF [80]. To date, the main disadvantages in using implanted hepatocytes are the delay of function upon implantation and the lack of proliferation without sufficient growth factors [83].

"Hepatocyte repopulation" has recently stimulated endeavors at improving the efficiency of cell engraftment and propagation. The goal of hepatocyte repopulation is a coordinated process of cell replacement in which exogenous cells are used to replenish the liver mass to its original state and facilitate hepatic homeostasis. In order for this to occur transplanted cells must have a growth and/or survival advantage over the damaged population and their must be space in the recipient organ for these cells to grow [84]. Subsequent to engraftment, the fundamental mechanism entails clonal proliferative stimuli induction and suppression of host cell mitosis [83]. Stimuli induction can come via loss of hepatic mass, reperfusion injury, massive endogenous apoptosis mediated by Fas-gene transfection or administration of hepatocellular mitotic stimulants [85]. The technology has garnered success in rodent models [86], and is deemed plausible as a treatment for metabolic disorders.

Although this technique has promise, it does have some obvious short-comings. Hepatocyte repopulation, in multiple models, has been shown to consistently and inherently be linked to with an increased risk of cancer development in the liver. To date the reasons why engrafted cells either produce normal versus cancerous liver histology has yet to be elucidated. However these cancerous events are thought to stem from either a diminished expression of gap junction protein connexin 32 and integrin protein IG-5-1, and the altered expression of matrix metalloproteinases 2 (MMP2) [87]. To be seen as a permanent modality for acute liver failure, more research and clinical trials are needed.

Extracorporeal Devices

The aforementioned modalities have resulted in the conception of the bioartificial liver (BAL) or hybrid liver support device. This two prong method functions by maintaining cultured immobilized hepatocytes (bio-component) in an exogenous bioreactor system (artificial component), while temporarily integrated into the patient's blood or plasma perfusion circuit. The objective of the BAL system is to either stabilize and support patients prior to orthotopic transplantation, act as a bridge for patients awaiting a suitable donor organ or operate as a conduit for liver regeneration [88]. To date, BAL extracorporeal devices such as HepatAssist, Extracorporeal Liver Assist Device (ELAD), Modular Extracorporeal Liver Support (MELS™), Bioartificial Liver Support System (BLSS™) and the Amsterdam Medical Center Bioartificial Liver (AMC-BAL™) have reached some level of clinical trial; however none have proven to be completely effective in suppressing all the events associated with liver failure.

The most appropriate hepatic cell source for extracorporeal devices is primary human hepatocytes. Theoretically, they provide all the necessary biological functions needed to maintain homeostasis. However the limiting factor is availability, as most eligible donor organs are used for transplantation [89]. Cryopreservation tactics were implemented to mollify the burden of availability, but offered little value as calamitous effects (i.e. detachment,

functional degradation, apoptotic and necrotic death) are induced by thawing [90, 91]. Moreover human hepatocytes are difficult to regenerate in vitro, are characterized by heterogeneity and low viability, express inadequate levels of liver-specific functions due to loss of gap junctions, originate from histologically impaired organs and pose complex logistical concerns [5, 92, 93].

Immortalized hepatocyte cell lines such as C3A stemming from hepatoblastoma cell lines have also been incorporated into support devices. Such cell lines hold a theorectical advantages over primary cells in that they are not mitotically inactive and can proliferate indefinitely, they secrete high albumin levels, but lack promise due to insufficient ureagenesis and amino acid metabolism [94]. Moreover, these sources also pose concerns for high risk transmission of potential tumorigenic cells [59, 95]. Adult and embryonic stem cells are currently being pursued as a final alternative. The utilization of adult stem cells as a surrogate has peaked the interest of many investigators, but the plasticity [96] and ability to efficiently differentiate and proliferate these cells remains a formidable challenge [97].

Due to abundant available quantities and their ability to maintain a highly differentiated state of functionality, primary porcine hepatocytes have been sought and used in the majority of clinically applied BAL reactors. Unlike C3A cell lines, porcine based hepatocytes maintain the necessary hepatocyte-specific function including but not limited to ammonia detoxification [89]. Albeit the great optimism of this cell type, many unresolved obstacles plague its efficacy in BAL systems. Foremost are the apprehensions regarding immunological complications emanating from xenogeneic protein influx [98], tumorigenicity, and the transmission of viral zoonoses, such as porcine endogenous retrovirus (PERV). Although no reports of human cross infection have been reported in BAL therapy, the theoretical chance of transmission, mutation and subsequent viral pathogenesis still looms [60, 99].

2.7.4 Tissue Engineered/Regenerative Medicine Constructs

The emerging and rapidly advancing knowledge base of tissue engineering exploits individual and mixed cell populations to create, restore, maintain, or enhance 3D tissues and organs [100]. Similar to implantation, the science excels under the notion that cell-infused exogenous implants can effectively replace diminished or non-existing function when placed in vivo. To this, cells are explanted and coaxed to grow on (biological or synthetic) bio: compatible, degradable and resorbable scaffolds which serve as a nano/micro-habitat for cellular support. In addition to support, it is vital that the construct's architecture and chemistry offer native tissue specific physio-chemical and mechanical cues that provide an environment which is conducive to the correct activation of downstream signaling pathways [101] and cell-to-substrate and cell-to-cell interactions.

More specifically, hepatic tissue engineering (HPT) focuses on creating an implantable, fully functioning liver expedient. Drawing parallels to extracorporeal adjuncts, HPT also makes use of various hepatic and nonparenchymal cell types, sources, spatial configurations and *in vitro* bioreactor culturing configurations. Parallels are also seen in promise and shortcomings. The promise is seen in the advances of culture techniques, short-term hepatic-specific physiology and anatomy, growth factor combinations and material modifications. However, HPT is hampered by issues pertaining to cell sourcing, co-culture schema, immune rejection, long-term viability, sustainable phenotypic expression and morphology, tissue reorganization and transport (i.e. nutrient, gas and waste) due to a lack of a viable hepatic vasculature.

2.8 Hepatocytes – 2D Cell Culture to 3D Bioreactor Studies

2.8.1 2D Hepatocyte Cultures

Primary hepatocytes are highly differentiated, attachment dependent epithelial cells, whose structural and functional integrity (i.e. phenotype) stems from regulatory interactions between unique DNA binding sites and the patterned expression *trans*-acting protein factors.

The use of primary in vitro hepatocyte cell cultures has been the principal model for elucidating the complexities of liver-specific functionality. Initial culture attempts utilized conventional methods involving suspension and hepatic platting on rigid substratums (i.e. plastic or ECM protein coated plates). Under such conservative conditions hepatocytes exemplified enhanced attachment [102], high proliferation kinetic, short-terms liver specific functionality [103] and in vivo-like cytoskeletal protein distribution and morphology [104]. However, as culture conditions progressed, drastic changes were observed in morphological intactness and polarity [105-107], a rapid decline in liver-specific enzyme activity [108-110], up-regulation of fetal and cytoskeletal proteins [111, 112] and sustained expression of proto-oncogenes [113].

The limitations displayed by conventional/simple substratum methodologies gave way to improvements in the approach towards restoration and sustainability of a differentiated hepatic phenotype. Hepatocytes cultured in a hepatic micro-architecture mimicking configuration (i.e. collagen gel sandwich) displayed sustained viability, competent liver-specific functionality and native-like morphology [114-116]. Furthermore, collagen gel sandwich cultures induced hepatic gap junction formation, bile canalicular repolarization, normal bile acid transportation [117-119], and xenobiotic biotransformation [120]. Likewise, superior hepatic biochemical differentia is noted when hepatocytes are cultured on rat liver membrane extracts [121, 122] and complex extracellular matrix materials: liver emanated biomatrices [123-125] and mouse derived sarcoma tissue [114, 116, 126]. Lastly, heightened levels of liver-specific functionality have also been noted when hepatocytes are cultured on modified natural and or synthetic materials, as multi-cellular aggregates or with nonparenchymal cells.

2.8.2 3D Implantable Porous Scaffolds and Perfusion Cultures

The fabrication of a synthetic liver organoid requires sustained cellular viability and metabolic activity. Additionally, successful guided tissue regeneration must incorporate the use of 3D highly porous matrices with an intrinsic network of interconnected channels that have biodegradation and or bioresorption characteristics. In tandem, porous constructs and dynamic perfusion systems have the advantage of producing an environment that mimics the hepatic sinusoid flow circuit, facilitate a differentiated phenotype, enhance neovascularization and elevate mass transport capacities. As well, cultures under continuous flow are more sensitive to hormone induced tissue function and have shown to improve viability, lifespan, metabolic output and vivo-like cellular reorganization. To this, the ideal scaffold and perfusion reactor system should collectively control the following variables [127, 128]:

- Accommodate high density seeding, uniform cell distribution, cell attachment, and spatial cellular reorganization (Aggregates/Spheroids & Angiogenesis)
- Promote efficient mass transfer of nutrients, gas mixture and nitrogenated waste, to and from cells, via convective and diffusive flow
- Regulate Oxygen tension, pH, temperature and pressure
- Control medium flow rate, shear stress and hydrodynamic stimulation/suppression
- Promote cellular adhesion and a sustainable differentiated phenotype
- Minimize cellular washout
- Facilitate the removal of acidic scaffold artifacts
- Retain possible newly synthesized ECM components within construct
- Prevent medium back mixing or recirculation between cellular constituents

The need to restore and protract hepatospecific functionalities and alleviate the deleterious stimuli imposed on hepatocytes by an exogenous environment demands a biphasic approach (i.e. Perfusion reactor, biodegradable/bioabsorbable polymer) that

effectively recreates and mimics the in vivo micro-domain prior to reimplantation. Initial studies that applied this scheme utilized synthetic Poly(*D,L*-lactic-*co*-glycolic acid) PLGA scaffolds. Under short-term culture conditions, Kim et al. [129] accomplished successful cell-substrate attachment, induce in vivo-like reaggregation and maintain a higher mean concentration of albumin in comparison to static cultures. Similarly, Park [130] and Fiegel et al. [131], used continuous flow conditions and PLGA augmented matrices to significantly improve cell viability, function and morphology in contrast to unmodified, static and negative control cultures. Likewise, biodegradable poly(L-lactic acid) (PLLA) with continuous flow [132, 133] and pulsatile flow [134] was also able to prolong liver specific function and instigate a cellular anatomy comparable to what is seen in vivo. In addition these physiochemical parameters, Torok et al. [135] was able to conclude that this configuration also fostered monoethylglycinexylidine (MEGX) expression, normal Cytokeratin 18 (CK18) distribution, homogenous glycogen storage and, intercellular junction and bile canaliculi formation. Analogous trends associated with cellular faculties, attachment and histological viability were evident with biodegradable polyglycolic acid (PGA) [136, 137]. However, in contrast to hepatic parenchymal and nonparenchymal co-culture physiology, Kaihara et al. [137] showed no significant effect on hepatospecific functionality when hepatocytes were cultured with nonparenchymal and sinusoidal endothelial cell.

Efforts with biomaterials polyurethane (PU) [138], Polyvinylalcohol (PVA) [139], and a loofa sponge [140]also preserved short –to- medium length culture periods where hepatospecific functionality was present. Conversely, the best results were obtained with porous galactosylated chitosan substrate, derived from dried fruit (*Luffa cylindrical)*. Chen and Lin [141], while using considerably high flow rates (34 ml/min), were able to induce spontaneous cellular reaggregation to form spheroid masses in excess of 300µm in diameter and suppress cellular damage caused by hydrodynamic shear stresses. Furthermore and

most importantly, albumin and urea synthesis were maintained at levels parallel to that seen in vivo for the duration of the culture.

2.9 Chitosan as a Biomaterial for Tissue Engineering Constructs

Chitosan (2-amino-2-dexoxy-β-D-glucan), is the fully or partially N-deacytlation derivatized form of chitin (Figure 1). By nature chitosan is a linear, hydrophilic, polyamine copolymer composed of two common *in vivo* amino sugar constituents; 80% D-glucosamine and 10% N-acetyl-D-glucosamine [142]. Depending on the source and preparation chitosan's molecular weight can range from 50 kDa to 1000 kDa with degrees of deacetylation between 50% and 90%.

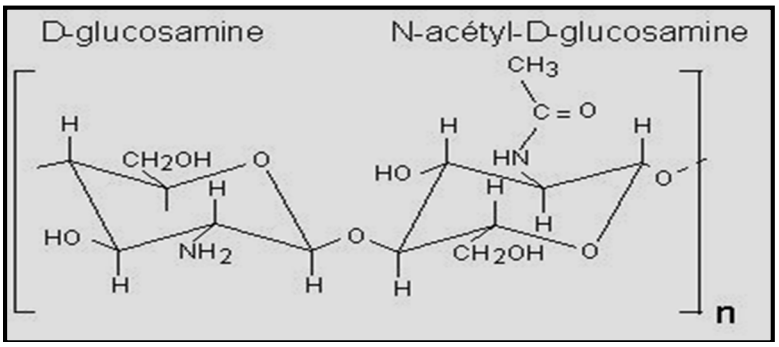

Figure 1: Structure of Chitosan Polysaccharide

Eliciting minimal foreign body reaction upon ingestion, implantation or injection, chitosan is deemed biocompatible. In addition the polymer possesses a marginal level of bioburden [143]. In vivo the polymer is bioresorbable and biodegradable via hydrolysis. Proteolysis, in foremost, is induced by lysozyme [144] however other proteolytic enzymes have also demonstrated nominal levels of enzymatic activity [145, 146]. Moreover the degraded artifacts (i.e. amino sugars) are excreted as carbon dioxide or coalesced into the synthesis of glycoproteins [147]. Considerable factors that are known to affect chitosan's degradation kinetics are molecular weight, water content, degree of deacetylation and molecular architecture.

At pHs below ~6.5, Chitosan assumes a cationic profile (i.e. linear polyelectrolyte and high charge (+) density) making it susceptible to electrostatic interactions with a myriad of negatively charged molecules including soluble proteins, proteoglycans and the extracellular matrix constituents, glycosaminoglygans (GAGS) [148]. These interactions are also consistent with anionic cell membranes which have been shown to enhance cellular growth, attachment, proliferations and cell-tissue reconstruction [149]. Chitosan's N-acetyl-D-glucosamine moiety, analogous to that found in GAGS, implies a certain level of bioactivity. Its presence stimulates macrophagic production of nitric oxide, thus upregulating phagocytic activity against pathogens and neoplastic cells and jointly affecting several unrelated biochemical processes such as the cytochrome chain [150, 151]. Moreover, chitosan and chitin are known to enhance *in vitro* and *in vivo* chemoattractivity in neutrophils [152].

Chitosan also possess an intrinsic level of bacteriostatic activity. The interaction between its reactive amino groups and the negatively charged microbial cell wall suppresses biosynthesis, thus accelerating death by hindering mass transport across the cell wall [153]. These amino groups as well as its reactive hydroxyl groups can be used in conjunction with or without each other to facilitate the amiable change of its chemical structure and soluble properties [154]. Furthermore, chitosan's physical characteristics in terms of porous structure and geometrical orientation can be altered through freezing rate, thermal gradient and shape manipulation [148].

2.10 Computational Fluid Dynamics (CFD) and Bioreactor Cultures

In the last decade computational fluid dynamics (CFD) has found usefulness in preliminary cells studies and has served as an adjunct to ongoing culture systems. Computational fluid dynamic modeling holds a comprehensive advantage over trial-and-error science by incorporating mass, momentum and energy conservation equations to quantify user defined metrics in steady state/unsteady state, laminar/turbulent flow and

Newtonian/non-Newtonian flow systems. Furthermore, the understanding of the complex fluid dynamic environment, prior to the experimental phase, allows for design optimization, modification, scale-up and determination of system efficacy.

In the early stages of micro-porous construct CFD modeling Raimondi et al. [155] attempted to characterize and quantify the flow fields and local hydrodynamic stress distribution imposed on the cellular constituents by experimental flow rates. This effort explored the use of a simplified 2-D geometry constructed from histological scaffold cross sections composed of randomly staggered 15µm diameter extruded rod-like fibers. The results were inconclusive due to heterogeneous scaffold architecture, construct oversimplification (2-D vs. 3-D) and the adopted boundary conditions used in simulation. The results were further confounded by the assumption that the shear stress inflicted on the 2-D structures would be comparable to a non-present cellular population irrespective of cell packing density. A more recent study conducted by Raimondi et al. [156] employed a scaffold mimicking, aggregate centered 3-D homogenous open-pore structure to ascertain a more realistic perfusion induced micro-shear environment. This approached proved to be better than the aforementioned in terms of predicting and quantifying applied shear stress, however such parameters that affect shear stress such as spatial position of multiple aggregate clusters in a finite space were not explored. CFD has also been used to correlate implied cellular hydrodynamic stresses at known micro-fluid dynamic conditions to 3-D construct micro-architecture (i.e. porosity and pore size). For example Boschetti et al. [157] were able to utilized an homogenous open-pore geometry with varying pore sizes and porosities to conclude that pore size has a strong influence on the shear stress level experienced by the cell population. Furthermore, they were also able to establish that porosity distinctly affects the statistical distribution of shear stresses, not its magnitude.

Micro-computed tomography (μCT) has been incorporated into CFD work to more accurately reconstruct the actual micro-structure of tissue engineering scaffolds [158-162]. In particular to simulated fluid flow Porter et al. [163] used this scheme in conjunction with lattice-Boltzmann method to determine the confined hydrodynamic load imposed on the internal walls of a reconstructed 3-D porous bone scaffold. Cioffi et al. [164] and Singh et al. [165] also used an analogous micro-computed tomographic method to recreate porous constructs to examine local shear stress distribution, flow fields and velocity profiles in a uni-axial and bi-axial rotational bioreactor.

In addition to calculating shear stresses, velocity profiles and flow fields, Williams et al. [166] was able to model steady state oxygen profiles of O_2 saturated media around a non-porous construct in a concentric cylinder bioreactor. By using a zero-order oxygen consumption model in conjunction with experimental mammalian oxygen consumption values, Williams was able to conclude that fluid phase oxygen transport to the nonporous construct was uniform and that oxygen concentrations within the bioreactor is not a limiting factor in terms of cell growth.

CHAPTER THREE: PERFUSION BIOREACTOR OPTIMIZATION, AND THE TANDEM EFFECTS OF DIRECT AND CONVECTIVE OXYGENATION ON HEPATIC FUNCTION

3.1 Introduction

Second to skin in size and the brain in complexity, the liver, and its hepatic constituents, are considered the epicenter for metabolic activity and homeostasis in the human body. The highly complex nature and architecture of the liver has burdened researchers with several challenges that has stifled the fruition of a successful implantable liver tissue engineered device. Major hurdles include reestablishing an in-vivo-like morphological, functional and polarized state that is lost upon disassociation from their nature ECM micro-environment. However because hepatocytes are highly metabolic and consume oxygen at a rate 10-fold that of any other cell type [167], the greatest challenge to a viable tissue engineered construct is an extended oxygen supply that can accommodate a densely scaffold-seeded hepatocyte mass of 80 to 100 million cells. Insufficient oxygen supply, in-vitro, can generate a number of intracellular changes that can affects how the liver processes glucose and vital nutrients [168]. Long-term exposure to O_2 limiting/hypoxic conditions would eventually cause a decrease in protein production and a disruption in cellular metabolism leading to ATP depletion. This also gives way to the metastable state of mitochondrial permeabilization transition (MPT), followed by lysosomal disruption, bleb coalescence and growth, cell swelling, ion dysregulation, enzyme degradation and eventual death either by apoptosis or necrosis [169, 170].

The goal of liver tissue engineering is to generate a functional 3-dimensional tissue substitute, in-vitro or de novo, that is morphological and phenotypically relevant with the intent to restore, replace or improve failing native tissue function [127, 171, 172]. Essential to the

success of such a device is the synergistic and dynamic interplay of the bioreactor/scaffold complex. The role of the bioreactor is to aid in the generation of functional liver tissue by maintaining an environment that is conducive to enhanced hepatocyte maturation, long-term viability and liver-specific functionality. It accomplishes this by: 1) maintaining a uniform spatial cell distribution post seeding [173]; 2) providing the necessary biochemical and biomechanical cues [174, 175]; 3) ensuring that the culture parameters (i.e. pH, O_2 tension, regulatory molecules, temperature and shear stress) are maintained at levels that resemble the native tissue microenvironment [176, 177]; 4) removal of heptaic by-products and 5) facilitate efficient external and internal mass transfer of nutrient, regulatory molecules and oxygen by diffusion and convection [127].

The second half of the complex is the scaffold construct which serves as a microenvironment that mimics the native tissue and fosters cell maturation. Scaffolds, for implantation, are composed of biocompatible and biodegradable materials that can provide the necessary mechanical support, and biochemical and biomechanical stimuli needed for optimal organ specific functionality [178]. Scaffold that have open, interconnected pore networks are essential to neo-tissue formation as they aid in cell nutrition, proliferation and/or migration, angiogenesis and serve as anchor points with the surrounding natural tissue structure post implantation [179-182].

Within the last decade researchers have sought to tackle O_2 transport limitations, in 3D hepatic cultures, by increasing the amount of available oxygen with synthetic or natural oxygen carriers and bioreactor culture systems. Shi and Coger [183] utilized perfluorocarbons (PFC) with Gelfoam gelatin sponge scaffolds in perfusion. They saw a 7.6 fold net increase in EROD activity (resorufin production rate) in cells culture with PFC vs. standard conditioned media. C3A cells cultured with PFCs in perfusion had 9 fold increase in the number of metabolically active cells. Another study conducted by Palmer and Chen

utilized bovine hemoglobin (BvHb) infused media in a hollow fiber bioreactor culture. Their results showed that hepatocytes within this experimental setup exhibited improved hepatic metabolism and drug clearance, and preserved higher hepatocyte specific functionality in comparison to controls with no BvHb [184].

In this study we sought to fabricate a viable 3-demesional chitosan scaffold embedded with gas permeable silicone tubing to accommodate high density cell seeding and simulate capillary-like direct oxygenation to adjacent hepatocyte cellular masses. We also designed and optimized a perfusion bioreactor system that seamlessly integrates with the aforementioned chitosan scaffold for long-term culturing. The main goal of this study is to evaluate the synergistic effect that the aforementioned bioreactor/scaffold complex has on the morphology, viability and phenotypic expression of densely seeded hepatocytes in culture. The working hypothesis is that an optimized bioreactor and optimized culture conditions, plus the concomitant effect of direct oxygenation and convective mass would lead to improved hepatocyte metabolic output.

3.2 Materials and Methods

3.2.1 Sources of Materials and Reagents

Medium molecular weight chitosan and glacial acetic acid were purchased from Sigma Aldrich (St. Louis, MO).

3.2.2 Scaffold Fabrication

For these studies, highly purified, medium molecular weight chitosan was employed (90% deacetylated, M=350 kDa) for three dimensional scaffold formation. The geometry of the porous construct is cylindrical in shape with dimensions of 2.5 cm height by 1.5 cm width. The scaffold fabrication process was adopted from the freezing and lyophilization principles and techniques employed by Matthew and Madihally [148]. The construct was formed in a

cylindrical metal mold fitted with a teflon rod to create a central port to facilitate uniform seeding and medium/nutrient perfusion. To perpetuate direct oxygenation of the cellular content, eight axially-orientated, gas permeable silicone tubes were incorporated into the chitosan construct. The three dimensional porous structure was formed by freezing a chitosan/collagen solution (1.5 wt%/.15% vol in .2M acetic acid). The freezing will be accomplished by immersing the chitosan/collagen-filled mold in liquid nitrogen for 10 seconds followed by immersion in a dry ice-chilled methanol bath for 24 hours. Subsequent to freezing, lyophilization was employed to remove pore trapped ice crystals. Scaffold rehydration and acetic acid neutralization was attained by immersion in 100% ethanol and sterilization by immersion in 70% ethanol followed by several washings in a phosphate buffer saline solution (PBS) and culture medium prior to cell seeding (Figures 2 and 3).

The pore direction and size were created and regulated by thermal gradient orientation and magnitude, respectively. Implemented during the freezing process, the gradient was created by using a scaffold-centered teflon tube containing 80℃ isopropanol. This application creates a tapered radial-orientated pore structure with the larger pores (100 to 400 µm) at the central port and the smaller pores (10 to 50 µm) at the scaffold periphery.

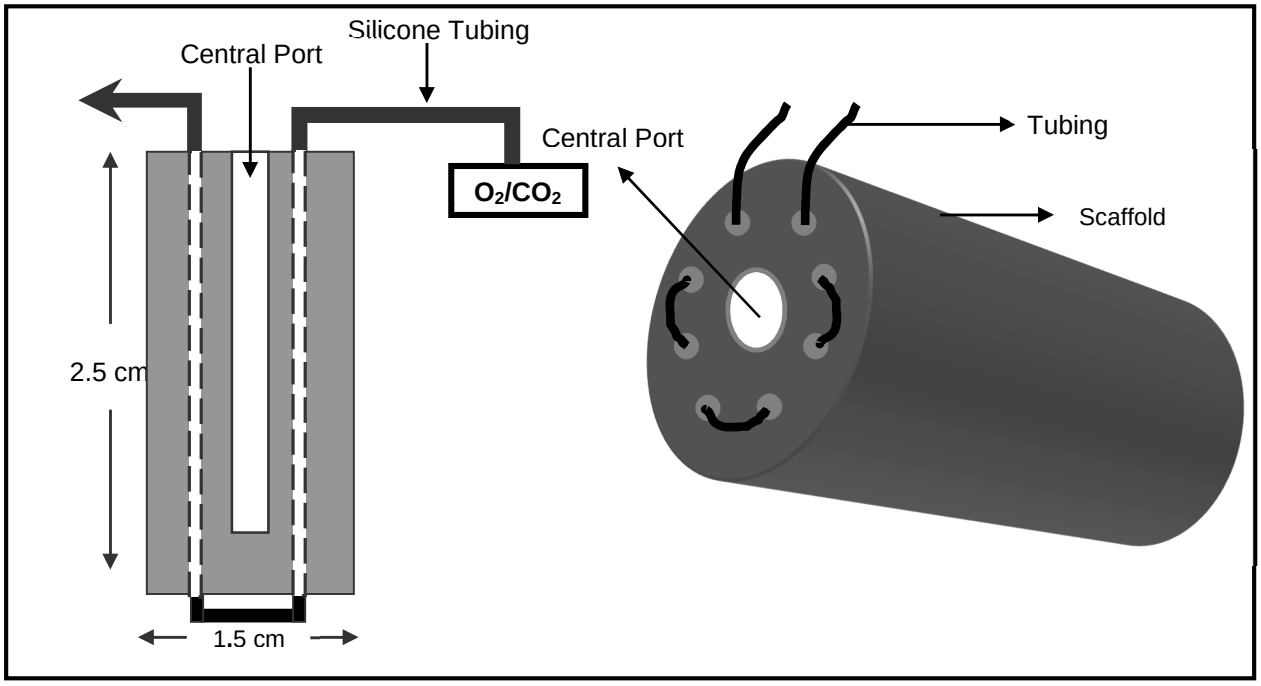

Figure 2: Schematic and 3D Rendering of Chitosan Scaffold with Silicone Tubing

Figure 3: Top, front and angled view of chitosan scaffold embedded with gas permeable silicone tubing

3.2.3 Hepatocyte Isolation

Hepatocytes were isolated from Fisher rats by a modified two-step collagenase perfusion technique. Post anesthetization by intramuscular ketamine and xylazine injection, the abdomen was open via midline incision. Subsequent to cannulation of the portal vein, the liver was flushed with 250 ml of Krebs-Ringer bicarbonate buffer (KRB) containing .4 mg/ml EDTA at a low constant flow rate. Upon complete evacuation of blood from the liver,

the perfusate was changed to 250 ml of KRBB containing .5 mg/ml collagenase (Type IV) and .3 mg/ml $CaCl_2$.$2H_2O$. Perfusion continued until the liver became flaccid and blanched in appearance, indicative of ECM breakdown and loss of anatomical structure. It should be noted that both solutions were maintained at 37•C water and circulated through sterile tubing via peristaltic pump. Upon completion of the enzymatic treatment, the liver was expunged and transferred to a beaker containing 50 ml of HBSS containing 2% bovine serum albumin. Cell liberation was achieved by blunt mechanical dissection of the Gissle capsule and mild organ agitation. The cell suspension was centrifuged at 500 rpm for 5 minutes and supernatant was removed by aspiration. Following two additional HBSS/albumin washes, cells were resuspended and aliquoted for assessment of cell density/concentration and viability. Said measurements were conducted under microscopic view using hemacytometer and trypan blue exclusion.

3.2.4 Culture Conditions

The medium used in all hepatocyte cultures was high glucose (4.5 g/L) Dulbecco's Modified Eagle's Medium (DMEM) with 4.5supplemented with the following additives: 10% Fetal Bovine Serum (FBS), 20 ng/ml Epidermal Growth Factor (EGF), 0.5 U/ml Insulin, 7 ng/ml Glucagon, 7.5 ng/ml Hydrocortisone, 200 U/ml Penicillin, 200 µg/ml Streptomycin and 20 µg/ml L-proline.

Subsequent to dynamic seeding and cell entrapment, hepatocyte cultures were maintained in a constant atmosphere of 95% O_2 air/5% CO_2. Cultures perfused with a more acidic medium (~ pH 7.2), were preserved in an atmosphere of 90% O_2/10% CO2. The respective atmospheric gas mixture applied to each culture was also supplied through oxygenation tubing. The flows rate applied in perfusion was approximated based on the cell number and literature values of hepatocyte oxygen consumption using the following equation:

$$Q_{(ml/min)} = \frac{OUR}{So_2[P_{in} - P_{out}]} N(t)$$

Where:

OUR = oxygen uptake rates of freshly isolated HCs (0.4 nmol/s/10^6 cells)

Q = medium flow rate, ml/min

So_2 = Solubility of oxygen in saline at 37℃ (1.29 nmol /ml/mmHg)

P_{in} = Inlet partial pressure (155 mm Hg)

P_{out} = Outlet partial pressure (5 mm Hg)

N = Number of viable cells in culture (million)

T = Time conversion factor (60sec/min)

It should be noted that the final value was doubled to mitigate mass transfer limitations.

Albumin protein synthesis and ureagenesis assays were performed to assess efficacy of bioreactor studies. The perfusion cultures contained a cell quantity of no less than 50 million. As a rule of thumb, the ratio of 1ml of culture medium per million viable entrapped hepatocytes per day was employed to determine the volume of medium circulating within the perfusion circuit. An additional 10 milliliters of extra medium was added to curtail any nutrient restrictions.

For the metabolic and protein synthesis comparison studies two double layer collagen sandwich culture systems were run in parallel with each bioreactor and utilized as controls. For these control cultures single cell hepatocytes were plated at a density of 1 million cells per 9.5cm^2 culture dish. Culture medium volume of 1ml per dish was used. Plated hepatocytes for the first 24 hours of culture were maintained on a single layer of collagen. On day two the unattached or non-viable cells were removed and the second layer of collagen was integrated into the system. The medium of 1ml per dish was maintained throughout the

cell culture. However for metabolic output assays, from day two onward, the final synthesis rates were doubled to account for the second ml of medium in the top collagen gel layer.

The medium was extracted and replenished daily for both culture systems. All samples were store at 4℃ until analysis were perfo rmed. Hepatocyte morphology and viability were ascertained by Hematoxylin and Eosin Y staining.

3.2.5 Metabolic Output Measurements

Enzyme Linked Immunoassay (ELISA) for Albumin

The rate of albumin secretion was quantified by an ELISA using an antibody specific to rat albumin. The assay is based on the principle of antibody capture with antigen competition. Immunoassay plates (96 well) were coated with 100 µl of coating buffer containing chromatographically purified rat albumin (Cappel), and incubated overnight at 4-8℃. The plates were washed four times with PBS/Twe en solution, then 50 µl of samples or standards and 50 µl of peroxidase-conjugated sheep anti-rat albumin antibody in PBS-Tween, the working solution was 1:10) (Bethyl Laboratories) was added and plates incubated again overnight at 4-8℃. The plates were washed ag ain and 100 µl of substrate mixture consisting of 25ml of substrate buffer and one capsule 10 mg of o-phenylenediamine dihydrochloride (OPD) (Sigma) and 10 µl of 30% hydrogen peroxide. The mixture was added to a row of wells every 10 seconds the reaction stopped after 5 min with 50 µl of 8 N sulfuric acid. Plates read immediately at 490nm and the optical density obtained using SOFT max Pro device (Molecular Devices Spectramax 250). The concentration of albumin is inversely proportional to the optical density measured. The standards were plotted on a semi-log standard curve. The unknowns are interpolated from the logarithmic fit of the standard curve.

Urea Assay

Urea secretion was measured using the diacetyl monoxime method which is a colorimetric analysis that directly determines the concentration of dissolved urea [85]. Collected samples were mixed well and 350 µl of each sample was transferred to microcentrifuge tubes, 25 µl of reagent A consisting of Diacetyl Monoxime 8.5g in 250 ml dH_2O (J.T.Baker) and 10ml Thiosemicarbazide solution,0.95g in 100ml dH_2O (TCI.Mark) is added and the solution was mixed, then 80 µl of reagent B consisting of 300ml concentrated sulfuric acid diluted to 535ml with dH_2O together with 0.5ml ferric Chloride solution,0.15g in 10ml dH_2O was added and the solution mixed well and placed in a water bath at 85℃ for 20 minutes. Urea nitrogen solution (150 mg/dl, Sigma) was used as a standard and treated the same way as the samples. Following the incubation, samples were cooled in tap water for 5 min, the water was changed and the samples cooled for another 5 min. 150 µl of standard and samples were transferred into a 96 well plate and the absorbance of the solution was read at 520 nm using a microplate spectrophotometer system. The concentration of urea was proportional to the obtained optical density (OD).

3.2.6 Histological Analysis

For histological examinations, scaffold samples, after each 7 day culture, were fixed in 4% paraformaldehyde for 2 days. The fixed samples were, processed, and embedded in paraffin, followed by microtome sectioning to obtain 5 µm thin horizontal slices. The sections were mounted on slides, deparaffinized, rehydrated and stained with Hematoxylin and Eosin (HE). Images were taken with a transmitted light microscope.

3.2.7 Statistical Analysis

The biochemical functional output of the hepatocytes for bioreactor design iterations 1 and 2 in sections 3.3.2(a) and 3.3.2(b) respectively, were calculated from single cultures.

The results from the third generation bioreactor cultures in section 3.3.2(c) were calculated form duplicate runs. The rates per day, where applicable, were averaged across duplicate runs and values are reported as mean ± standard deviation.

3.3 Results

3.3.1 Scaffold Characterization

Scanning Electron Microscopy was utilized to characterize the pore size at the scaffold's central port and periphery. This technique was also used to assess the orientation and sloped gradient of the interconnect pore structure from the central port to the periphery. Post fabrication, scaffold were vertically and radially cut, and gold sputter coated before characterization. We observed pore sizes ranging from 100-400 microns in the central port/fluid inlet and 10-35 microns at periphery/fluid outlet (Figure 4). The internal pore structure exhibited a high level of interconnectivity with a radial, tapered orientation decreasing from the central port to the periphery by a magnitude of 10.

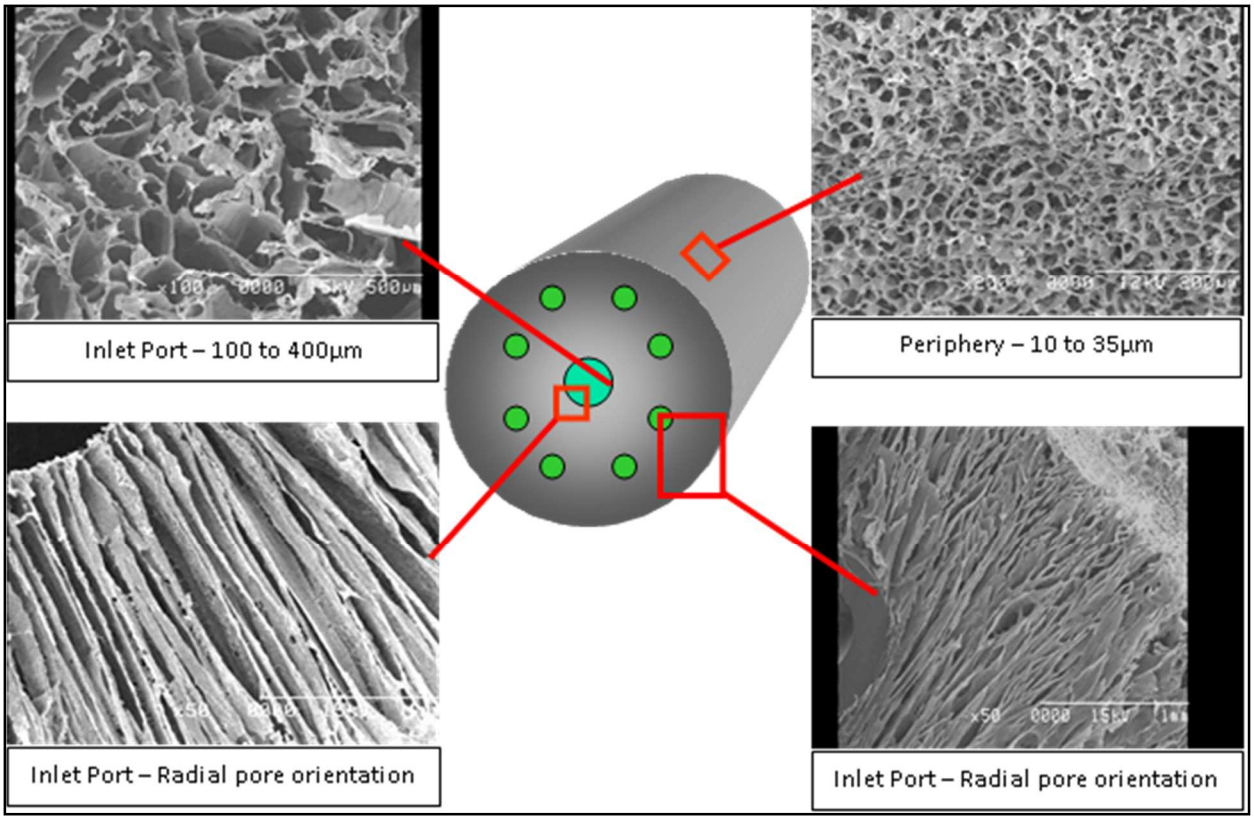

Figure 4: Scanning Electron Micrograph images of 3-dimensional chitosan scaffold. Vertical cut shows the pore size in the central port/fluid inlet (a) and scaffold periphery/fluid outlet (b). Radial cuts show tapered orientation and magnitude of interconnect pore structure at the inlet (c) and outlet (d).

3.3.2 Bioreactor design/optimization and the effects of 3D chitosan scaffold with direct and convective oxygenation on hepatocyte phenotypic expression

The reactor system was designed and developed with four goals in mind: First, accommodate high density seeding and even cell distribution; Second, provide sustained direct oxygenation to hepatocyte entrapped scaffolds, through integrated gas-permeable silicone tubing; Third, ensure adequate mass transfer via radial perfusion and, convective and diffusive flow; Fourth, maintain in vitro liver-specific functionality for the duration of the experimental run.

Scaffolds were seeded with 50, 80 and 85 million hepatocytes at a density of one million cells/ml and a flow rate of 20 ml/min. Seeding was conducted using oxygenated

medium, direct scaffold oxygenation via semi-permeable tubing. The bioreactor system, during seeding, was seated on a flat cold pack to minimize temperature fluctuations. The cold environment aided in maintaining hepatocyte viability and mitigated metabolic behavior until cells were adequately housed in the chitosan scaffold. Seeding duration continued until desired seeding density was achieved. This information was ascertained by retrieving and counting the remaining cells in suspension every 10 minutes. Once the desired density was achieved the remaining cell suspension was removed and the perfusion system was replenished with fresh culture medium. Subsequent to seeding and medium replenishment the reactor system was relocated to a climate controlled incubator and cultured at 37˚C for the duration of the experiment. Experiments conducted with the first and second bioreactor designs were cultured under 95% air/5% CO_2 balance. The experiments with third iteration bioreactor design were conducted under 90% air/10% CO_2 balance.

3.3.2(a) First Generation Bioreactor Design and Results

The first generation bioreactor system (Figure 5) was fashioned from a 45 ml glass jar which served as the cell seeding and perfusion/culture chamber. The medium reservoir/bubble trap was fabricated from a 10 ml polysulfone tube. The reservoir was fitted with a .22 µm filter which served as a sterile air vent. Before entering the culture chamber the conditioned medium first passed through 3 meters of coiled gas permeable silicone tubing (2 mm ID) that was placed in a sealed bag purged with a 95% air/5% CO_2 mixture. The sealed enclosure regulated the pH and functioned as an oxygenator for the culture medium. Upon exiting the perfusion chamber medium was pumped to the reservoir/bubble trap then the oxygenator and then back to the culture chamber. This particular perfusion circuit ensured the consistency of the gas mixture and pH were maintained before entering the culture chamber and cell seeded scaffold. The flow rate needed for cell survival was estimated based on cell mass and reported values of nutrient consumption. Circulation was

achieved by means of a peristaltic pump placed between the reservoir and oxygenator. Stopcocks were used for sampling during seeding for cell counts and viability measurements. They were also used for acquiring sample aliquots during the culture and medium exchange. The entire perfusion unit was sterilized and maintained in a 37℃ incubator for the duration of the culture. The system was replenished with fresh medium every 24 hours and sample aliquots were stored at 4 ℃ for later metabolic an alysis. In this trial the scaffold was seeded with 50 million hepatocytes and cultured for 21 days. The duration of the seeding process was 35 minutes.

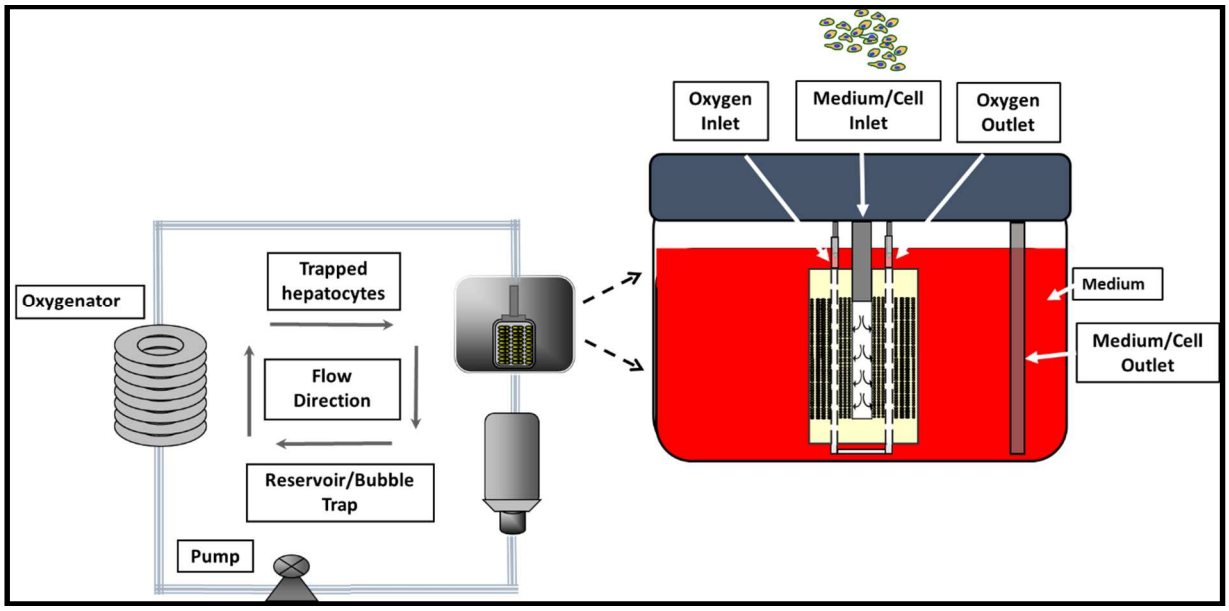

Figure 5: Schematic of first generation perfusion culture circuit with expanded, detailed schematic of the bioreactor chamber. The bioreactor image shows the fluid path from inlet to outlet, oxygenation tubing and, orientation and position of the scaffold with seeded hepatocytes.

Figure 6 shows a plot that compares albumin secretion for the perfusion and control cultures over time. For the duration of the experiment, the perfused hepatocytes were able to secrete albumin. However it is clearly evident that the levels of activity, when compared to the control culture, are significantly depressed. Although albumin synthesis declined

continuously, measurable amounts were still noticeable at day 21. The highest level of synthesis, 3.72 µg/million cells/day, was seen on day 5.

Figure 7 shows similar trends in ureagenesis. However, urea production was seen to slightly increase by day 4, but declined immediately thereafter and maintained low levels for the duration of the culture. The highest level of production was seen on day 4 with a value of 10.08 µg/million cells/day.

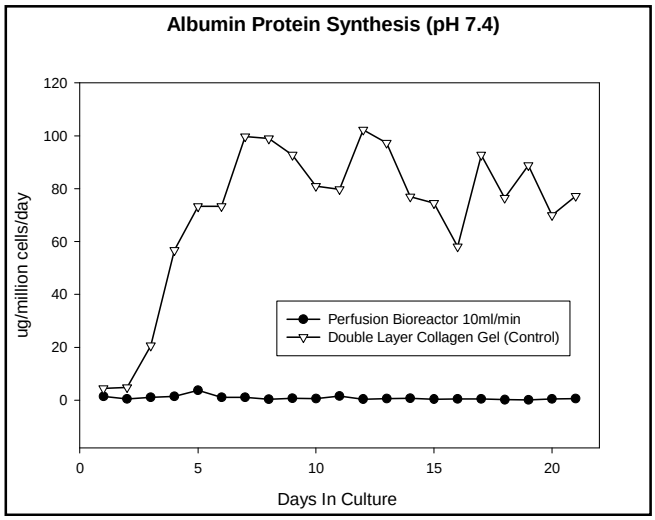

Figure 6: Rate of albumin synthesis produced by hepatoctyes cultured in first generation bioreactor system at a flow rate of 10 ml/min vs. double layer collagen gel control. Secretions rates for control were significantly higher when compared to perfusion bioreactor model.

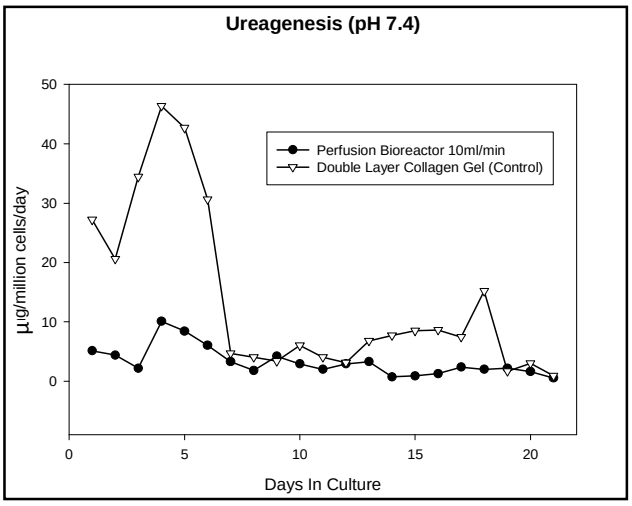

Figure 7: Rate of Ureagenesis produced by hepatocytes cultured in first generation bioreactor system at a flow rate of 10 ml/min vs. double layer collagen gel control. Secretion rates for control significantly outpaced those exhibited by the perfusion culture.

Mild hepatocyte aggregation was noticed at the conclusion of the culture. The extent of aggregation was confined to near the central port (Figure 8 A and B) and the oxygenated tubing (Figures 8 C and D). Aggregates in these regions assumed a liver-like morphology with noticeable variation in size and geometry. Aggregates located in close proximity to the central port were more numerous, contained an elevated aggregate mass and were more spherical in shape, in comparison to those near the oxygen tubing. In terms of viability, single cell hepatocytes exhibited no viability, while aggregated cells displayed signs of minimum viability at best. Viable cells within aggregates from both regions were observed, to a greater degree, on the periphery than the midsection. It was concluded that cells in this region of the aggregate died from necrosis due to oxygen and nutrient deprivation.

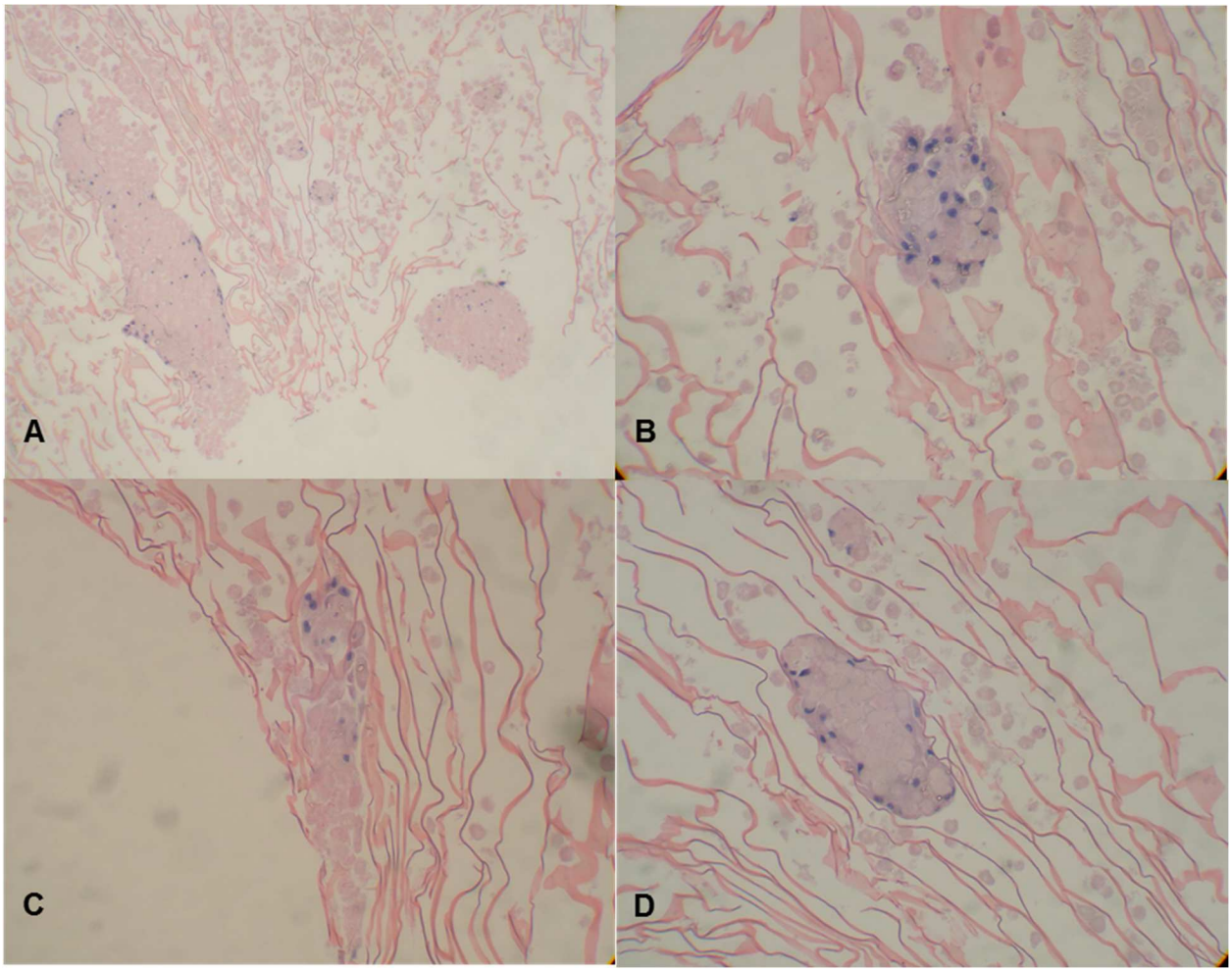

Figure 8: H&E staining of hepatocyte seeded in the high oxygenated regions of the scaffold post 21 days of culture in first generation bioreactor system. A & B) Cell aggregates at the central port, C & D) Cell aggregates adjacent to integrated oxygenation tubing. A & C were taken with a 5x objective magnification lens. B & D were taken with a 10x objective magnification lens.

Many difficulties, with the current bioreactor design, were encountered during multiple culture runs. These issues included, but were not limited to, scaffold reorientation during the cell seeding or culturing process. Adhesive seal breakage at reactor/luer and reservoir/luer connection points which lead to medium leakage and subsequent contamination. Lastly on multiple occasions uneven pressure throughout the perfusion circuit lead to medium overflow in the reactor chamber and the emptying of the reservoir which introduced bubbles into the

system. Because of these issues a second full experiment could not be reproduced and a second generation bioreactor design was implemented.

3.3.2(b) Second Generation Bioreactor Design and Results

The need for a second generation perfusion reactor system stemmed from multiple design flaws with its predecessor that hindered reproducible long-term cultures. Such flaws included scaffold reorientation during seeding and culture, and inefficient cell seeding due to cells being ejected from the top of the central port instead of being seeded into the scaffold. The reactor also experienced material and adhesive failure on several occasions at reactor cap and luer lock connection points respectively. This lead to pressure differentials and uneven fluid flow across both chambers. This flaw was due to sterilization process (autoclave) which ultimately lead to device failure during culture. To address these issues the second generation system was completely fabricated from heat tempered glass with the lure/tubing connections integrated into the cap (Figure 9). The scaffold reorientation issue was resolved by adding a basket to the perfusion chamber which immobilized the scaffold during the seeding and culture periods. A cap, used to seal the scaffold-perfusion tubing interface, mitigated cell pluming during the seeding process and back pressure fluid flow which previously allowed media to flow out of the central port versus through the scaffold. Lastly the reactor cap and chamber were fabricated to accommodate o-ring which created a secure seal between the parts and helped to maintain even pressure across the flow circuit. The geometry and flow circuit of the new system resembled that of its predecessor however the fluid capacity of the perfusion chamber was greater at 60 ml versus 45 ml.

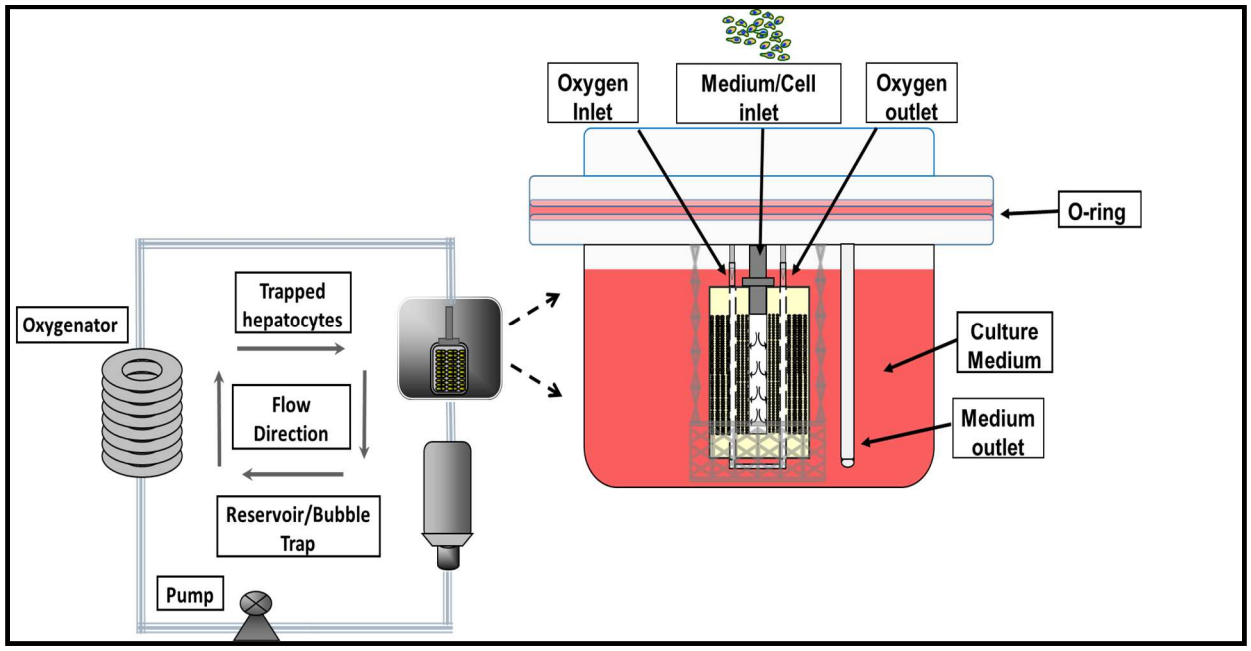

Figure 9: Schematic of second generation perfusion culture circuit with expanded, detailed schematic of the bioreactor chamber. The bioreactor image shows the fluid path from inlet to outlet, oxygenation tubing and, orientation and position of the scaffold with seeded hepatocytes.

This experiment sought to evaluate the efficacy of the second generation perfusion bioreactor system with our chitosan scaffold embedded with semipermeable silicone tubing for diffusion based oxygenation. Just as important was to asses if this complex better supports hepatocyte-specific functionality, morphology and viability throughout the culture period. In this trial the scaffold was seeded with 80 million hepatocytes and cultured for 7 days. The seeding for this trial slightly deviated from the previous in that direct oxygenation, via the integration silicone tubing, was implemented during the process. The seeding process did not exceed 15 minutes.

The results in Figure 10 showed that hepatocytes in the perfusion culture were able to sustain secretion over the duration of the 7 day culture period. The initial synthesis rate of the perfusion culture surpassed that of the control and reached its peak on the second day with a maximum output of 11.67 µg/million cells/day. However, over the next four days,

production rates displayed a consistent decline as compared to the control which saw value increase throughout the culture. The lowest rates for the bioreactor culture were seen on day 6 with values of 1.99 µg/million cells/day.

The results from the urea secretion assay (Figure 11) showed that hepatocytes cultured in the perfusion system had drastically lower function when compared to the control. Ureageneis, like albumin synthesis, exhibited higher synthesis rates at the onset of the culture when compared to the control (9.16 vs. 4.92 µg/million cells/day). However as the culture progressed urea secretion continued to decline with the lowest value of 1.62 µg/million cells/day on day 6.

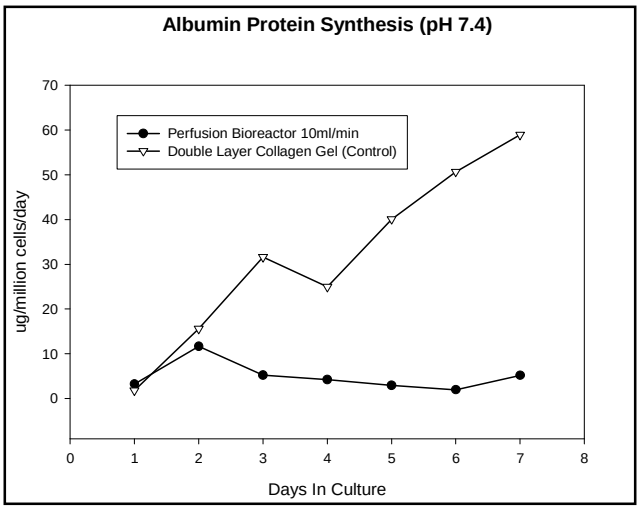

Figure 10: Rate of albumin synthesis produced by hepatoctyes cultured in the second generation bioreactor system at a flow rate of 10 ml/min vs. double layer collagen gel control. Secretions rates for control were significantly higher when compared to perfusion bioreactor model.

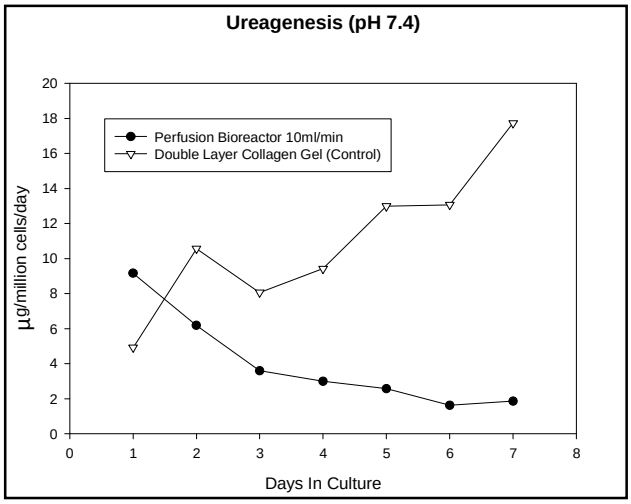

Figure 11: Rate of Ureagenesis produced by hepatocytes cultured in the second generation bioreactor system at a flow rate of 10 ml/min vs. double layer collagen gel control. Secretion rates for control significantly outpaced those exhibited by the perfusion culture.

At the end of the experiment histology showed mild to strong aggregation throughout the scaffold. Again, aggregates varied drastically in size and geometry with higher concentrations near the high oxygenated regions (i.e. Central port and the oxygenated tubing) (Figures 12 A and B, C and D). Viable cells in these areas were once more only noticed when only encapsulated in a collective mass. The position of active cells within the various aggregated showed no finite pattern given that functioning cells were observed at the boundary as well as in the aggregate interior. In contrast to the previous culture, aggregation was also observed in areas around the scaffold periphery. However, aggregates viewed at the construct perimeter revealed a smaller collective mass with little to no viability.

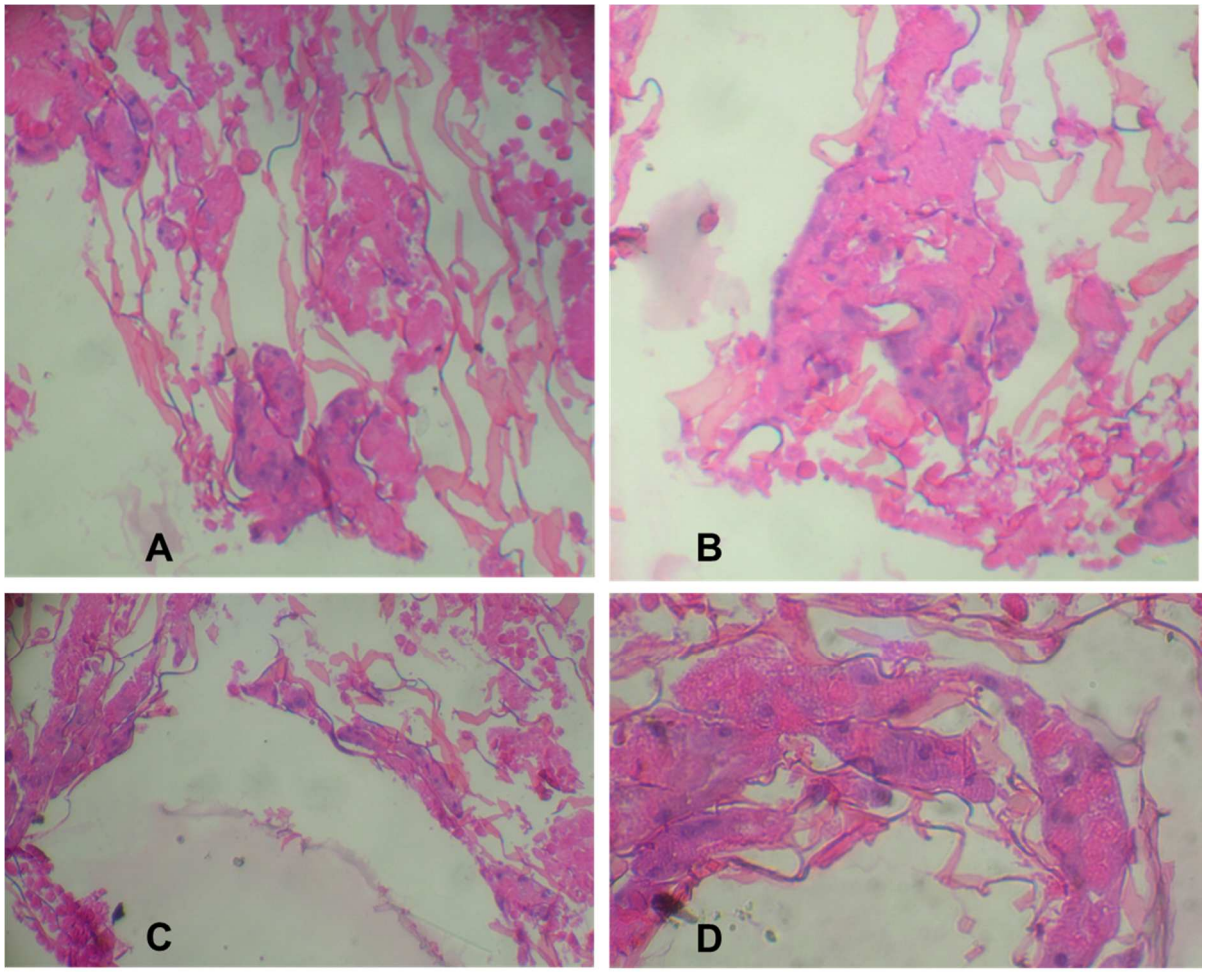

Figure 12: H&E staining of hepatocyte seeded in the high oxygenated regions of the scaffold post 7 days of culture in second generation bioreactor system. A & B) Cell aggregates at the central port. C & D) Cell aggregates adjacent to integrated oxygenation tubing. A & C were taken with a 5x objective magnification lens and B & D were taken with a 10x objective magnification lens.

Although the design modifications did improve hepatocyte phenotypic expression as exhibited by the increased metabolic and protein outputs. This system, like the first generation bioreactor, did experience multiple functional issues which hindered it performance during the seeding and culturing processes. Such problems included inefficient fluid recirculation through the perfusion circuit. This functional flaw lead to cells settling out of suspension on the chamber floor during the seeding and subsequent culture period. Being that the geometry and configuration of this system was analogous to its predecessor, these finds would suggest this was an issue with the first generation system too. Lastly the unsturdy

nature of the glass material made it quite challenging to handle and manipulate during both processes. This gave way to contamination during media exchange, compromised scaffold integrity during reactor system integration and, breakage while transporting and in storage. Due to these issues the reproduction of meaningful data was impossible and prompted a complete system redesign.

3.3.2(c) Third Generation Bioreactor Design and Results

The bioreactor/seeding chamber system in this iteration consisted of a 20cc chamber that served as the culture chamber and a 60cc chamber which served as a medium reservoir and bubble trap (Figures 13 and 14). In this iteration scaffold/reactor integration was accomplished quite easily by one person. In addition to being an entrance and egress for the direct oxygenation, the cannulas also served as anchor points for scaffold stabilization when attached to the embedded silicone tubing. Once attached and fully integrated into the system the scaffold was seated on and supported by a wire mesh. The cells, during the seeding process, and the path of media during the culture flowed in from the top of the culture chamber, into the scaffold and egressed through the bottom of the chamber. A stopcock was placed between the culture chamber outlet and media reservoir for samples acquisition and medium changeover. The flow circuit for this bioreactor resembled that of the previous two iterations. The complete system was autoclaved and assembled under sterile conditions before being used in seeding and culture applications.

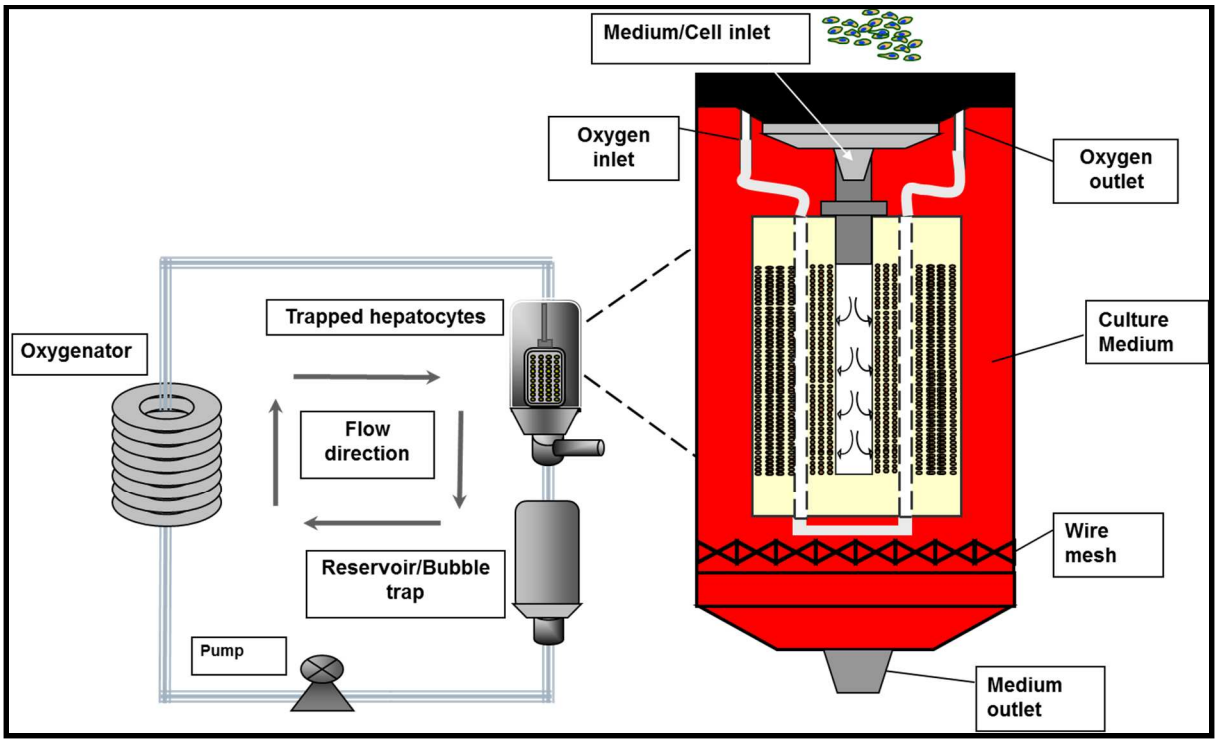

Figure 13: Schematic of complete third iteration perfusion culture circuit with expanded, detailed schematic of the bioreactor chamber. The bioreactor image shows the fluid path from inlet to outlet, oxygenation tubing and orientation of trapped hepatocytes.

Figure 14: Bioreactor culture setup showing cell seeded scaffold, medium reservoir and oxygenator

This experiment sought to evaluate the effect that direct oxygenation and convective transport, with the third generation bioreactor system, have on hepatic biochemical output, viability and morphology. In addition to the redesigned bioreactor chamber we also decreased pH of the culture media to ~7.2 by doubling the percent concentration of CO^2. The rationale behind this was to have the pH of the medium mimic portal venous conditions, thereby exposing the hepatocytes to a more in vivo-like milieu. In this trial the scaffolds were seeded with an average of 85 million hepatocytes and cultured for 7 days. The seeding process did not exceed 15 minutes.

The rates for protein synthesis for experiment are exhibited in Figure 15. In general the albumin rates for the plated control exceeded those of the perfusion reactor system. However rates, for the duration of bioreactor culture, did not fall below 4.17 ug/million cells/day. This was not seen in previous experiments. Additionally this perfusion culture kept pace with the static control until day three with average levels peaking on day four (9.58

ug/million cells/day). Thereafter the rates of production were considerably distant. It should also be noted that for the duration of the culture, day-to-day production levels exhibited only minor fluctuations versus a continuous downward trend seen in the previous cultures.

Mean urea synthesis for each day of culture can be seen in Figure 16. Although ureagenesis was measureable for each day, it seemed to follow the common trend of elevated production at the onset followed by a stable decline in output. The highest level of production, 11.797 and 10.17 µg/million cells/day, were seen on day 1 and 2 which did surpass the control values of 10.6 and 8.5 µg/million cells/day for both days respectively. Nonetheless, outputs during this run were consistently higher than those seen in the previous trial.

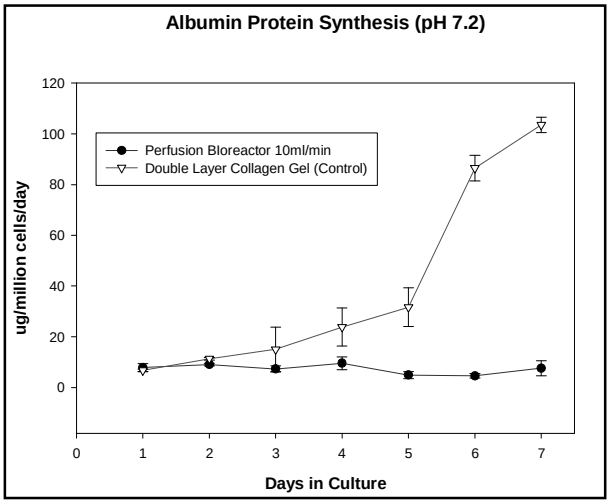

Figure 15: Rate of albumin synthesis produced by hepatoctyes cultured in third generation bioreactor system at a flow rate of 10 ml/min vs. double layer collagen gel control. Secretions rates for control were significantly higher when compared to perfusion bioreactor model. Error bars represent standard deviation of 2 replicate measurements.

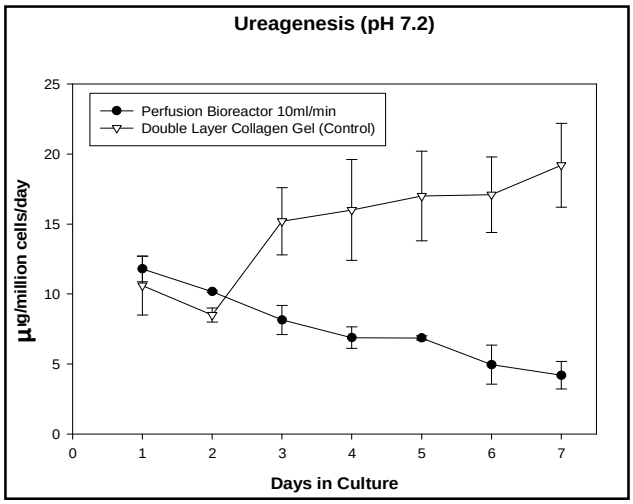

Figure 16: Rate of Ureagenesis produced by hepatocytes cultured in third generation bioreactor system at a flow rate of 10 ml/min vs. double layer collagen gel control. Secretion rates for control significantly outpaced those exhibited by the perfusion culture. Error bars represent standard deviation of 2 replicate measurements.

Upon experimental cessation, histological examination showed the cellular constituents were less likely to retain their single celled appearance, thus favoring intense aggregation in multiple scaffold regions. Heavy aggregation was yet more prominent in and around the high oxygenated areas (Figure 17 A to D). In contrast to prior trials, more aggregation was detected at the construct's outer radius. It was also observed that the cellular masses resembled an ellipsoid-like geometry as appose to an irregular configuration. Viable cells were found randomly dispersed within most aggregates located in the so called high oxygenated areas, however the level of functionality was not elucidated.

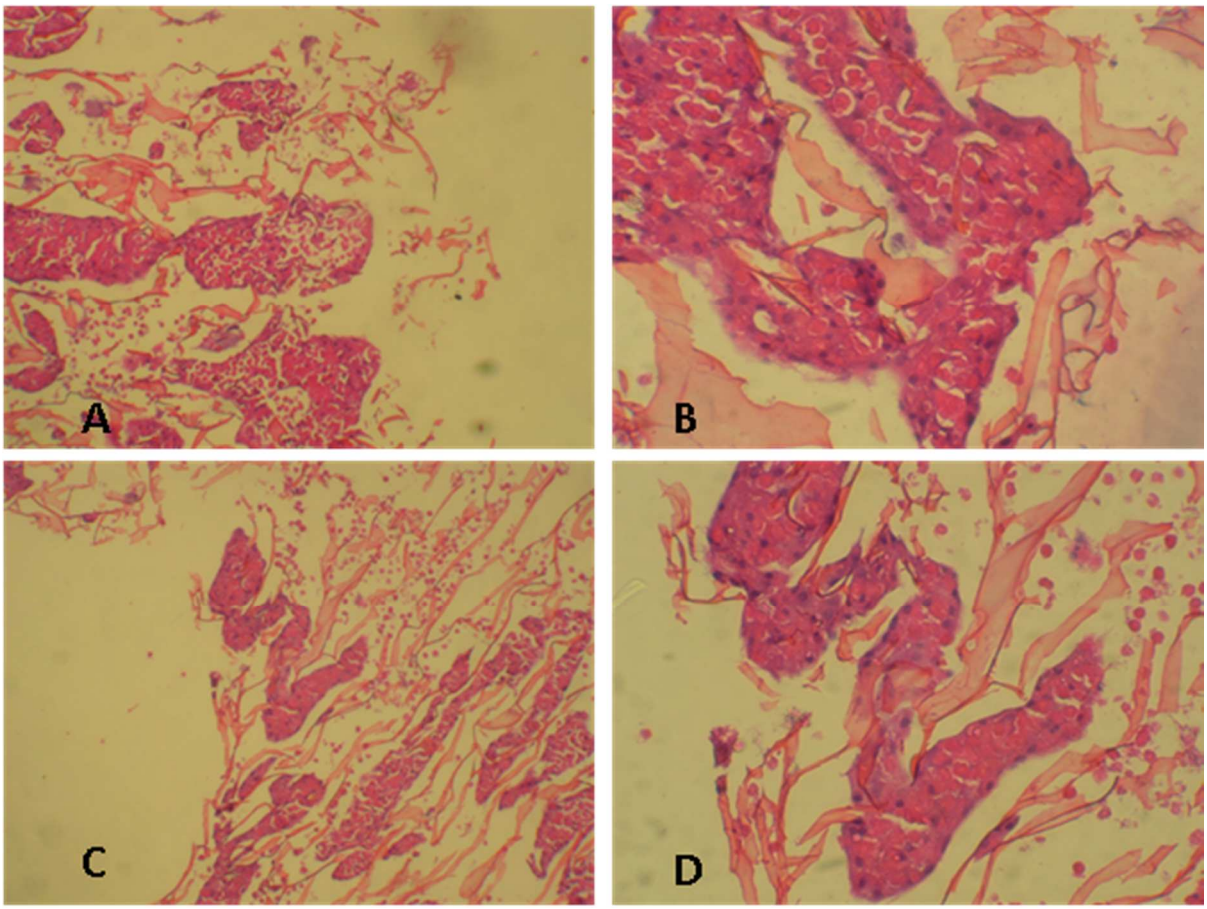

Figure 17: H&E staining of hepatocyte seeded in the high oxygenated regions of the scaffold post 7 days of culture in third generation bioreactor system. A & B) Cell aggregates at the central port, C & D) Cell aggregates adjacent to integrated oxygenation tubing. A & C were taken with a 5x objective magnification lens and B & D were taken with a 10x objective magnification lens.

In addition to measuring against a control, results from all three designs were plotted together and compared versus each day in culture. In order to accurately compare and draws conclusions across the three designs, results on days 8 to 21 from the first generation bioreactor were omitted from the figures. Figure 18 shows the compared results for albumin synthesis versus each day in culture for the three bioreactor systems. When compared it is quite evident that production levels from the first generation system pales in comparison to generation 2 and 3. Only do rates on day 5 for the first generation system exceed those from the other bioreactors. Similar trends in activity, for the most part, can be seen in the second

and third generation systems. Other than day 7 for both systems and day 4 for the third generation reactor – production levels increase on 1 and 2, and decrease thereafter.

A paired t-test was performed on all samples from each system; there was no statistically significant differences in albumin synthesis rates between hepatocytes cultured in the second and third generation systems. However there was a significant differences in generation 1 vs. 2 and generation 1 vs. 3 ($p > .05$).

Urea synthesis rates comparing each bioreactor over 7 days of culture are shown in Figure 19. Similar to the compared albumin rates, the third generation system, for ureagenesis, outperformed the other two systems. As expected when compared, trends for the second a third generation system are similar in that increased rates at the onset followed by declining expression as the culture progressed. The first generation reactor also followed a similar trajectory until day 4 where a spike in production is seen followed by a precipitous drop in activity. The reason for this increased synthesis is unclear.

A paired t-test was performed on all samples from each system; there was no statistically significant differences in albumin synthesis rates between hepatocytes cultured in the first versus second, and first versus third generation systems. However there was a significant differences in generation 2 vs. 3 reactors ($p > .05$).

Based on the results from the three different bioreactors, the third generation configuration was chosen as the system to be used to evaluate the effects that shear stress, generated by varying flow rates, has on hepatocyte viability, functionality and morphology.

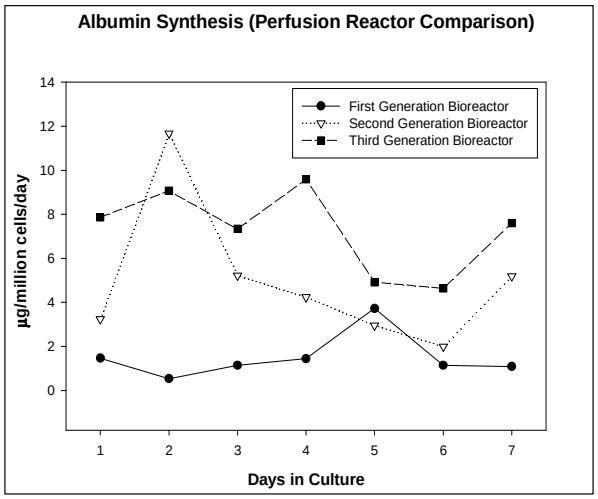

Figure 18: Albumin protein synthesis rates for hepatocytes cultured in first, second and third generation perfusion bioreactors. Days 8 to 21 were excluded from the first generation reactor culture to better compare the outputs rates between the different reactors.

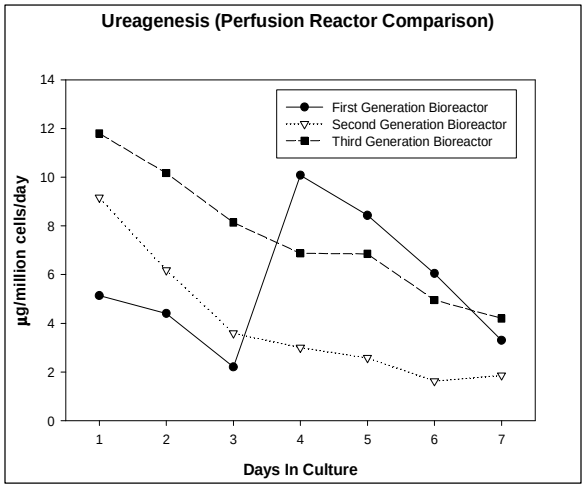

Figure 19: Ureagenesis rates for hepatocytes cultured in first, second and third generation perfusion bioreactors. Days 8 to 21 were excluded from the first generation reactor culture to better compare the outputs rates between the different reactors.

3.4 Discussion

The ultimate goal of hepatic or liver tissue engineering is to make an implantable, liver equivalent that is comparable to the native organ in size, cell density and functionality. Being that hepatocytes are highly aerobic, the science has been stymied due to the lack of a viable substrate that can bio-mimetically recapitulate the oxygen tension of the hepatic

microenvironment. Studies have attempted to satisfy this demand by using decelluarized livers as pre-vascularized scaffolds, designing bioreactors that minimize mass transfer limitation, hepatocyte encapsulation with VEC cells and oxygen carriers – to name a few. However results, although promising have not produce a viable solution.

The bi-phasic approach in this study was to; 1) investigate the synergistic effects of bulk convective mass transport (perfused oxygenated media) and capillary-like direct oxygenation on hepatocyte functionality and 2) design a perfusion bioreactor system that could accommodate both modes of oxygen delivery.

The level and trend of protein synthesis increased with each bioreactor design iteration. The greatest difference was noticeable between the first and second design iterations. There were several possible reasons for this. All of which are debatable, however it's believed that the two main contributors are; 1) the cap that created a seal at the scaffold inlet. This aided in directing flow through the structure thus minimizing reverse flow possibly caused by back pressure from the scaffold's tapered porous structure and cellular inhabitants. This facilitated better mass transfer of oxygenated media and nutrients, and removal of waste by-products. Lastly, this drastically reduced the seeding time and subsequent cell-to-ECM integration period which enabled the hepatocytes to reestablish their lost polarized state more quickly. 2) Implementing direct oxygenation during the seeding process. It has been shown that hepatocytes consume three-fold more oxygen during or shortly after the inoculation process [185]. Because of this it is not unreasonable to deduce that the superior functional capacity, was partially due to the support that the additional oxygen provided during the seeding process.

Similarly, there were two major modifications made to the third generation system that brought about a significant improvement in phenotypic expression and viability when compared to the previous generation. The pH of the culture media was acidified and reduced

to 7.2 which brought it more in-line with the average hepatic intracellular pH*i* of 7.16 [186]. Studies conducted by Halladay et. al [187] determined that the intracellular pH*i* of hepatocytes, in culture, equilibrates to that of its culture media, which in this case is 7.4. This could explain the difference in functionality because a more acidic intracellular pH has been shown to protect hepatocytes against the onset of cell death especially during time of ATP depletion [188]. Secondly the size and volume capacity of the culture chamber were drastically reduced and the chamber floor was slightly tapered at the outlet. The flat bottom and wide diameter design of the second generation reactor allowed thousands of cells to fall out of suspension and settle on the chamber floor either during seeding or culturing. The design proved to have inadequate media recirculation characteristics which could have led to zones of stagnant or "no" flow and pH imbalances in these areas. It was also suspected that waste by-products from viable cells or toxic substances released from dead cells that settled out and adversely affected the culture. This could have also contributed to the reduced performance from the first bioreactor system.

It was noticed that the urea and protein production from second and third generation bioreactor cultures surpassed that of the control on the first and/or second day. When taken into physiological context this makes perfect sense. Vinken et al. [189] and Hewitt et al. [190] both showed that hepatocytes, once disassociated from the liver capsule, become depolarized and when cultured on monolayers experience a progressive loss of liver-specific function and morphological abnormalities. It was not until the second collagen layer was added, which created a 3D substrate, that a markedly increase in function which observed in the control cultures. This trend was not seen in the first generation system. It is likely due to the cells being ejected from the top of central port instead being seeded into the scaffold during the seeding process. This contributed to the extended time period for cells outside of an ECM-like milieu (scaffold) and subsequent depressed cellular activity. It is also believed

that the extended seeding period, a consequence of the pluming effect, prolonged the exposure of the already entrapped cells to harmful hydrodynamic forces which are known to compromise hepatocyte functionality [191-193]. The harmful effects that prolonged exposure to excessive shear stress have on hepatocyte viability will be discussed in detail in a later chapter.

Advanced hepatocyte aggregation and the frequency of aggregation are two factors believed to have played a significant role in enhanced performance of reactors 2 & 3 over 1. In both systems increased levels of aggregation was observed in high oxygenated areas (inlet and adjacent to oxygen tubing). Viable hepatocytes, when clustered, can form gap junctions which are essential to hepatocyte function and survival as they provide pathways for communication between adjacent cells and regulate a number of liver-specific functions [194, 195]. Although not characterized in this study the lack of aggregation and gap junctions could be one reason, amongst several, as to why depressed functional activity was observed in reactor version 1. Additionally the cells on the periphery of these aggregates are most likely in contact with the scaffold and form integrin mediated adhesion anchor points – which too are need for cell survival through, but not limited to, the beta1-ILK-pAkt pathway [196, 197]. In addition to minimal O2 limitations, this would point to why more viable cells were localized around the aggregate periphery. It should be also noted that the same aggregation contributed to the subpar functional performance of these same two system. From the H&E stains the 2-dimension measurements of numerous aggregates are several hepatocytes in width and length. The unknown, but critical, characteristic that also complicates this even further is the height of each aggregate. Hepatocytes that are more than 1 to 3 mm away from an oxygen or nutrient source will succumb to mass transfer limitations [198]. This is evident as more hepatocytes in the interior of the aggregates are non-viable. Those that do survive will function at depressed levels. What exacerbates the issue is not being able to

remove non-viable cellular matter as this is known to release noxious degraded substances which could injure an otherwise healthy cells or accelerate the cell death machinery of a fragile adjacent cell.

Several reactor modifications contributed to the final bioreactor design. Such modifications, as stated in the previous section, enhanced the overall performance and sustainability of the hepatocytes in culture. The results from the third generation study were compared to data (not published) reported by a previous colleague who used a similar scaffold structure but different bioreactor design. Albumin production in both studies were maintained for the duration culture. In the study conducted by my colleague an average peak synthesis rate of 2.88 ug/million cells/day was reported on day 1 followed by a sharp decline. The average peak production rated for this study, as seen on day 5, exhibited a 22.5% (3.72 ug/million cells/day) increase over the aforementioned rate. The compared results clearly show that the bioreactor design in this study better supports hepatocyte-specific functionality and viability.

Metabolic Rates: Comparison with Oxygen Carrier Augmented Cultures

To date the lion's share of research dealing with oxygen supplementation for enhancing hepatocyte viability and metabolic performance has not focused on usage with 3D scaffolds for implantation modalities. Instead research efforts have utilized oxygen supplementation, in the way of perfluorocarbons (PFC) and hemoglobin-based O_2 carriers (HBOC), for extracorporeal liver devices or toxicity screening. It has been well documented that functional and morphological characteristics of hepatocytes, primary or cell lines, differ based on their in-vitro milieu, substrate/ECM or end-point therapeutics. Because of this it would be difficult to provide conclusive comparisons with the results from this study and the research done with O_2 medium supplements. However trends in metabolic activity and viability, in perfusion bioreactor cultures only, will be compared.

The only study, to date, that has evaluated a 3D scaffold construct for implantation purposes, in perfusion supplemented with PFC for enhanced oxygenation, exhibited significantly lower rates of albumin synthesis when converted and compared to this study's 3rd generation bioreactor setup. Shi and Coger [183] cultured HepG2/C3A hepatocytes in Gelfoam ® gelatin sponge (Pharmacia & Upjohn) for 48 hours and saw an average rate of 600 ng/million cells/day vs. 9.070 ug/million cells/day in this study. Although a true comparison cannot be made between the rat hepatocytes in this study and human HepG2/C3A cells it was surprising to see there was no significant difference between the PFC supplemented culture and control. This would suggest that PFC, in this instance, had no functional effect. In contrast to Kinasiewicz et al. [199] who saw increasing albumin synthesis from the onset of his bioreactor culture supplemented with PFC vs. the control. However it should be noted that the scaffold was composed of mineral fibers coated with type I collagen. This could be the pitfall of PFC emulsions in perfusion scaffold cultures. Unlike Hollow Fiber or 2D bioreactors, which allows unfettered flow of PFC emulsions through the extracapillary space or over a cellular monolayer respectively, the micro-porous structure of a scaffold could be too small or random thereby hindering PFC passage through its interior and nullifying its intended effect.

Perfluorocarbons, under the right experimental conditions can prove useful in enhancing liver-specific functionality. However from a true physiological perspective hemoglobin-based oxygen carries (HBOC) would seem to be the better alternative. HBOCs can increase oxygen solubility 70-fold over that of regular aqueous media vs. 10-fold for PFC. Moreover HBOCs exhibit a binding/dissociation curve similar to that of RBCs and they bind/release O_2 in ranges that are physiologically relevant [200].

Albumin synthesis did not correlate well with Sakai et. al [200] for rat hepatocytes cultured in perfusion with lipsome-encapsulated hemoglobin (LEH) supplemented media.

Although data is only reported for the first 24hr the culture exhibited rates of ~45 ug/10^5 cells/day vs. this study which reported 11.797 ug/million cells/day on day 1. In a follow-up study which extend the culture duration to 4 days, rates from adult rat hepatocytes exceeded 40 ug/million cells/day on day 2 of the culture. This value was halved for fetal rat hepatocytes under similar culture conditions. These results are contrary to conventional data in that fetal hepatocytes tend to be more functional than their adult counterparts. However LEH could have an adverse effect on less mature hepatocytes. Despite the gap in albumin protein synthesis there is a slight trend in that production decreases as the culture progresses. This being true-to-form form for most hepatocyte cultures.

Chen and Palmer [184], with a hollow fiber bioreactor reported rates ranging from 0.4 - 0.8 ug/hr/10^6 cells. Activity was maintained for at least 2 weeks. In this study (3rd generation reactor) hepatocytes seeded chitosan scaffold with direct and convective oxygenation were also able to maintain hepatic viability and protein synthesis for the duration of the culture albeit at lower levels (4.6 – 9.589 ug/10^6 cells/day). It is believed that the discrepancy in functionality is attributable to poor oxygen solubilization in aqueous media. It could also be further postulated that because auxiliary oxygen is being added to the system by way of the gas permeable tubing, there is a chance that excess oxygen could have caused mitochondrial free radical oxygen species formation and contributed to further loss of function.

When comparing the results from the two HBOC groups it's clear that Sakai et al outpaced the later even though both cultures contained a form of HBOC. This could be due to the fact that free hemoglobin (Hb) outside of red blood cells can be toxic because of high redox activity which can lead to reactive oxygen species generation and subsequent cellular damage [201]. The liposome-encapsulated Hb, the formulation used by the Sakai group, prevents free Hb leakage - which could account for increased functionality.

Studies that utilized hemoglobin-based oxygen carriers (HBOCs) or perfluorocarbons (PFC) did not evaluate ureagenesis as a metric for hepatic functionality. For this reason ureagenesis results from this study were not mentioned in this section.

3.5 Conclusion and Future Work

In this chapter the feasibility of improving the viability and hepatocellular functionality by optimizing the bioreactor design and culture conditions has been demonstrated. Factors such as media acidification, improved bioreactor design, and convective and direct oxygenation contributed to increased hepatic metabolic output. When compared to reported data from previous studies in our lab, the final system in this study exhibited better performance over a seven day culture period.

The next chapter will utilize computational fluid dynamic simulations to investigate the influence that varying inlet volumetric flow rates have on hepatocyte oxygen uptake, fluid flow characteristics around and between the entrapped cellular aggregates and shear stress imposed on these cells. The shear stress and oxygen concentration along the length of the scaffold will be elucidated. These parameters in conjunction with the flow characteristics will be used to better understand the scaffold/cellular micro-environment under perfusion. It is believed that achieving and understanding this information will help to further optimize our culture conditions and improve hepatocyte functionality.

CHAPTER FOUR: COMPUTATIONAL FLUID DYNAMICS ASSESSMENT OF HOW MASS FLOW RATES AFFECT FLUID FLOW PROFILES, SHEAR STRESS AND OXYGEN CONSUMPTION IN A CELL-INFUSED MICROENVIRONMENT

4.1 Introduction

There are many factors that have to be addressed before an “off the shelf” tissue engineered construct can be successfully seeded with the appropriate cell type configuration, cultured under optimal conditions and seamlessly integrated into the human body. Such factors include bioreactor and scaffold design, scaffold location, initial flow rates and mass transport attributes [202]. These factors have been explored as a “Black box” with random assumptions and iteratively-derived empirical data which has proved to be very costly, time consuming and mentally taxing. More importantly such approaches have led to inconclusive or incorrect results that inevitably lead to in-vitro graft and/or host/graft failure. Over the last two to three decades researchers have looked to computational fluid dynamics (CFD) or computer-aided mathematical models as a tools to help guide the discovery process by addressing and subsequently mitigating the number of unknowns pre- in-vitro. The advantage that CFD offers is that it allows for the prediction, comprehension and characterization of certain phenomenon (i.e. fluid flow, consumption/secretion kinetics and hydrodynamic stress profiles, spatial and temporal cell seeding distribution, and volumetric and mass flow rate estimates) that are occurring within and around the scaffold/bioreactor complex at the macroscopic and microscopic scales.

One of the earlier publications that utilized computational fluid dynamics as a precursor to their experimental works was by Block and Talalla [203]. Although rudimentary in comparison to today’s CFD models they, with a set of seven assumptions, were able to

further their understanding of derangements of cerebral spinal fluid (CSF) dynamics which helped to shed light on symptomatic low-pressure hydrocephalic states in man. Since then CFD and computational biological modeling has been integrated into just about every facet of basic medical research. It been utilized in research fields such as tracheobronchial air flow/particulate transport motion [204, 205], vascular remodeling [206, 207], hemodynamics [208-210] and tissue engineering [211-213]. Recently Guyot et. al [214] recently utilized CFD to elucidate the shear stress magnitude and distribution along the fluid/neo-tissue boundary during growth. The 21-day experimental validation culture was carried out with Ti6Al4V Scaffolds seeded with Human Periost-Derived Cells (hPDCs). From their work they were able to discern that there is a significant difference in shear stress imposed on the cells at the fluid interphase vs that seen on cells within their porous construct. They were also able to elucidate how pore geometry affected that magnitude of mechanical stress during culture and neo-tissue formation.

Hepatic tissue engineering has benefited tremendously from computational fluid dynamic and computer aided mathematical modeling. These simulation tools have proven to be a critical adjunctive measure to empirical data generation for predicting bio-physiological phenomena such as hydrodynamic stress [215, 216], metabolic function [215, 217], the effects of oxygen carries on oxygen transport [218-220] and oxygen consumption [221-224] within the scaffold/cellular microenvironment in invitro and invivo settings. Debbaut et al. developed a numerical and CFD model to simulate complex micro-circulatory blood perfusion from the macroscopic level to the sinusoidal terminal unit in a healthy liver. Using vascular corrosion casting with high resolution micro-CT, a 3D image-based of the liver vascular was rendered and used to study fluid mechanical properties during sinusoidal perfusion. From this unique model of the of the lobule unit which had the *z*-axis parallel to the liver central vein they were able to ascertain pressure, flow resistance and permeability tensor differences in

the *z*-direction from those in the *r* and *θ*-directions. From the study it was concluded that the immediate result of these findings was that the sinusoidal circulation behaves in an anisotropic manner. Moreover they also pointed out the deficiency in their model in that it the shear stress levels generated did not fully reflect that of what is seen in vivo. Conversely, they more resemble what is seen from a machine perfused organ before transplantation [216] . This work was followed up by Peters et. al [225] who used the same vascular corrosion casting with high resolution micro-CT and computational fluid dynamics to study the micro-perfusion and permeability in a cirrhotic liver. They were able to show that anisotropic permeability within a cirrhotic liver was highest in the direction parallel to the central vein and lower values were in the radial and circumferential direction. Their macro-circulation model also indicated that regenerative nodules within the cirrhotic liver increases intrahepatic vascular resistance beyond 65 vol.%. of the regenerative nodules.

Despite the advances that CFD and computer aid numerical modeling have made toward understanding metabolic and fluid flow phemena within the scaffold/cellular microenvironment the internal flow, hydrodynamic and oxygen consumption profiles of certain micro-structures impregnated with single and multi-cellular masses still lacks a certain level of understanding. With the use of well-defined engineering principles, we are able to approximate certain flow characteristics at localized regions within our porous construct. What is also not understood in our cultures is how the change in internal flow rates at the inlet, which affects oxygen consumption and the mechanical stress imposed on the cells, correlates with overall cell health based on experimentally derived parameters. To gain insight into the in vitro hydrodynamic stress and oxygen concentration distribution, and fluidic microenvironment, in this study a small segment of the cell seeded porous construct was designed and meshed, and simulated with the ANSYS GAMBIT and FLUENT software packages respectively. In this model oxygen consumption/availability, shear stress and fluid

flow were analyzed at varying inlet flow rates. The parameters for hepatocyte oxygen consumption (VM and KM) and culture medium pO2 parameters were obtained from literature values that were experimentally derived. To simplify the simulation the culture medium took on the characteristics of water and modeled as an incompressible, isothermal, Newtonian fluid.

4.2 Materials and Methods

4.2.1 Computer Model of Hepatocyte-Infused Porous Scaffold

The inspiration and thought process that brought about the geometry that simulated the multi-cellular aggregated infused interconnected porous structure can be seen in Figure 20. The geometry modeling and grid generation (i.e meshing) were both conducted with the software package GAMBIT (ANSYS, Concord MA). In addition to fluid flow and hydrodynamic stress profiling, part of the rationale behind the geometry was understand how oxygen consumption of the cells adjacent to the central port affected oxygen availability and subsequent functionality and viability, of cell downstream without the support of direct oxygen supplied by the impregnated gas permeable tubing. Essentially the simulation and generated data only pertains to cells positioned between and not assisted by direct oxygenation facilitated by the gas permeable tubing. The modeling and mesh generation could have been expanded to accommodate the full scale scaffold however to reduce computation time to convergence and computing expenditures the geometry was reduced to the interconnectivity, cell seeding and fluid trajectory that stems from a single pore in the scaffold's central port region to its outlet at the scaffold's perimeter.

The pore size corresponding to the central port was 400μm. The height and length of the porous geometry was 100um and .75cm respectively. The size of the inlet pore and, the pore height and length were derived from the actual scaffolds used in the experimental

bioreactor cultures. The conditioned medium that we assumed to be equilibrated to the gaseous atmosphere created by the oxygenator entered the structure through the single pore inlet. A constant normal velocity profile was set as the boundary condition at the fluid inlet. The oxygen concentration at the pore inlet was also set to be constant at 21 mol/m^3. The medium perfused through the porous zones while making contact with every aggregate on all sides. The culture medium exited the porous geometry through 64 significantly smaller pores all of which have an “outflow” boundary condition set at zero pressure.

The tapered pores structure or channels from the inlet port to the scaffold periphery was created by the sequential bifurcation of contiguous segments within the scaffold interior. Each bifurcation doubled the number of pores in the subsequent segment. Spheroids were incorporated into each pore to simulate multiple aggregated cell masses. Each aggregate was design to occupy a significant majority of the pore volume. The geometry was meshed using a tetrahedral protocol and “WALL” boundary conditions were assigned to the pore walls and to the outer surface of each spheroid. The “WALL” boundary condition for the spheroids and pore walls were also coupled with non-slip boundary conditions at the solid-fluid interphase. The inlet mass flow rates were determined by experimental volumetric flow rates and the assumption of equal-distribution of flow between each pore of the central port. Lastly, the simulation was conducted using single precision, segregated solver.

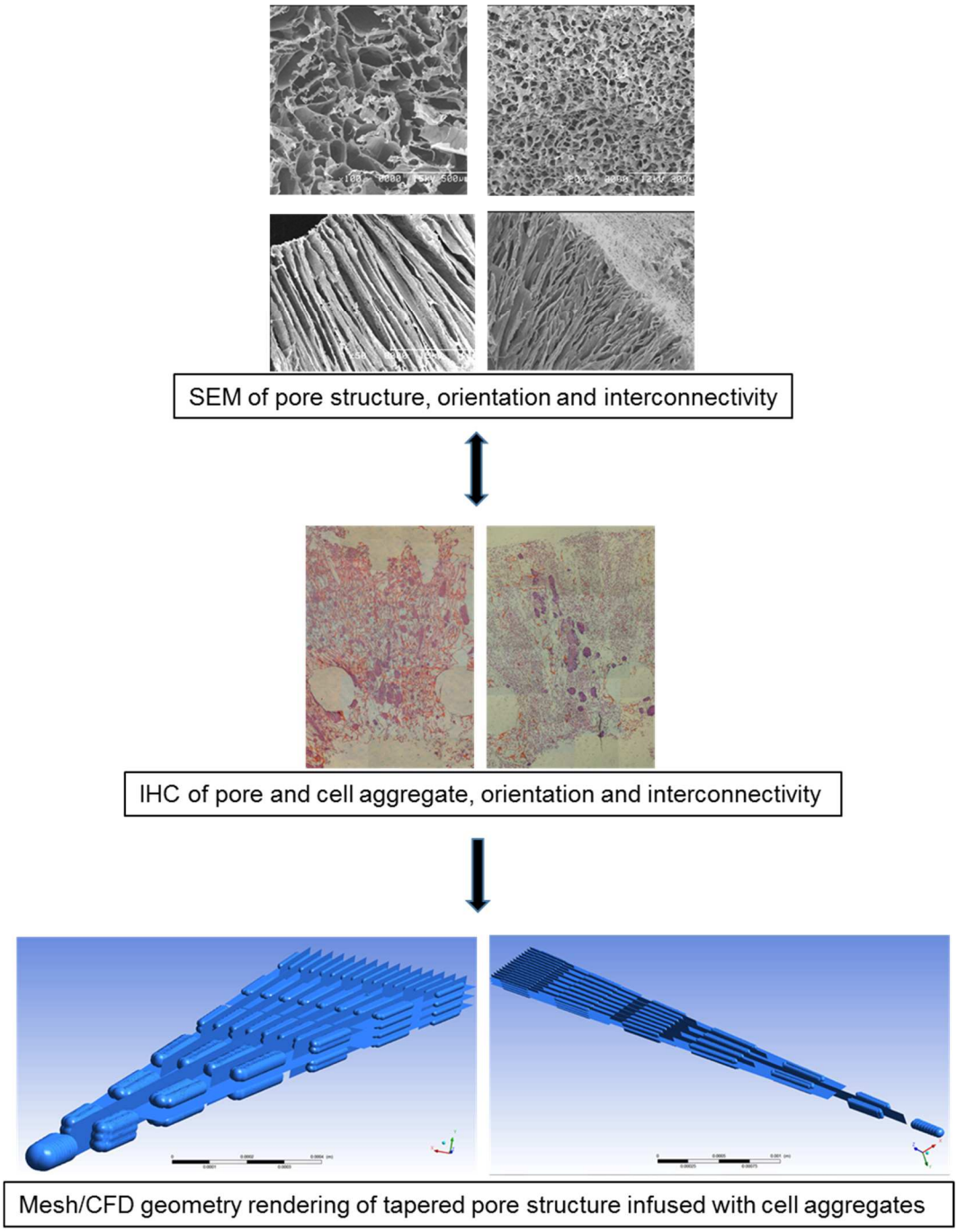

Figure 20: Rationale, workflow and final rendering for cell-infused pore structure for CFD simulations

4.2.2 Modeling Fluid Flow

To simulate fluid flow, the commercial computational fluid dynamic (CFD) software pack Fluent 15.0 (ANSYS, Concord MA) was implemented to solve the velocity field by using the Navier-Stokes equation for a incompressible, isothermal Newtonian fluid. Equations 1 and 2 represent the mass and momentum conservation equations.

$$\frac{\partial \rho}{\partial t} + \nabla \cdot (\rho \vec{v}) = 0 \quad (1)$$

$$\frac{\partial}{\partial t}(\rho \vec{v}) + \nabla \cdot (\rho \vec{v}\vec{v}) = -\nabla p + \nabla \cdot (\mathrm{T}) + \rho \vec{g} + \vec{F} \quad (2)$$

Where ρ denotes density of the culture medium, $\vec{v}$ is the velocity field and p represents pressure. Additionally, $\rho \vec{g}$ is the gravitational body force and all the external body forces on the volume are represented by $\vec{F}$. For Newtonian fluids a component of the latter equation includes the stress tensor T.

The stress tensor T is given by:

$$T = \mu \left[(\nabla \vec{v} + \nabla \vec{v}^{t}) - \frac{2}{3} \nabla \cdot \vec{v} I \right] \quad (3)$$

Where μ is the molecular viscosity and I is the unit tensor. Lastly the second term within the brackets represents the effect of volume dilation.

The shear stress on the surface of each aggregate structure is dependent on the density and viscosity of the culture medium. In general shear stress is proportional to the rate of change of the shear strain S_{xy}, with the components of tensor S_{xy} given by the equation below, and u_{xy} components of the velocity vector.

$$S_{xy} = \mu \cdot \left(\frac{\partial u_x}{\partial y} + \frac{\partial u_y}{\partial x} \right) \quad (4)$$

However in the Ansys Fluent solver when the mesh is fine enough to resolve the viscosity-dominated sublayer, the wall shear stress is obtained from the laminar stress-strain relationship:

$$\frac{u}{u_T} = \frac{\rho u_T y}{\mu} \quad (5)$$

If the mesh cannot resolve the viscous sublayer (i.e. too coarse) then the law-of-the-wall is employed:

$$\frac{u}{u_T} = \frac{1}{k} \ln E \left(\frac{\rho u_T y}{\mu}\right) \quad (6)$$

Where u is the velocity parallel to the wall, u_T is the shear velocity, y is the distance from the wall, k is the von Karman constant (.4187), and $E = 9.793$. The culture media was modeled with a density of 1000 kg/cm^3 and a dynamic viscosity of 1x10^{-3} kgm^{-1}s^{-1}. The inlet mass flow rates were applied at the entrance of the porous structure. The outlet boundary condition was set to a zero pressure outflow and the barriers that made up the interconnected porous structure, including top, bottom and side enclosures, and the spheroids that simulated the hepatocyte aggregates were give the designated boundary condition of "no-slip" walls.

4.2.3 Modeling Species (Oxygen) Transport and Consumption

To simulate species/oxygen transport and uptake, Fluent solved the steady-state equations (Eq. 7 and Eq. 8) for the convection and diffusion processes that involves dissolved oxygen in our media.

$$\frac{\partial}{\partial t}(\rho Yn) + \nabla \cdot (\rho \vec{v} Yn) = -\nabla \cdot \vec{J}n + Rn \quad (7)$$

where

$$\vec{J}n = -\rho Dn,m \, (\nabla Yn) \quad (8)$$

In Equation 7, Yn represents that local mass fraction of each species n. Rn is the net rate of production of species n by chemical reaction. $\vec{J}n$ in Equation 8 represents the diffusion flux for species n and Dn,m is the mass diffusion coefficient for species n. In the simulations species consumption only occurred at the surface of the "WALL" boundary conditions that were assigned to the surfaces that formed the cell aggregates. The ANSYS Fluent software

models this type of reaction as a "wall surface reaction" which is governed by the general rth equation:

$$\sum_{i=1}^{N_g} g'_{i,r}\, G_i \;+\; \sum_{i=1}^{N_b} b'_{i,r}\, B_i \;+\; \sum_{i=1}^{N_s} s'_{i,r}\, S_i \;\overset{K_r}{\Leftrightarrow}\; \sum_{i=1}^{N_g} g''_{i,r}\, G_i \;+\; \sum_{i=1}^{N_b} b''_{i,r}\, B_i \;+\; \sum_{i=1}^{N_s} s''_{i,r}\, S_i \quad (9)$$

where G_i, B_i and S_i represent the gas phase species, the bulk solid species and the surface absorbed (or site) species, respectively. N_g, N_b, N_s are the total number of these species. $g'_{i,r}$, $b'_{i,r}$, $s'_{i,r}$ are the stoichiometric coefficients for each reactant species *I*, and $g''_{i,r}$, $b''_{i,r}$, $s''_{i,r}$ are the stoichiometric coefficients for each product species *i*. K_r is the overall forward reaction rate constant. In Equation 9 only the species involved as reactants or products will have non-zero stoichiometric coefficients. All species not involved in the reaction will drop out of the equations.

Oxygen consumption by the structures that simulated primary rat hepatocyte aggregates inside the porous construct was modeled by the additional user-defined function (UDF) term based on Michaelis-Menten kinetics (Eq. 10). The UDF was only implemented on the surface "WALLS" of the aggregate structures.

$$\frac{dS}{dt} = -\frac{Vmax \bullet C_{O_2}}{Km + C_{O_2}}\,(N_{cell}) \quad / \text{(condition - } C_{O_2} > F_{O_2}) \qquad (10)$$

where V_{max} is the maximum volumetric oxygen consumption (mol • s^{-1} • $cell^{-1}$), Km is the Michealis-menten constant corresponding to the oxygen concentration at which consumption drops to half of its maximum, N_{cell} is the number of cells per aggregate and $\frac{dS}{dt}$ is oxygen flux at the cell surface.

To realistically describe the oxygen consumption and hydrodynamic conditions within the scaffold/bioreactor complex, several key elements and assumptions had to be factored into the CFD simulation:

i. Equal flow and cell seeding distribution through each inlet pore in the experimental scaffold's central port region.

ii. Cell number (N_{cell}) per aggregate in each segment of the structure was determined by the percent volume of the segment in relation to the volume of the whole structure divided by the number of aggregates in the segment.

iii. Inlet pore velocity for CFD simulation is determined by the volumetric flow rate at the central port (experimental) divided by the number of pores in the central port region.

iv. At any given point along the length of the scaffold $C_{O_2} > F_{O_2}$ (2 x 10^{-2} mol/m^3) which is the concentration at which hepatocytes are deemed non-functional due to hypoxia [170]

The parameters used in the simulations are experimentally derived from rat hepatocytes. These parameters can be seen in the Table 1.

Table 1: Parameters for computational fluid dynamics (CFD) model at 37℃

Parameter	Symbol	Value	Units	Ref.
Inlet O_2 concentration	S_{O_2} in	.21	mol/L	[226-228]
O_2 diffusivity in aqueous media	D $O_{2,}$ *aq*	$3x10^{-9}$	m^2/s	[226, 227, 229]
Medium Viscousity (water)	μ	$1.0x10^{-3}$	$Kgm^{-1}s^{-1}$	
Medium Density	ρ	1,000	kgm^{-3}	
Max Hepatocyte Consumption Rate	V_{max}	$4.8x10^{-17}$	$mol•s^{-1}•cell^{-1}$	[230]
Michaelis-Menten Constant	K_m	$7.39x10^{-3}$	mol/L	[222]
Bioreactor Inlet Flow Rates	n/a	5, 10, 15	mL/min	n/a

Table 2. Mesh element parameters for the number of cells and cell aggregates per pore segment

Pore segment	# of mesh elements	Vol. of Elements	Aggregate surface area	# of aggregates per segment	# of cells per aggregate
1	3910	1.99E-13	1.03E-07	1	343
2	6628	1.98E-13	1.18E-07	2	196
3	5000	2.27E-13	1.09E-07	4	118
4	3912	1.85E-13	9.13E-08	8	95
5	3746	1.11E-13	5.86E-08	16	43
6	2994	8.30E-14	4.18E-08	32	20
7	1186	3.61E-14	1.84E-08	64	9

4.2.4 CFD Simulation Workflow

Each computational fluid dynamic simulation was carried out in two stages. The first stage involved solving equations 1 and 2 which are the mass and momentum conservation equations respectively. From here we were able to assess the hydrodynamic stress distribution and fluid flow profile with the pore structure. Simulations were conducted at the mass flow rate values of 3.68×10^{-6} g/s, 6.737×10^{-6} g/s and 1.01×10^{-6} g/s which correspond to the experimental culture flow rate values of 5, 10 and 15 ml/min respectively at the scaffold central port inlet.

After the solutions for the stead-state equations were obtained, a second simulation was run to solve for the species transport and Michaelis Menten equations. All three simulations assumed that the full scaffold was seeded with 1×10^8 cells and these cells were distributed evenly into each pore within the scaffold's central port. Table 2. provides a list of the detailed parameters that were utilized in the oxygen consumption simulations. This segment of the simulation provided information about the oxygen uptake and distribution along the length of

pore structure. This simulation was conducted for each experimental flow rate. It should be noted that only shear stress data was generated for $1.47x10^{-5}$ g/s and $1.84x10^{-6}$ g/s which corresponds to the central port inlet volumetric flow rate of 20 ml/min and 25 ml/min. The reason for this decision was our mass transport expectations were exceeded at the lower flow rates and the shear stress thresholds at these volumetric flow rates were surpassed. In total higher volumetric flow rates would extend the dynamic range of higher concentrated oxygen supplied to the cells, however these higher flow rates imposed shear stresses that would render the cell non-viable and not able to take advantage of the oxygenated environment.

4.3 Results

4.3.1 Computational Fluid Dynamics Results for Fluid Flow and Velocity Profile

Figures 21 to 23 shows and compares the results from the steady-state simulation results for the cell-infused tapered pore construct with the inlet mass flow rates of $3.36x10^{-6}$ g/s, $6.737x10^{-6}$ g/s and $1.01x10^{-5}$ g/s, which corresponds to the experimental volumetric flow rates of 5 ml/min, 10 ml/min and 15 ml/min, respectively at the scaffold's central port inlet. The arrows illustrate the fluid flow profile and velocity vector distribution. The side, top, bottom and internal pore walls were omitted from the images to better display the transitional differences in vector magnitude along the length of the structure. Fluid velocity is illustrated by color with red denoting areas of high velocity and dark blue for areas of zero flow. Also images of porous structure were taken only from the first three aggregate segments as these were the regions of high fluid flow. The maximum and minimum velocities for 5, 10 and 15 ml/min were .0007 - .0028 ft/s, .0010 to .0040 ft/s, and .0010 to .0040 ft/s respectively. High velocity flow for each flow rate was typically in the area near the inlet of the pore structure and progressively decreased as flow moved towards the outlet. However in the tight spaces between the cellular aggregates and the pore walls there are abrupt changes in fluid velocity. In these areas the fluid velocity doubles in comparison to scaffold segments without

aggregates. This was consistent for each simulated condition. In all simulated conditions flow was not halted based on the pore volume occupied by the aggregates. Lastly, the simulation showed that fluid recirculation around or after each aggregate segment was not an issue.

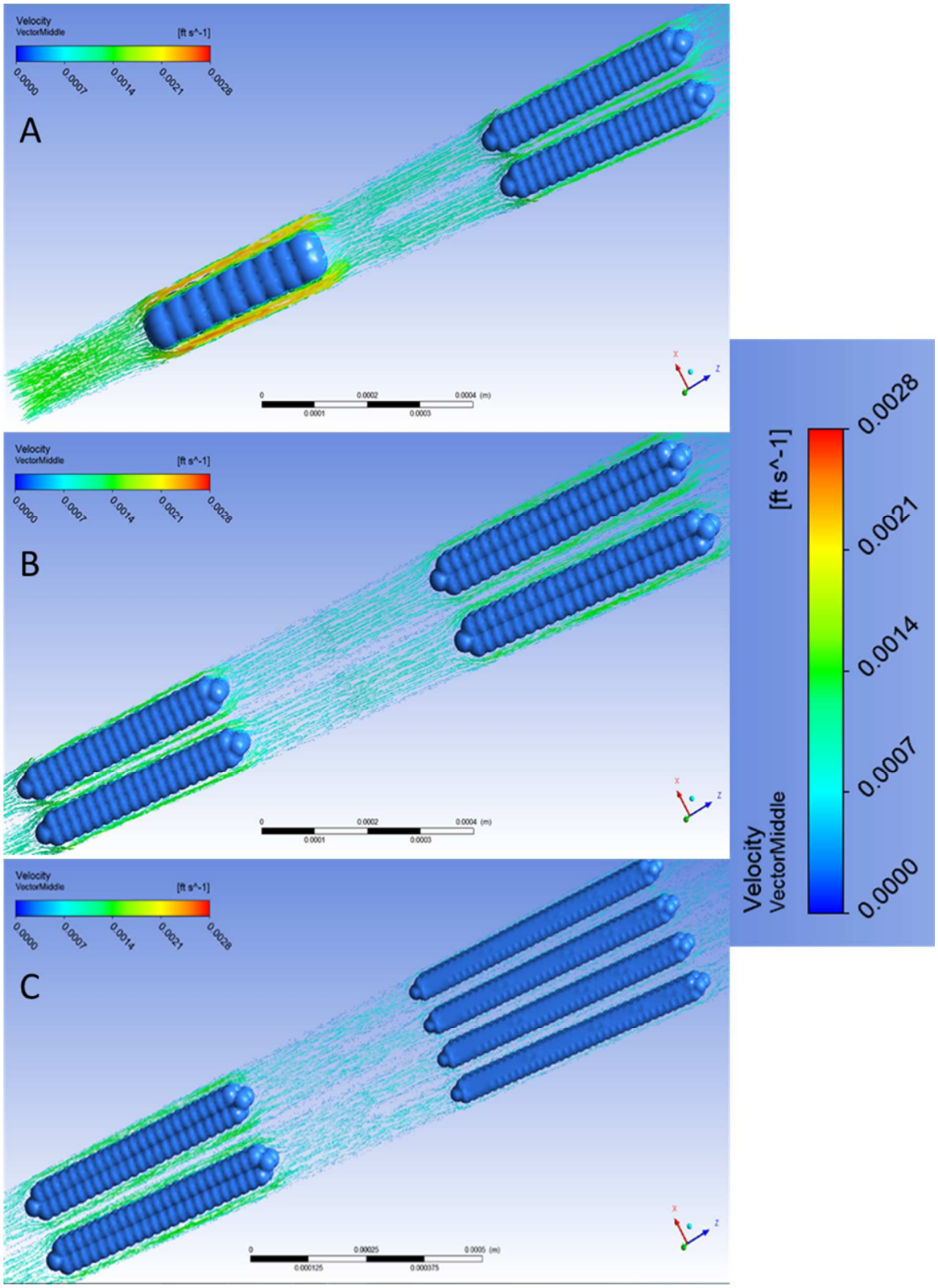

Figure 21: Velocity vector distribution and fluid flow profile through the first 4 bifurcating segments from the pore port inlet for the mass rate of 3.36 x10^{-6} g/s, which corresponds to the volumetric flow rate of 5 ml/min at the scaffold's central port inlet

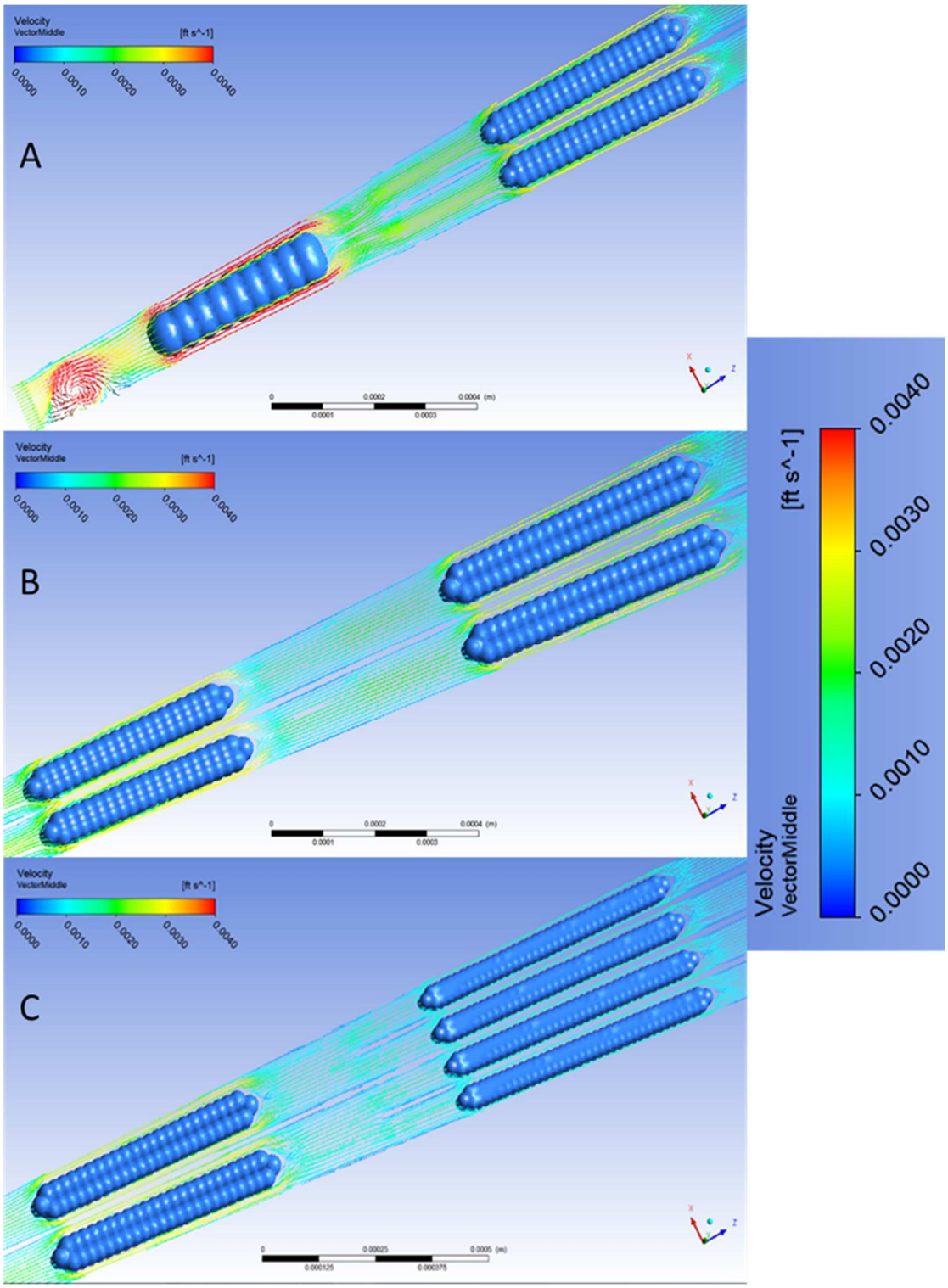

Figure 22: Velocity vector distribution and fluid flow profile through the first 4 bifurcating segments from the pore port inlet for the mass rate of 6.737 x10^{-6} g/s, which corresponds to the volumetric flow rate of 10 ml/min at the scaffold's central port inlet

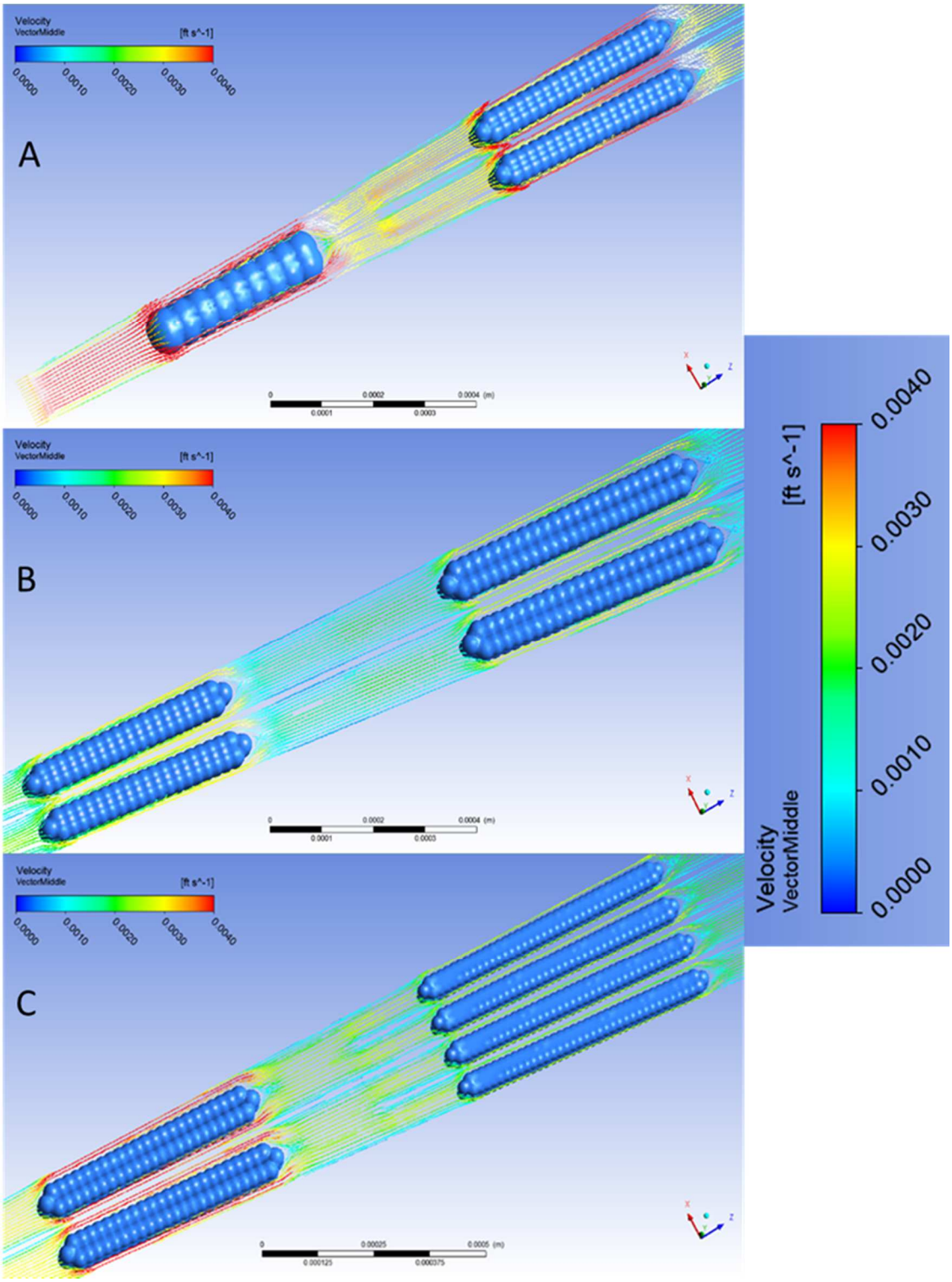

Figure 23: Velocity vector distribution and fluid flow profile through the first 4 bifurcating segments from the pore port inlet for the mass rate of 1.01 x10^{-5} g/s, which corresponds to the volumetric flow rate of 15 ml/min at the scaffold's central port inlet

4.3.2 Computational Fluid Dynamics Results for Wall Shear Stress

Hepatocyte function, in perfusion cultures, is negatively modulated by the presence of excessive shear stress. In the simulation we assessed shear stresses for values that correspond to experimental flow rates 5, 10 and 15 ml/min at the central port inlet. Since shear stress is directly related flow velocities, in general shear stress at the wall intensified as the inlet flow rate increased for each simulation. However within each simulation, the shear distribution from inlet to outlet were inconsistent. We saw that elevated shear stresses were located at the pore inlet and decreased somewhat uniformly towards the outlet. This can be attributed to the reduction of the flow caused by tapered bifurcated segments of the pore geometry. The shear stress values exhibited in Figures 24 to 26, for each flow rate ranged from .21 Pa (2.1 dynes/cm^2) to .017 Pa (.17 dynes/cm^2) at 5ml/min, .027 Pa (2.7 dynes/cm^2) to .35 Pa (3.5 dynes/cm^2) for 10 ml/min and .45 Pa (4.5 dynes/cm^2) to .035 Pa (.35 dynes/cm^2) at 15ml/min. The side, top and bottom walls of the pore structure were omitted from the shear stress images to better display the contour gradients. It should be also noted that the wall shear stress values imposed on the aggregate surfaces, in all three simulations, did not exceed the threshold value for compromised cell functional as put forth by Tilles et. al at 5 dynes/cm2 [192]. This would indicate that the cells, at least on the outer surface of each aggregate, were not adversely impacted by the shear stress generated by the experimental flow conditions.

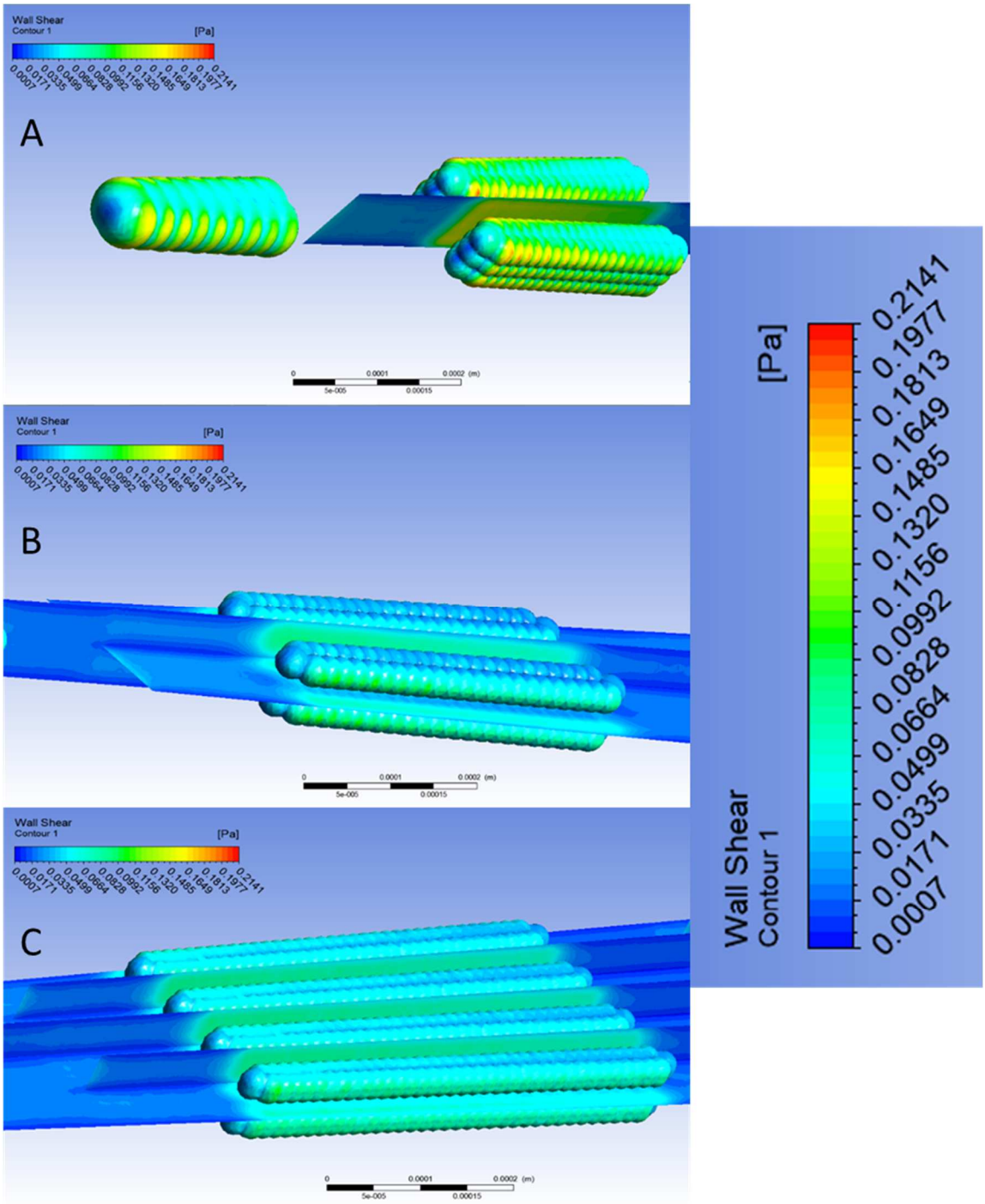

Figure 24: Contour plot of flow induced shear stress distribution imposed on cell aggregate surfaces through the first 4 bifurcating segments from the pore inlet along the axial length of the porous construct. The simulation was conducted at a mass flow rate of 3.36 x10^{-6} g/s which corresponds to the experimental volumetric flow rate of 5 ml/min at scaffold central port inlet.

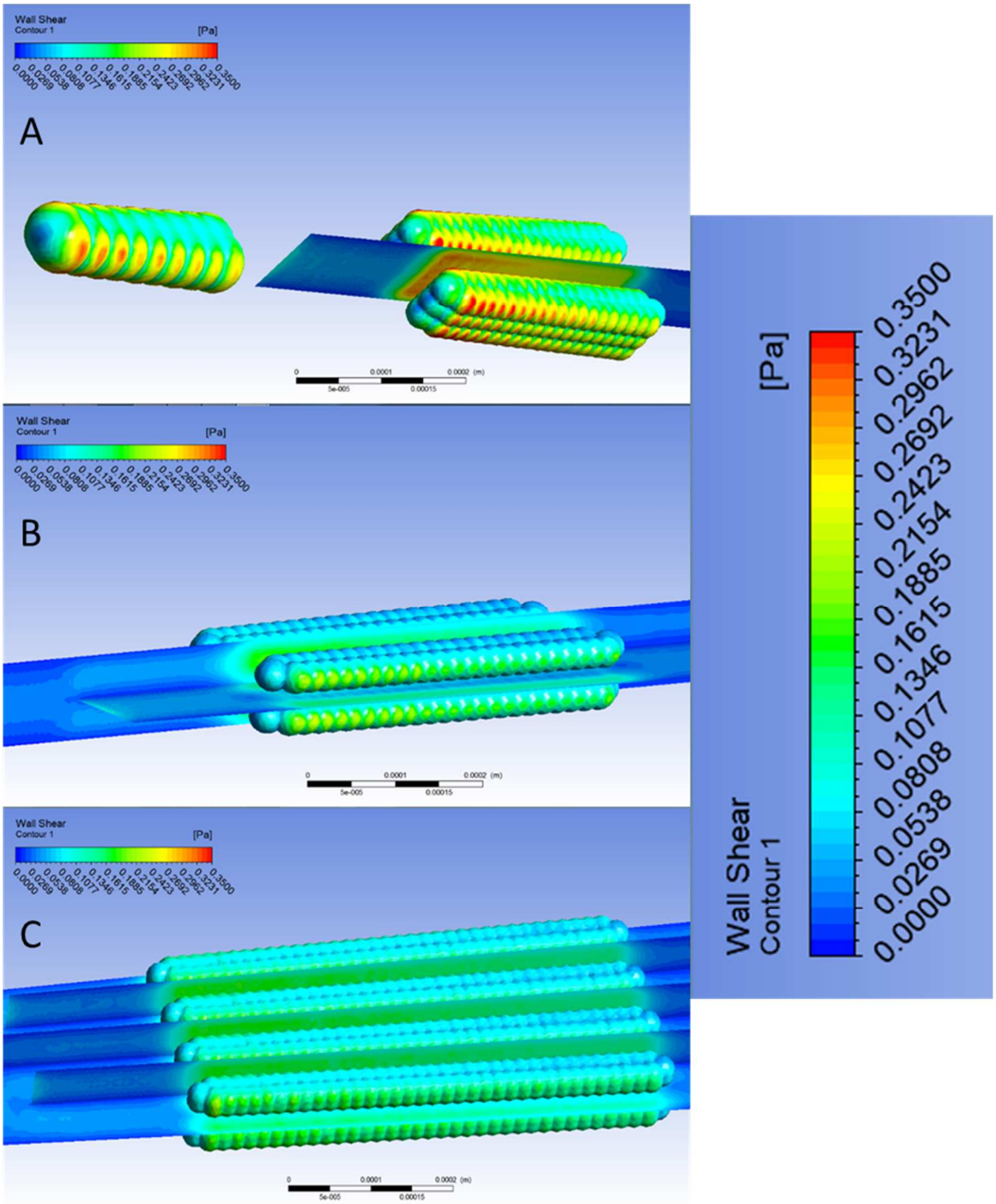

Figure 25: Contour plot of flow induced shear stress distribution imposed on cell aggregate surfaces through the first 4 bifurcating segments from the pore inlet along the axial length of the porous construct. The simulation was conducted at a mass flow rate of 6.737 x10^{-6} g/s which corresponds to the experimental volumetric flow rate of 10 ml/min at the scaffold central port inlet.

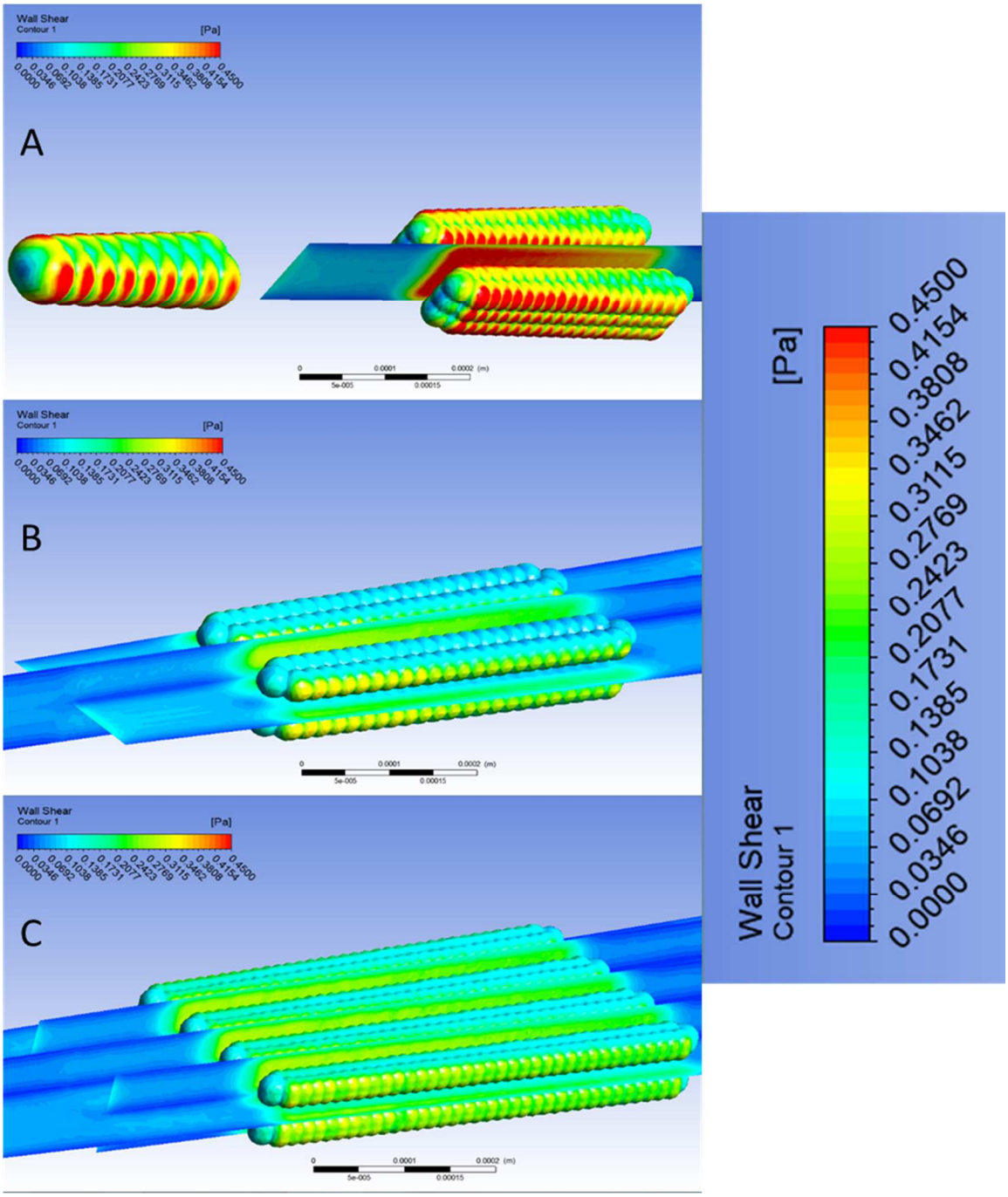

Figure 26: Contour plot of flow induced shear stress distribution imposed on cell aggregate surfaces through the first 4 bifurcating segments from the pore inlet along the axial length of the porous construct. The simulation was conducted at a mass flow rate of 1.01 x10^{-5} g/s which corresponds to the experimental volumetric flow rate of 15 ml/min at the scaffold central port inlet.

Partial simulations were also conducted for mass flow rates $1.47x10^{-5}$ g/s and $1.84x10^{-5}$ g/s which corresponds to the volumetric flow rate of 20 and 25 ml/min at the scaffolds central port inlet. The full gambit of simulations comprising of oxygen consumption was not conducted for these rates as hydrodynamic stress imposed of the cells aggregates in each segment exceeded 5.0 dynes/cm^2, which has been documented as the threshold for compromised hepatocyte functionality. From the shear simulations at $1.47x10^{-5}$ g/s the shear stress values ranged from .024 - .982 Pa (.24 – 9.82 dyne/cm^2) at the port inlet to the construct midpoint and .073 - .894 Pa (.73 – 8.94 dyne/cm^2) from the midpoint to the periphery. From Figure 27 it is clearly evident that every aggregate in each segment is experiencing flow induced stress over 5.0 dynes/cm2 with first two aggregate segments seeing this value or higher on more that 50% of its surfaces. The level of shear does subside towards the middle of the construct but increases towards the periphery with aggregates in segments 5, 6 and 7 experiencing levels at or over the threshold of 5.0 dyne/cm^2 on a third of their surfaces.

Similar trends, but at higher shear levels, were exhibited for the simulation at $1.84x10^{-5}$ g/s. At the pore inlet to midpoint of the construct the shear stress levels ranged from .048 – 1.247 Pa (.48 – 12.47 dyne/cm^2) and .036 – 1.224 Pa (.36 – 12.24 dyne/cm^2) from the midpoint to the periphery. From Figure 28 every aggregate in each segment, except the third, have shear stress at or greater than 5.0 dynes/cm^2 on more than 50% of its surfaces. In fact aggregates in the first two segments are showing shear levels that exceed the aforementioned threshold on more than two-thirds of their surfaces. If validated, these results would suggest that in an experimental setting, more than 66% and 50% of hepatocytes, located on the aggregate surfaces, would succumb to shear mediated apoptotic death at the pore inlet and mid-to-periphery respectively.

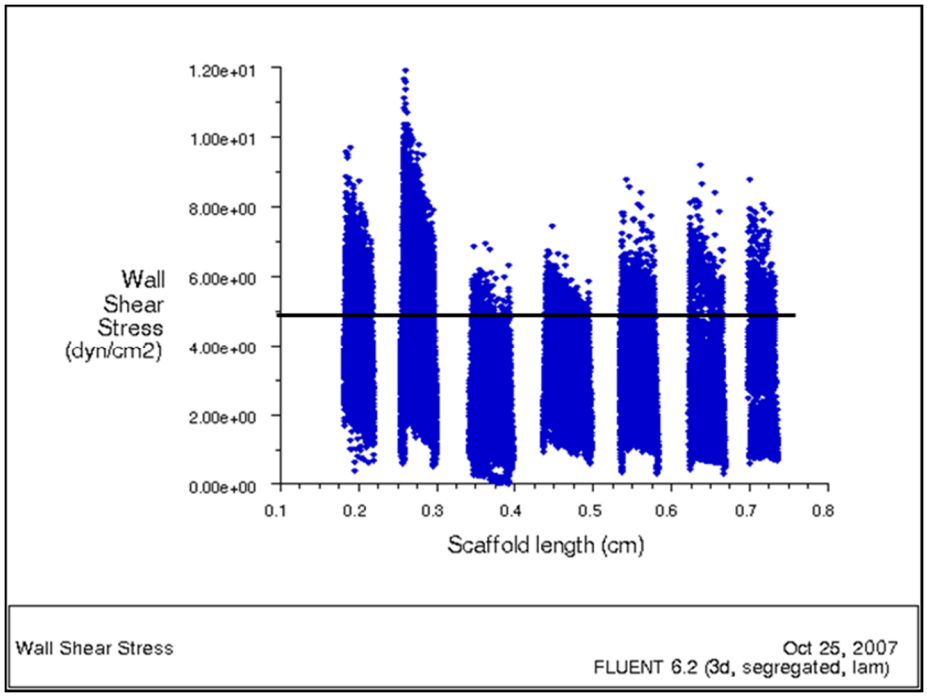

Figure 27: Wall shear stress levels of aggregate containing segments at the mass flow rate of 1.47×10^{-5} g/s (20 ml/min)

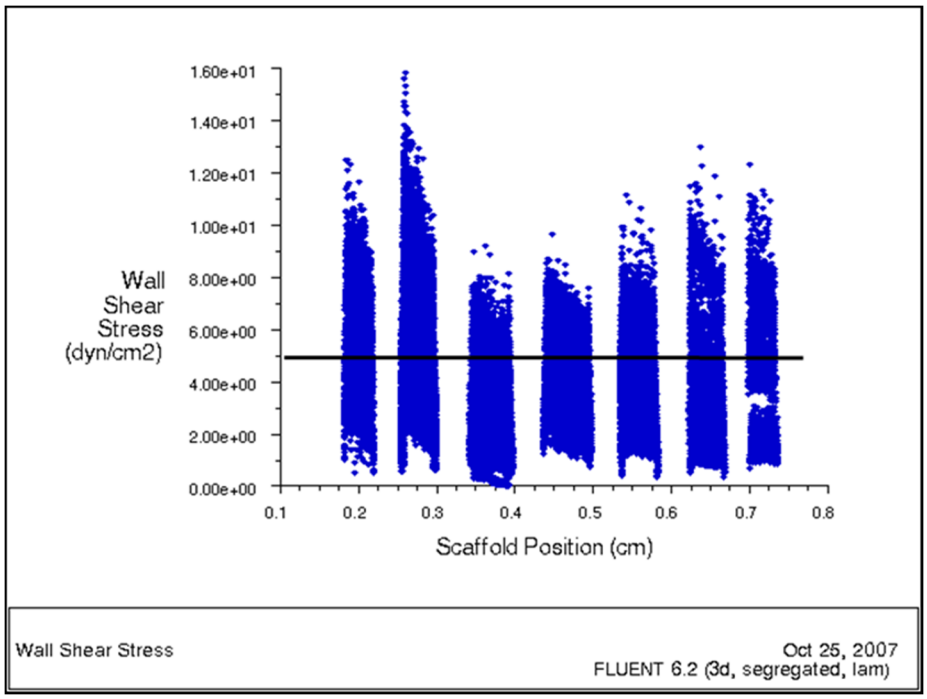

Figure 28: Wall shear stress levels of aggregate containing segments at the mass flow rate of 1.84×10^{-5}g/s (25 ml/min)

4.3.3 Computational Fluid Dynamics Results for Oxygen Consumption

Figures 29, 31 and 33 provide the steady state contour profile of O_2 consumption and concentrations for each simulated mass flow rate condition. Moreover the figures shows how oxygen consumption occurred around the cell aggregates and, based on aggregate number and cell number per aggregate. Oxygen concentration is shown by color gradient, with the red representing areas of higher concentration and dark blue signifying regions of zero oxygen. In addition to oxygen uptake distribution Figures 30, 32 and 34 also provide information about where transitional changes in oxygen uptake occurred along the axial length of the construct.

The impact that flow rate had on mass transport and oxygen consumption was very evident when comparing all three simulations. The contour plots in Figures 29, 31 and 33 show a less gradual color gradient change in oxygen concentration as the simulated inlet mass flow rates increase from $3.68x10^{-6}$ g/s (5 ml/min) to $1.01x10^{-5}$ g/s (15 ml/min). Table 3 also shows the gradient flux in each cell aggregate containing segment decreases with increased inlet flow rates. When comparing $3.68x10^{-6}$ g/s (5 ml/min) to $1.01x10^{-5}$ g/s (15 ml/min) the average change in each segment was ~3-fold except in the second segment where there was a ~4-fold change. When contrasting $6.737x10^{-6}$ g/s (10 ml/min) and $1.01x10^{-5}$ g/s (15 ml/min) the majority of segments saw a 2-fold change, except for segments one and six. Both of which saw a 1.5-fold change.

The effects of flow rate on oxygen consumption is further supported by the percent change of oxygen consumption per aggregate containing segments. From Table 4 we can see that in the first segment of cells, which happens to have the largest cell density, the percent change in oxygen consumed decrease by 3-fold when the lowest and highest inlet flow rates are compared. The same can be said for the next two successive segments where the changes are ~5-fold and ~4-fold respectively. The fifth cell segment is where the most

drastic shift can be seen between the highest and lowest rates. Here there is an exact 9-fold difference in the percent change in oxygen consumption. The last two segments could not be quantified in this manner as the oxygen concentration at the mass flow rate of $3.68x10^{-6}$ g/s was zero.

By increasing the inlet flow rate we were able to improve oxygen transport, and one could deduce nutrient transport as well, to cells at the midpoint and more towards the periphery of the construct. If the first simulation at $3.68x10^{-6}$ g/s (5 ml/min at the actual scaffold central port inlet) is used as a baseline, as we increased the flow rate to $6.737x10^{-6}$ g/s (10 ml/min) and $1.01x10^{-5}$ g/s (15 ml/min) oxygen availability increased by 42 and 100% at the construct's midpoint and, 51 and 100% at the periphery respectively. 100% was reported for both flow rates at the periphery because oxygen availability, assessed by reported concentration, for the baseline condition was zero. When the $6.737x10^{-6}$ g/s (10 ml/min) and $1.01x10^{-5}$ g/s (15 ml/min) mass flow rates are compared, the oxygen availability increased by 15% at the midpoint and 52% at the periphery for the latter. Of the three simulations, the lowest mass flow rate was the only condition in which oxygen concentration fell below the threshold for compromised functionality (2×10^{-2} mol/m^3) by hypoxia. Based on Figure 30 this occurred at .575 cm into the construct, which would indicate that cells residing in the last 29% of the scaffold's interior were cultured in a hypoxic environment.

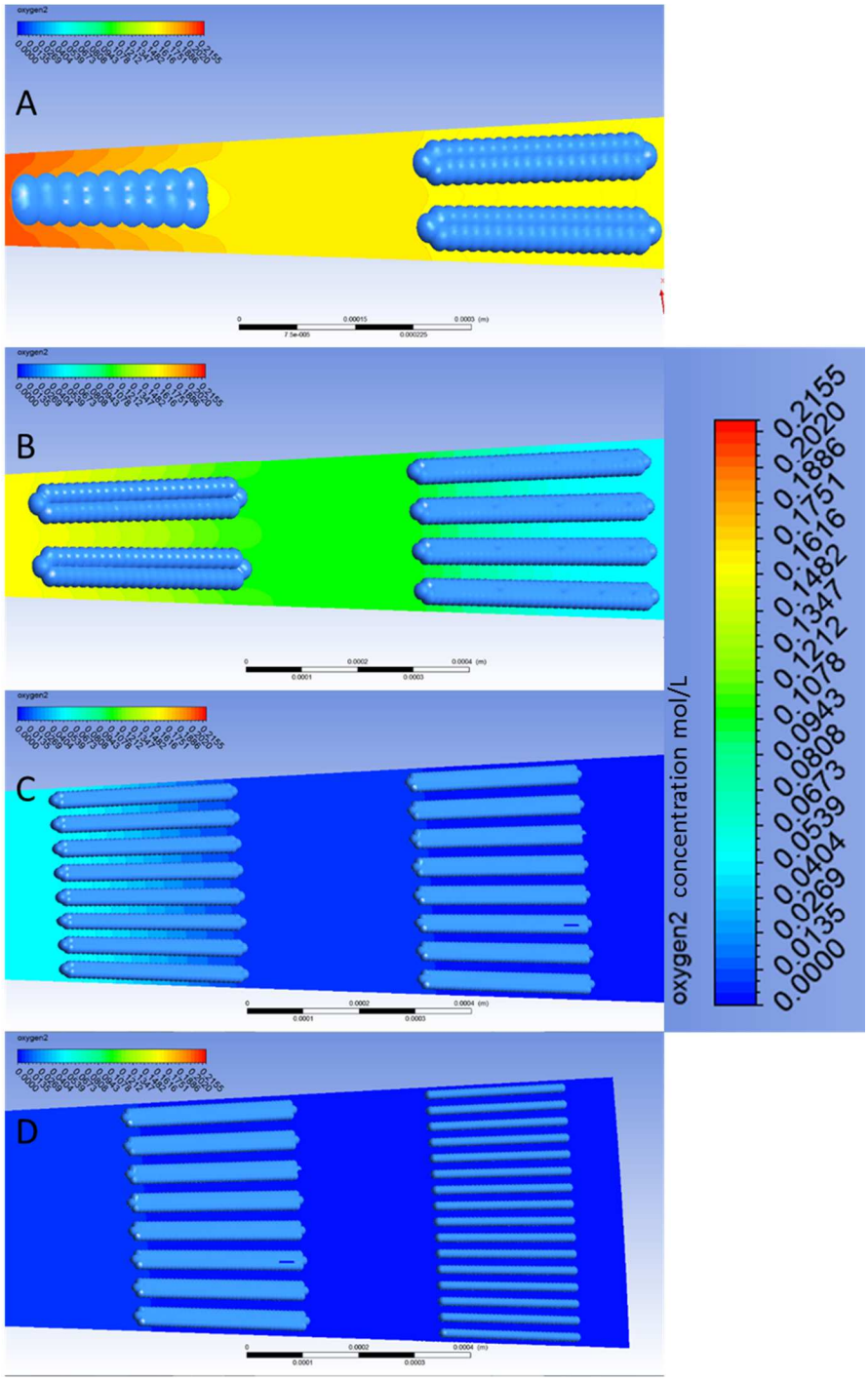

Figure 29: Contour plot of steady state oxygen distribution along length of porous structure with infused cell aggregates. Simulation was conducted at mass flow rate of 3.36 x10^{-6} g/s (5 ml/min at scaffold central port inlet) with a constant oxygen inlet concentration of .21 mol/L. Dark blue color indicates hypoxic regions where $C_{O_2} < F_{O_2}$

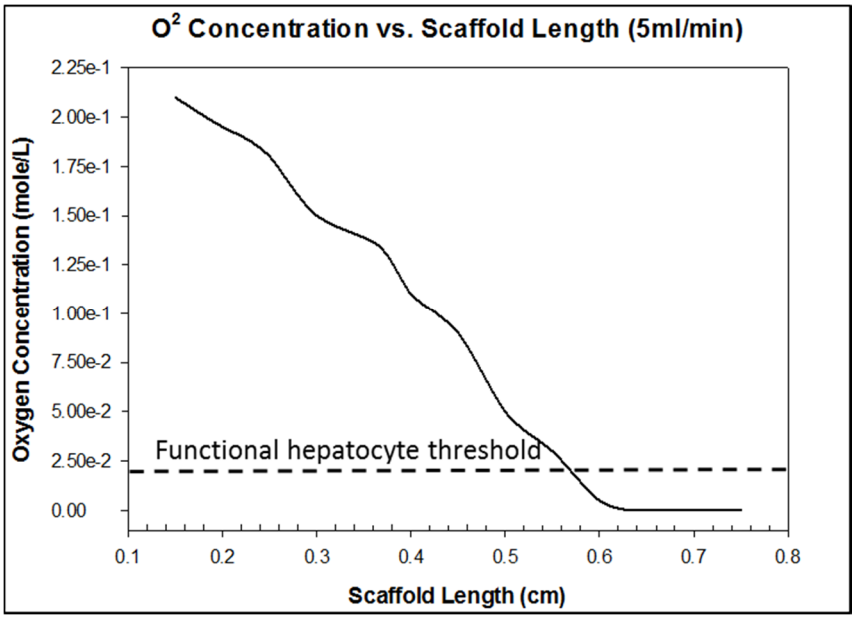

Figure 30: Oxygen concentration profile along the axial length of the porous construct at inlet mass flow rate of 3.36 x10^{-6} g/s (5 ml/min at scaffold central port inlet) with a constant oxygen inlet concentration of .21 mol/L

Mass Flow Rate (g/s)	Segment 1 (1/343) (450um)	Segment 2 (2/196) (400um)	Segment 3 (4/118) (500um)	Segment 4 (8/95) (700um)	Segment 5 (16/43) (500um)	Segment 6 (32/20) (400um)	Segment 7 (64/9) (400um)
3.86x10-6	-0.67	-0.88	-0.70	-0.86	-0.90	n/a	n/a
6.737x10-6	-0.33	-0.38	-0.40	-0.43	-0.60	-0.63	-0.62
1.101x10-5	-0.22	-0.20	-0.24	-0.29	-0.32	-0.40	-0.38

Table 3: Concentration flux (gradient) across the length of cell aggregate(s) per sequential segment. Units for gradient values are in (mole/L)/cm. The values in the parenthesis represent the number of cell aggregates in the associated segment followed by the number of cells per aggregate. The second set of parenthesis contains the aggregate length in um.

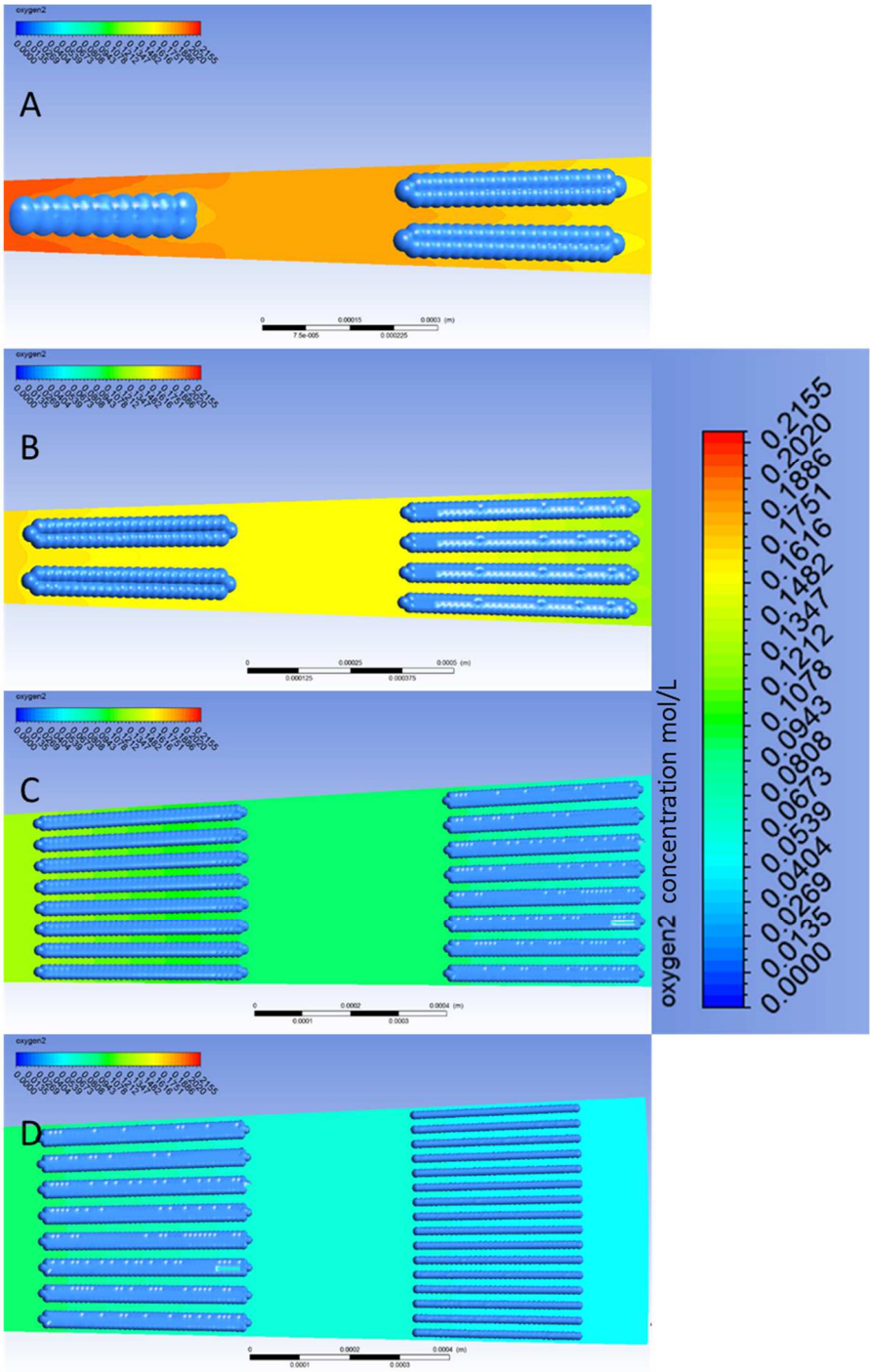

Figure 31: Contour plot of steady state oxygen distribution along length of porous structure with infused cell aggregates. Simulation was conducted at mass flow rate of 6.737 x10-6 g/s (10 ml/min at scaffold central port inlet) with a constant oxygen inlet concentration of .21 mol/L.

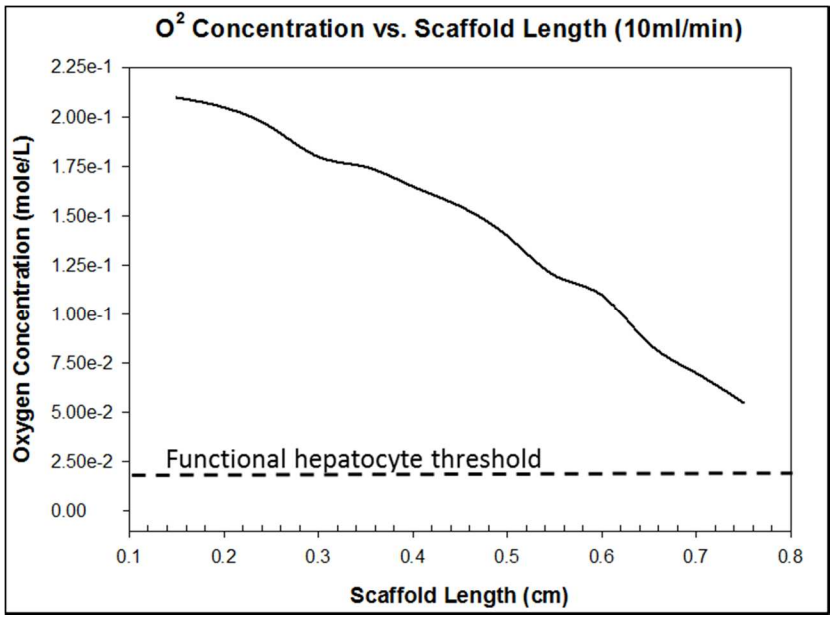

Figure 32: Oxygen concentration profile along the axial length of the porous construct at the inlet mass flow rate of 6.737×10^{-6} g/s (10 ml/min at scaffold central port inlet) with a constant oxygen inlet concentration of .21 mol/L

Mass Flow Rate (g/s)	Segment 1 (1 / 343)	Segment 2 (2 / 196)	Segment 3 (4 /118)	Segment 4 (8 /95)	Segment 5 (16 /43)	Segment 6 (32/20)	Segment 7 (64/9)
3.86x10-6	14.20%	19.40%	24.10%	54.50%	90%	n/a	n/a
6.737x10-6	7.10%	8%	11.10%	19%	23%	25%	33.30%
1.101x10-5	5%	4%	6.25%	11.10%	10%	11%	12%

Table 4: Percent change in oxygen consumption per successive aggregate(s) containing segment. The values in the parenthesis represent the number of cell aggregates in the associated segment followed by the number of cells per aggregate. n/a means that oxygen concentration at that segment was zero

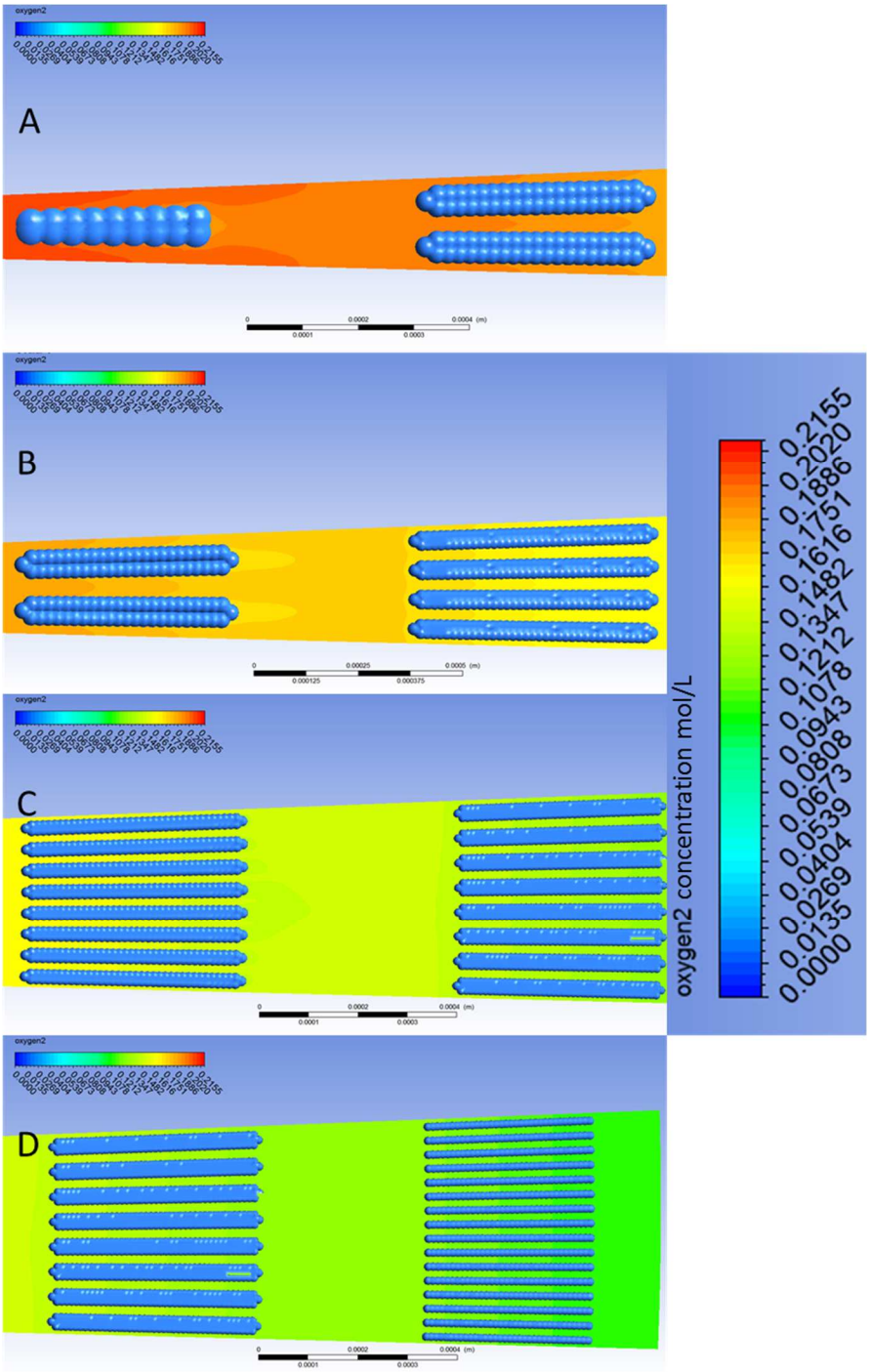

Figure 33: Contour plot of steady state oxygen distribution along length of porous structure with infused cell aggregates. Simulation was conducted at mass flow rate of 1.01 x10^{-5} g/s (15 ml/min at scaffold central port inlet) with a constant oxygen inlet concentration of .21 mol/L

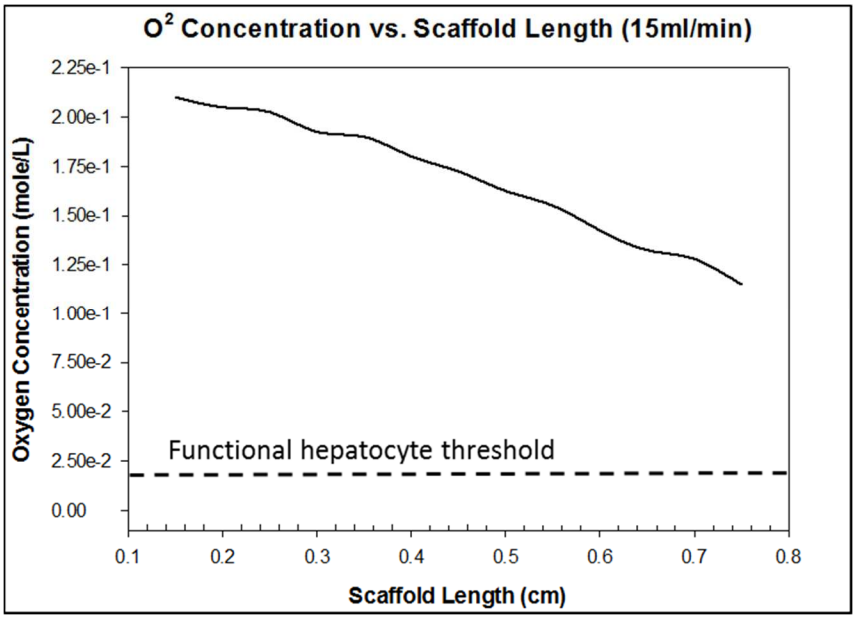

Figure 34: Oxygen concentration profile along the axial length of the porous construct at inlet mass flow rate of 1.01 $x10^{-5}$ g/s (15 ml/min at scaffold central port inlet) with a constant oxygen inlet concentration of .21 mol/L

4.4 Discussion

Computational fluid dynamic models have provided much needed insight into how external stimuli influence cellular processes in fluidized, three dimensional micro-environments. In this study we reconstructed our cell seeded, porous chitosan scaffold, at the single pore level, to predict how flow, at varying magnitudes, effects oxygen consumption and availability experimentally. Furthermore the CFD model was used to provide insight about the flow characteristic within our hepatocyte/scaffold microenvironment and to predict the hydrodynamic forces imposed on these cells in vitro. The overarching goal of this work was to use the information garnered from these simulations to help predict cellular outcomes pre-culture and to optimize the experimental design process.

The geometric rendering of the cell infused scaffold and CFD model are felt to be good representations of our experimental scaffold. The porous structure of the model accurately represents that of our scaffolds due to inlet pore sizes match (high end for scaffold at 400 µm), and both pores structures are radial and linear, tapered and interconnected. Although not measured, but from a qualitative perspective both have similar tortuosity. Also similar to our in vitro system, the aggregates in our model occupy a significant amount of the pore volume. The rationale for incorporating aggregates was that they more accurately resembles our scaffold/hepatocyte complex which in turn will better predict the internal flow patterns of media in and around our cells which affect velocity and shear distribution, and oxygen consumption. From the CFD simulations we were able to show how velocity progressively decreased along the axial length of the scaffold in the segments between the aggregates. The decrease in velocity was mostly attributed the bifurcating nature of the tapered interconnected porous structure. The velocity vector distribution for each mass flow rate condition showed that fluid flow in the structure was laminar. The vectors also showed that flow, mainly due to a low mass flow rate at the pore inlet, was orderly with essentially no eddies or swirls which would suggest that the Reynolds number for each simulation, along the length of the construct was under the threshold that would transition laminar to turbulent flow. This would also suggest that media was able to travel the distance of the scaffold and that the transportation of nutrients and oxygen to cells was not disrupted. However it should be noted that there was slight recirculation at the pore inlet for the mass flow rate of 6.737^{-6} g/s (10 ml/min) condition but this was resolved before the fluid reached the first aggregate. The magnitude and color of the velocity vector arrows would indicate that the flow profile, despite the aggregates, still

followed a typical parabolic shape for laminar flow in that the velocity at the pore walls was zero.

Shear or hydrodynamic stress at certain magnitudes is beneficial to some cells and essential to others such as endothelial cells that line our vasculature system. However at certain levels, which are cell type dependent, shear stress can disrupt essential cellular processes and produce calamitous effects. In dynamic scaffold culture, predicting shear stress levels inflicted on the cells along the fluid trajectory in the matrix is virtually impossible. What can be simply said is that levels increase with increasing flow rates. Understanding or being able to predict, with confidence, the shear stress level within a matrix's microenvironment could be the difference between device success and failure. In this study we utilized computational fluid dynamic simulation to ascertain shear stress levels within our scaffold microenvironment and extrapolated these finds to elucidate the shear effects on our hepatocytes. According to our computational results, shear stress for the three lower flow rates remained below the needed threshold. However the mass flow rates of 1.47×10^{-5} g/s (20 ml/min) and 1.84×10^{-5} g/s (25 ml/min) produced forces that were well above this threshold and would have been deemed as unsafe perfusion culture conditions. Shear stress is a proportional to the velocity magnitude and what was noticed from our model is that velocity doubled in the tight spaces around the aggregates in relation to previous sections without aggregates. This perfectly logical as shear forces increase with decreased flow area. This would indicate that shear flow distribution, if flow is not occluded, is dictated by aggregate position and how much of the aggregate occupies the scaffold void volume. In an in vitro setting where spatial distribution of cell aggregates can only be partially controlled (pore size and direction) the flow and subsequent shear force distribution would not be consistent throughout which is in

agreement with this model. For these reasons it is felt that model is a good predictor of the magnitude of stress internally.

Others have used CFD simulations to predict shear stress levels imposed on their cells in culture. For those whose cells are cultured in monolayers [231-234] it is feasible to assume that cell layer in contact with fluid is flat and can be modeled as the surface of the planar surface of the perfusion reactor and given a "WALL" boundary condition. However for bulk 3-D scaffold models who experimental cultures utilize high cell densities but assume that this aspect's contribution to the system's shear profile is insignificant, it is felt that these models don't accurately represent the microenvironment and will generate unreliable data. Using a dynamic cell growth model Lesman e. al [235] was able to show how shear stress distribution is effected by increasing cell densities. Lesman's demonstrated that occlusion of the flow field, in this case, by escalated cell compaction which reduced the scaffold void volume, increased the level of shear experienced by the surfaces of the cells in the fluid path. Melchels et al. [236] also described the impact that cell dispersal and relative densities have on the magnitude and spatial distribution of shear stress in fluidized scaffold. In the CFD model, Mechel's type G scaffold configuration showed that by increasing the relative cell density by 20% the average shear stress increased 3-fold. The model also demonstrated that past 30% relative cell density shear stress levels plateaued. The model was not pushed passed 75% relative cell density. It is speculated that convergence issues with the simulation could have or did pose an issue.

Oxygen transport limitations have always posed serious problems for cells seeded in bulk scaffold constructs. The solution of increasing fluid flow to increase the transport

distance of oxygen is no longer a rationale nor viable solution. Thus it is important to the success of a perfused tissue engineered device that the correct balance is struck between increased mass transport efficiencies and damaging shear effects. In this segment of the study we looked at how increasing inlet flow rates modulated shear stress and more importantly oxygen transport distance within porous construct. From our results were we able to show that within our scaffold, with the experimentally comparable cell densities, increased flow does decrease the intensity of the consumption gradient along axial length of our scaffold. A similar trends were seen by Cioffi et. al [237] who utilized a micro-CT rendered scaffold to investigate how increased flow effected oxygen gradients along the length of chondrocyte infused construct. It was discerned by increasing inlet flow rate from .03 to .3 ml/min the percent oxygen availability could be increased by 26% at the scaffold's periphery. Podichetty et. al [221] also demonstrated that the oxygen distribution from the scaffold inlet to outlet could be increased by ~57% with a volumetric flow rate increase from 1- 15 ml/min.

In establishing a volumetric flow rate ($3.68x10^{-6}$ g/s $\rightarrow$ 5 ml/min at the scaffold central port inlet) that can simulate medium flow from inlet to outlet while producing the least amount of shear stress, what we saw in terms of oxygen consumption and availability is that the last 29% (.575 cm away from inlet) of the scaffold that contained cells was a hypoxic environment. This can be attributed to the increased residence or interaction time of the oxygen molecules with the aggregate surface. Lawrence et. al [238] explained that residence time distribution (RTD) is "a measure of dispersal of a molecule in a flowing medium owing to the combined action of a velocity profile and molecular diffusion". In this scenario residence time is dependent on the fluid velocity

and oxygen consumption rate. Devarapalli et. al [239] looked at how flow rates and residence time distribution affected oxygen uptake distribution across 6 different cell types. Essentially what he saw across all cell types is as you decrease the inlet flow rate, residence time increase and oxygen availability decrease along the fluid flow trajectory. In terms of hepatocytes, in his system the flow rate of 1ml/min increased the residence time enough to where oxygen levels with, at the outlet, were zero. In a future but similar experiment from the same lab, while using a hepatic model it was also concluded that increased fluid flow at the reactor inlet produced better oxygen availability at the reactors outlet [221].

4.5 Conclusion and Future Work

Computational fluid dynamic models used in this study provided needed information about our scaffold's microenvironment and how varying flow rates might impact shear stress, oxygen consumption and fluid motion within its interconnected porous architecture. The results presented in this study showed that under the right conditions the transport of key nutrients to the entrapped cells would not be hampered by the porous nature of construct. Moreover the models also demonstrated that under the two highest flow rates, oxygen transport limitations, that are known to plague bulk scaffold constructs, and are exacerbated by the highly aerobic nature of hepatocytes, can be overcome with minimal damage due to shear effects. More importantly, for the scope of the objectives, the simulations showed that the model is works. Just as important the study demonstrated that the model can be scaled up to accommodate more clinically relevant cell densities and experimental input to help predict how certain stimuli might influence cellular processes pre-in vitro and aid in the optimization of future experimental designs.

Understanding how closely the data generated from the CFD model correlates to the actual in vitro experiment is just as important as the model itself. This would lend to the model's credibility and efficacy. That said in the following chapter perfusion bioreactor studies with cell numbers and flow rates matching that of the model will be conducted to validate the model predictions. It is hypothesized that the flow rate which produced the best oxygen transport profile with shear stresses below the damaging threshold of 5 dynes/cm^2 will produce the best viability and metabolic outcomes.

CHAPTER FIVE: EVALUATION OF HOW SHEAR STRESS AND MASS TRANSFER AFFECT HEPATOCELLULAR-FUNCTIONALITY, MORPHOLOGY AND VIABILITY: EMPIRICAL ASSESSMENT OF CFD SIMULATIONS

5.1 Introduction

Shear stress is the hydrodynamic force induced by liquid-based friction against the cell membrane. The mechanical stimulus, caused by shear stress, affects the cell-specific and morphological behavior, and adhesion properties of several cell types in in-vivo and in-vitro. Depending on the cell type and function, shear stress can be deleterious or essential to proper phenotypic expression. Regarding the latter, shear stress imposed on the endothelium has been shown to regulate vascular morphogenesis, atherosclerosis and blood pressure. When acting directly on endothelial cells, shear stress inhibits apoptosis [240], activates Ca^{2+} influx [241], triggers signaling cascades which modulate gene expression and cytoskeletal remodeling by reducing cell contractility via decreased VE-cadherin tension and increased tension on PECAM-1 [242]. Ueda et al. demonstrated that shear stress exhibited a positive effect on odontogenic cells by upregulating the expression of both epithelial and mesenchymal ondontogenic-related mRNAs after 2hrs of exposure, and increase protein expression and better in-vivo integration after 12 hours of exposure when compared to the control [243].

In-vivo hepatocytes are principally shielded from shear stress by vascular endothelial cells. However past evidence suggest that hepatocytes do experience a certain level of direct shear stress through small pores in the sinusoidal endothelium [244] or experience force passively from being in contact with sinusoidal endothelial cells that are stretching due to shear stress imposed by portal blood flow. This would suggest that shear stress or force, to

some degree, is essential to normal hepatocellular functionality in-vivo. The effects of shear stress, in-vivo, are further boosted after partial hepatectomy, where increased hemodynamic forces imposed on hepatocytes are partially responsible for triggering cell proliferation [245].

Hepatocytes exposed to hydrodynamic forces that don't exceed harmful threshold values are known to produce greater rates of albumin and urea secretion in comparison to static cultures. Kan et al. initially observed improved ammonia removal and ureagenesis in hepatocyte co-cultures with nonparenchymal cells under shear stress [246]. Similar results were observed by Yu et al. and Shuler et al. in uni-directional and bi-directional perfusion reactors respectively [247, 248]. In both instances, and in similar cultures alike, elevated hepatic performance is attributed to increased gas, nutrient and metabolite exchange which is limited, from a mass-transport perspective, in static cultures. In addition to increased liver specific function, shear stress, when moderately applied, inhibited liver tissue destruction [249] and contributed to higher collagen secretion from hepatocytes [250].

Conversely data also suggest that moderate to excessive levels of shear stress can prove to be quite detrimental to hepatocyte functionality over time. Although a definitive threshold has yet to be established, most likely because certain bioreactor configurations present shear differently, some have stated that at 5 dynes/cm^2 activity begins to collapse [192]. Sato et al. reported shear stresses greater than 1.0 Pa (10 dyne/cm^2) caused hepatocytes to assume a morphology analogous to endothelial cells which negatively influenced their metabolic capacity when culture periods exceeded 3 days [251]. However others have reported enhanced cytochrome P-450 monooxygenase, P-450IA1 (CYP1A1) expression in response to higher hydrodynamic stress [252].

A viable bioreactor/scaffold complex necessitates adequate convective mass transport as hepatocytes are highly metabolic and sensitive to oxygen concentrations. In perfusion systems where hepatocytes are not shielded from shear by encapsulation (i.e.

alginate or endothelial cells) and flow is parallel to all hepatic surfaces and deemed non-physiological, a delicate balance between flow rate, which facilitates good mass transfer and shear stress, must be adhered to. In the previous chapter we conducted CFD simulations at 5, 10, 15, 20 and 25 ml/min to elucidate the relationship between volumetric flow rates, shear stress and mass/oxygen transport in our cell seeded scaffold/reactor complex. In this chapter we looked to empirically evaluate how these flow rates from the CFD simulations, with direct oxygenation, effected cell morphology (i.e. aggregation), viability and metabolic output. The overarching goal was to find the optimum flow rate that produced the best biochemical and morphological outcome. Furthermore we sought to validate the CFD model as a future tool that could be used as the building block for understanding how more complex oxygen transport/delivery systems, nutrient uptake and flow could work within our perfusion reactor/scaffold complex.

5.2 MATERIALS AND METHODS

5.2.1 Sources of Materials and Reagents

Medium molecular weight chitosan and glacial acetic acid were purchased from Sigma Aldrich (St. Louis, MO).

5.2.2 Scaffold Fabrication

Scaffold fabrication technique, scaffold dimensions and materials used in making the scaffolds for the experiments conducted in this chapter are consistent with those used in chapter 3.

5.2.3 Hepatocyte Isolation

The technique, type of rats and reagents used to isolate and purify the hepatocytes used in these experiments were consistent with those from chapter 3. Briefly, the hepatocytes were isolated from Fisher rats by a modified two-step collagenase perfusion technique.

5.2.4 Culture Conditions

The medium makeup (i.e. components and concentrations) and seeding protocol used for the experiments conducted in this chapter were similar to those used in chapter 3. However in this chapter all cultures were maintained in an atmosphere of 90% air/10% CO_2 which preserved the pH at ~7.2. This pH is more consistent with the physiological acidity of the liver and intracellular pH of its hepatic constituents.

Albumin protein synthesis and ureagenesis assays were performed to assess efficacy of the bioreactor studies. The volume of medium in the bioreactor system and concentration of cells seeded in each scaffold were factored into both calculations. Similar to chapter 3 two double layer collagen sandwich culture systems were run in parallel with each bioreactor and utilized as controls. The protocols for cell concentration, volume of medium used and top collagen layer integration were consistent with those used in chapter 3.

The medium was extracted and replenished daily for both culture systems. All samples were stored at 4℃ until analysis were perf ormed. Hepatocyte morphology and viability were ascertained by histology using Hematoxylin and Eosin Y staining. All experiments in this chapter and going forward were conducted with the third generation perfusion bioreactor system and flow circuit (Figure 35).

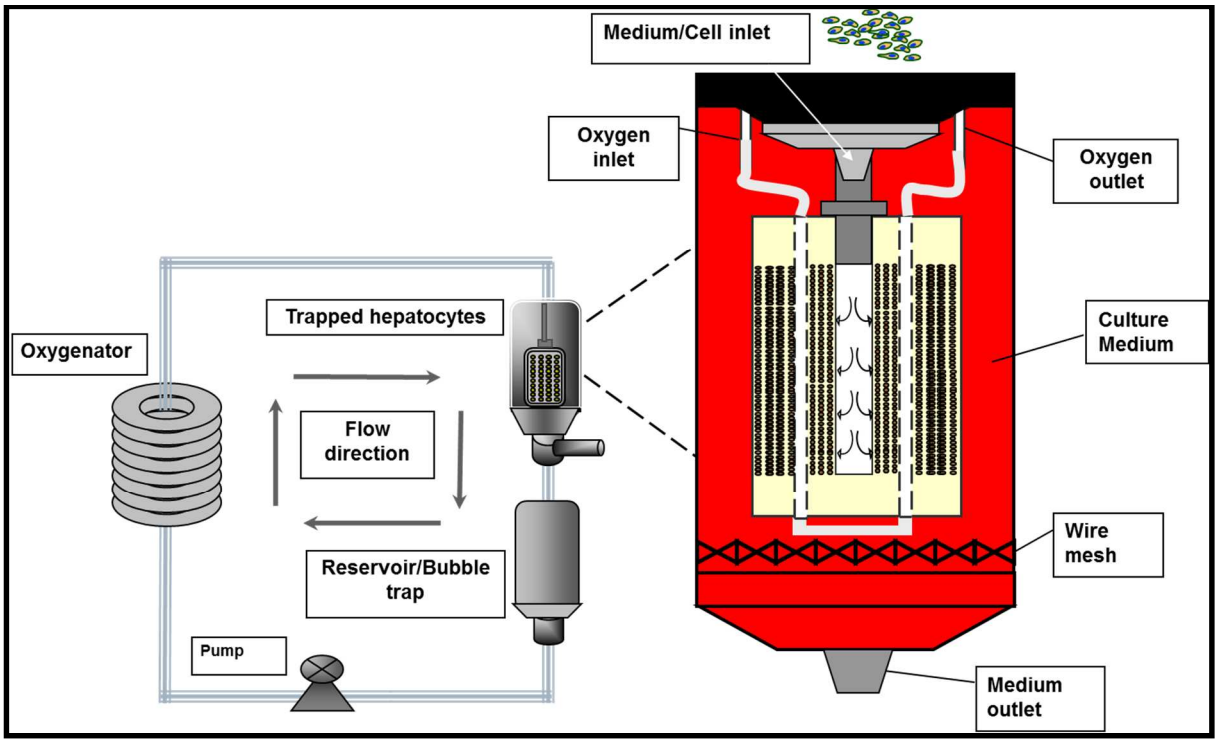

Figure 35: Schematic of complete third generation perfusion culture circuit with expanded, detailed schematic of the bioreactor chamber. The bioreactor image shows the fluid path from inlet to outlet, oxygenation tubing and orientation of trapped hepatocytes

5.2.5 Metabolic Output Measurements

Enzyme Linked Immunoassay (ELISA) for Albumin

The protocol, reagents and instrumentation used to perform the ELISA assays for these experiments were consistent to those from chapter 3.

Urea Assay

The protocol, reagents and instrumentation used to perform the urea colorimetric assays for these experiments were consistent to those from chapter 3.

5.2.6 Histological Analysis

The protocol, reagents and instrumentation used to perform the histological analysis for these experiments were consistent to those from chapter 3.

5.2.7 Statistical Analysis

The biochemical functional output of the hepatocytes were calculated from duplicate runs. The rates per day were averaged across duplicate runs and values are reported as mean ± standard deviation.

5.3 Results

5.3.1 Effects of Direct Oxygenation (Static Bioreactor Culture)

The goal of this experiment was to evaluate the effects that direct oxygenation, without the assistance of convective transport via media perfusion, has on the biochemical functionality and morphology of the hepatocytes in this culture system. In both experiments the scaffolds were seeded with an average of 101 million hepatocytes and cultured for a duration of 7 days. The scaffolds were seeded at a flow rate of 20 ml/min until the desired cell number per scaffold was achieved. In both cases the cell seeding process did not exceed 15 minutes.

In general, the culture did remain functional throughout the duration of the 7 day period. As seen in Figure 36, protein synthesis, although very depressed and flat, was measureable on every day. The highest rate of synthesis was noted on day 1, with an average value of 0.727 µg/million cells/day. Surprisingly this was the only day that the hepatocytes in both cultures experienced any convective oxygen transport, which occurred exclusively during the 15 minute seeding process. A precipitous drop in protein synthesis was seen from day 1 to day 2. However levels from day 2 to 7 exhibited slight fluctuations.

The mean urea synthesis for each day can be seen in Figure 37. Similar to albumin protein synthesis, ureagenesis was highest on the first day with a value of 0.534 µg/million cells/day. Based on evidence presented earlier it is no coincidence that the highest rate of production was seen on the day that the cells were exposed to flow, albeit for a very short time frame. The rate of production saw slight downshifts as the culture progressed. The sixth

day of the culture saw the greatest difference in urea output of 98.9% between the static reactor system and the control.

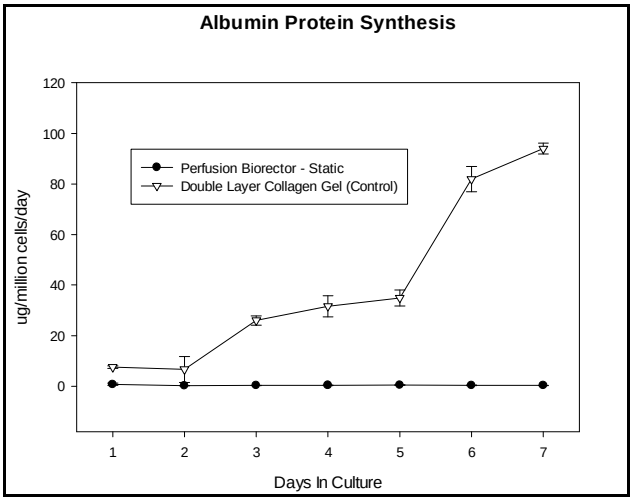

Figure. 36: Rate of albumin synthesis produced by hepatoctyes cultured with direct oxygenation and no perfusion vs. double layer collagen gel control. Error bars represent standard deviation of 2 repeated measurements.

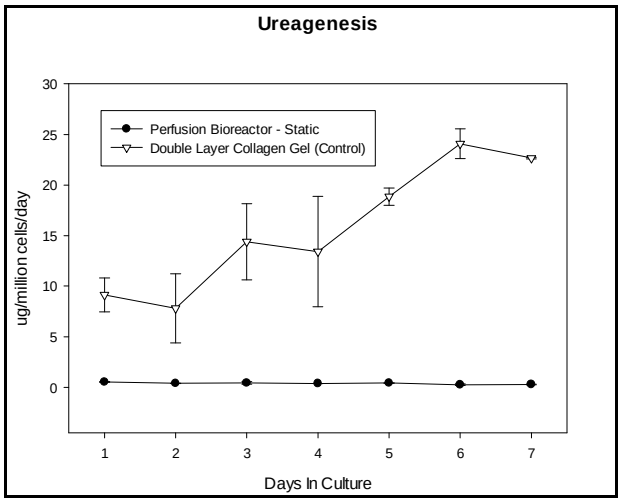

Figure. 37: Rate of Ureagenesis produced by hepatocytes cultured with direct oxygenation and no perfusion vs. double layer collagen gel control. Error bars represent standard deviation of 2 repeated measurements.

Figure 38 shows a segment of the scaffold cross section between two direct oxygenation tubes. It's quite evident that all viable hepatocytes were clustered in close proximity to the only oxygen source in the culture. Hepatic aggregation was nonexistent in

the area between the oxygen tubes or at the scaffold periphery. Given that aggregation is essential to cell viability it is assumed that all single hepatocytes died of necrotic factors caused by lack of essential nutrients provided by convective transport. Viable cells within each cluster were mostly seen at the edges of the aggregates indicating that hepatocytes within the interior were deprived of oxygen (Figure 39 A to C). In addition to access to oxygen, hepatocytes at the aggregate periphery probably remained viable because shear was not a factor. A lesser number of small aggregates were seen slightly downstream of the oxygen source. It is plausible that these cells remained functional only because: 1) they were able to cluster during the seeding process; and 2) they were able to take advantage of the nutrient containing medium not consumed by the large number of non-viable single cells. Lastly, because hepatocytes can be motile in culture it can be deduced that the minimal level of aggregation that occurred away from the oxygenation tubing, post seeding, was attributed to these cells utilizing oxygen not consumed by the non-viable population to remain functional and form multi-cellular masses.

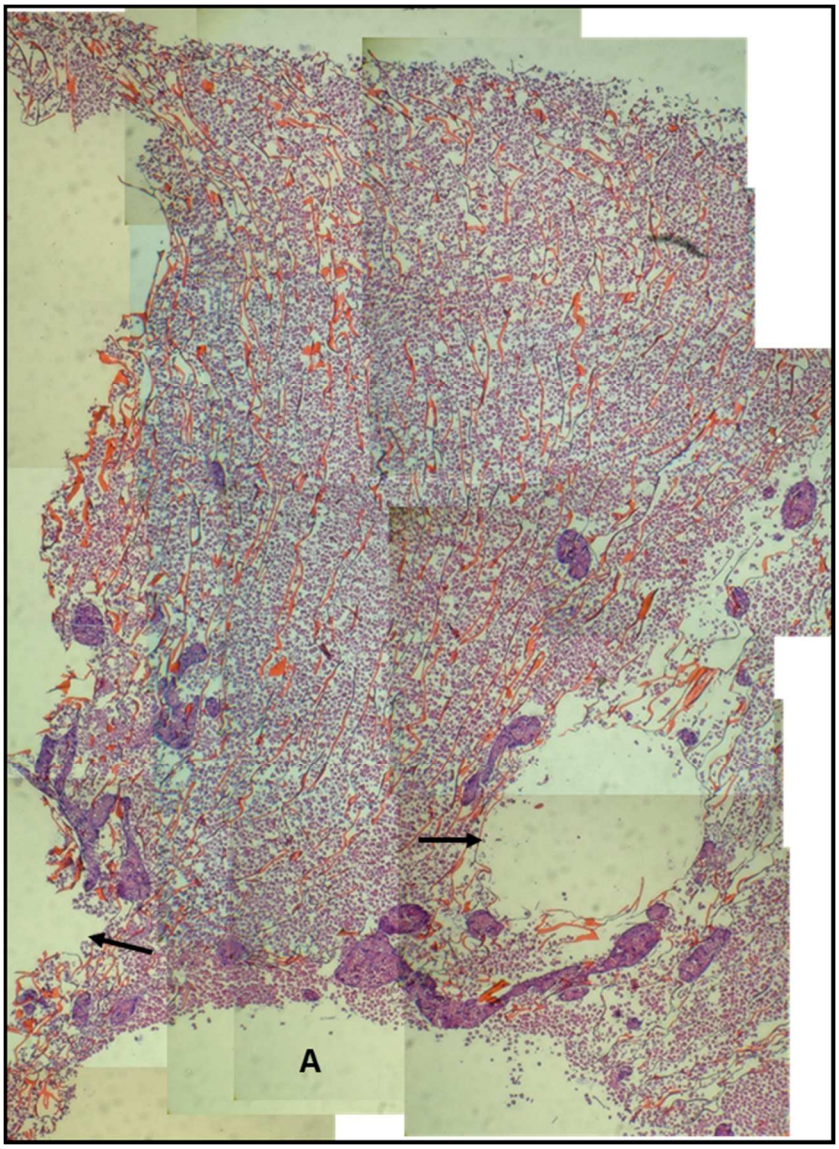

Figure 38: Histological montage (H&E stain) of static bioreactor culture (only direct oxygenation). Arrows are pointing to embedded semi gas permeable tubing for direct oxygenation. A is positioned in the central port inlet.

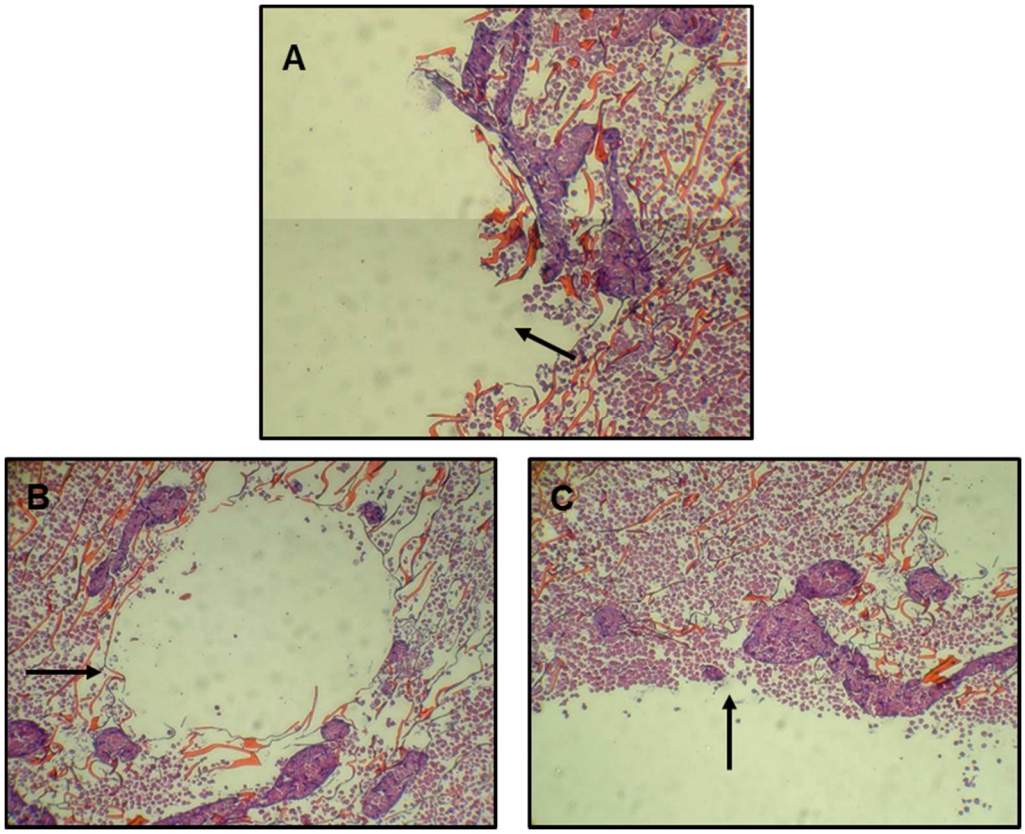

Figure 39: Enlarged images of high oxygenated sections within scaffold from static bioreactor culture (only direct oxygenation). A) arrow is pointing to area where gas permeable oxygenation tubing was embedded. B) arrow is pointing to area where gas permeable oxygenation tubing was embedded. C) Arrow is pointing in the direction of flow from the scaffold central point inlet.

5.3.2 Effects of Direct Oxygenation and Convective Transport at 5 ml/min

The goal of this experiment was to evaluate the effects that direct oxygenation, with convective transport facilitated by perfusion at 5ml/min has on liver-specific functionality, viability and morphology. The scaffolds used in both experiments were seeded with 100 million and 105 million hepatocytes, respectively and cultured for a duration of 7 days. The scaffolds were seeded at a flow rate of 20ml/min until the desired cell number per scaffold was achieved. In both cases the cell seeding process did not exceed 15 minutes. Cells were seeded in a 90% air/10% CO_2 atmosphere. After the seeding process the flow rate was quickly switched to 5ml/min for the duration of the seven day culture.

Albumin synthesis, in general, was maintained over the 7 day period of the culture with average peak levels reaching 12.894 µg/million cells/day on the first day (Figure 40). Similar to the static culture, rates of production, in this condition, dropped significantly going into the second day (~4 fold decrease). However from the second day to the cessation of the culture, protein synthesis remained constant at an average of 3.5 ± 0.59 µg/million cells/day, with the lowest rates seen on day 5 (2.66 µg/million cells/day). When compared to the control, the experimental culture yielded 41.6% more albumin on the first day. Day 2 was the point where the control surpassed the experimental culture. At the conclusion of the culture, the control was producing 95% more albumin than the perfusion condition.

Urea secretion results (Figure 41) show that hepatocytes cultured in perfusion had lower function compared to the control. Unlike albumin, urea secretion was consistent throughout the culture with only minor fluctuations in rates between 24 hour periods. However it should be noted that expression, albeit slightly, did decline as the culture progressed. The maximum and lowest synthesis were seen on day 1 and 7, with values of 5.46 and 3.14 µg/million cells/day respectively. This represented less than a two-fold change. When both days are juxtaposed to the control a 1.7–fold and 7.1–fold difference in levels were observed.

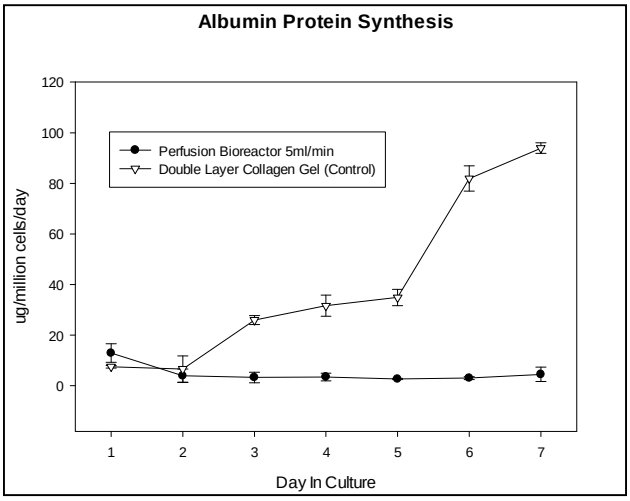

Figure. 40: Rate of albumin synthesis produced by hepatoctyes cultured with direct oxygenation and 5 ml/min perfusion vs. double layer collagen gel control. Error bars represent standard deviation of 2 repeated measurements.

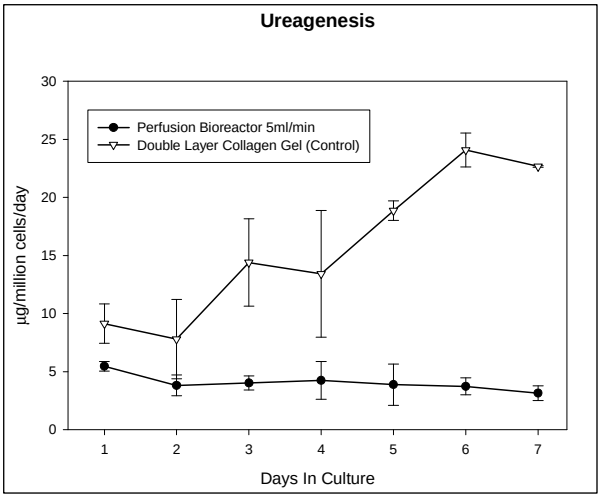

Figure. 41: Rate of urea produced by hepatoctyes cultured with direct oxygenation and 5 ml/min perfusion vs. double layer collagen gel control. Error bars represent standard deviation of 2 repeated measurements.

Figure 42 is a reconstructed montage that represents a one-eighth segment of the scaffold cross-section. The overwhelming majority of hepatocytes within the section are not aggregated, which based on hepatic physiology would clearly suggest that they are non-viable. Cell aggregation was evident and concentrated between the embedded oxygen tubing, but not in close proximity to the tubing. There was insignificant spheroid formation

and cell viability towards the periphery of the scaffold. Unlike the static culture, in this condition, aggregation was not prevalent around the fluid inlet which, like areas adjacent to the tubing, is considered a region of high oxygen tension. The fact that little to no viable cell spheroids are visible around the oxygen tubing is counter to data presented in previous sections. Because the aggregation process in perfusion scaffold cultures is usually flow mediated it's very plausible that this is simply due to the poor flow distribution which is characteristic at low flow rates such as this one. Of the cells that did aggregate, they took on more of an elliptical geometry that was in-line with the direction of the fluid trajectory. Figure 43 A, B and C show that viable cells were interspersed throughout the body of smaller spheroids. However for larger spheroids in the same images viable cells were more concentrated at the periphery which would suggest that cells positioned towards the interior succumbed to death via oxygen and nutrient deprivation.

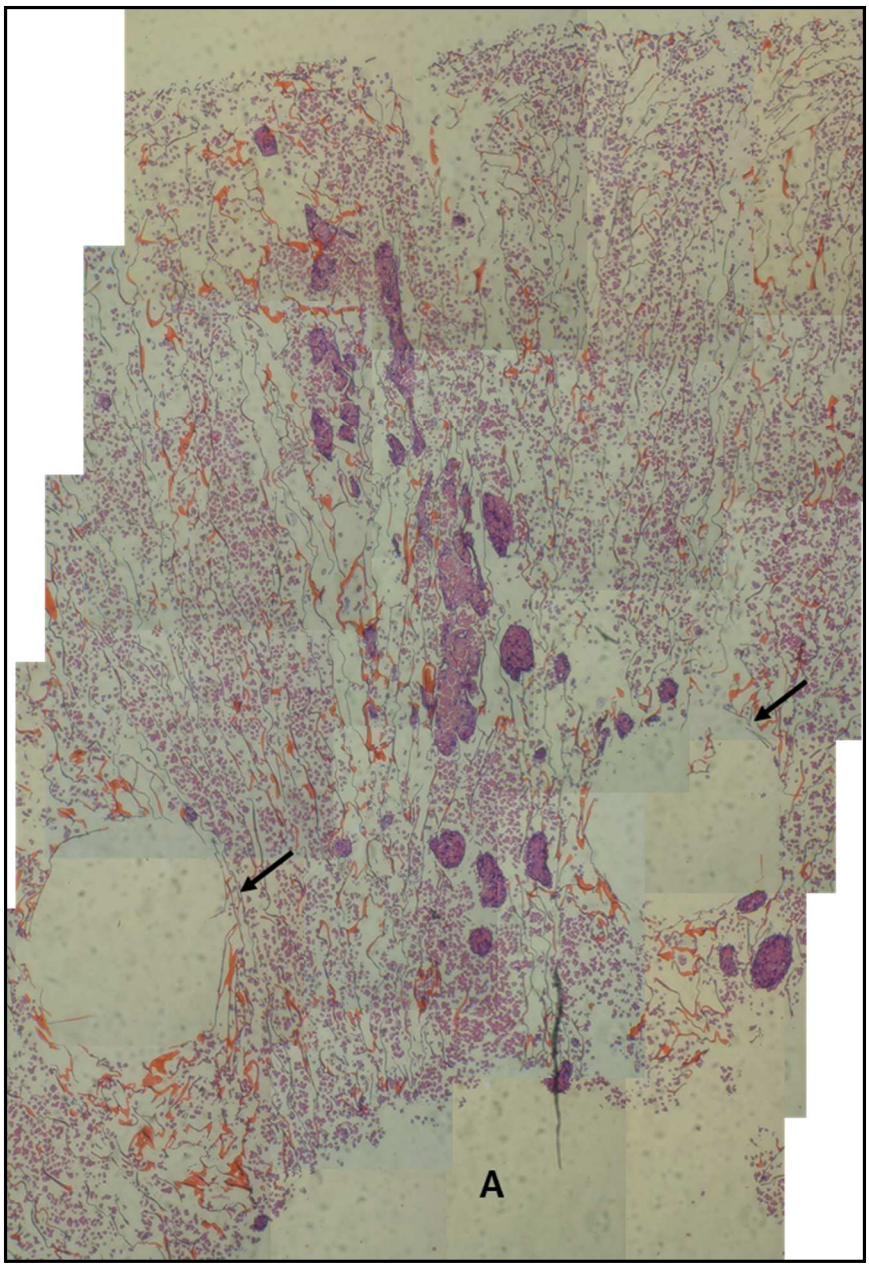

Figure 42: Histological montage (H&E stain) of 5 ml/min bioreactor culture with direct and convective oxygenation. Arrows are pointing to areas where direct oxygenation tubing was present during the culture. A is positioned in the central port inlet.

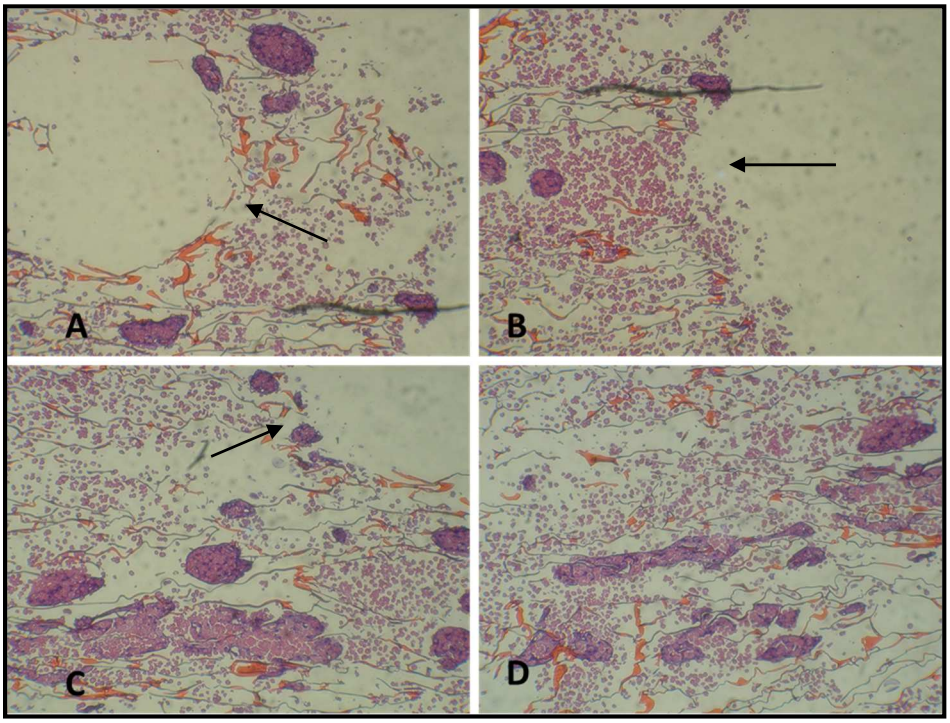

Figure 43: Enlarged images of high oxygenated sections within the scaffold from 5ml/min perfusion culture. Images A) and C) arrow are pointing to area where semi-permeable oxygenation tubing was embedded. B) Arrow is in central port area and pointing in the direction of the fluid path. D) Spheroids in mid-section of scaffold towards scaffold perimeter

5.3.3 Effects of Direct Oxygenation and Convective Transport at 15 ml/min

In this experiment, the volumetric flow rate of 15 ml/min was utilized to ascertain how it affected mass transport within the scaffold micro-environment and its causal effect on cellular respiration, viability and geometry. The scaffolds used in both experiments were seeded with 95 million and 100 million hepatocytes, respectively and cultured for a duration of 7 days. The scaffolds were seeded at a flow rate of 20 ml/min until the desired cell number per scaffold was achieved or if the number of entrapped cells did not significantly change over time. In both cases the cell seeding process did not exceed 15 minutes. Cells were seeded in a 90% air/10% CO_2 atmosphere. After the seeding process the flow rate was quickly switched to 15 ml/min for the remaining timeframe of the culture. It should be noted that the histology stains for the montage and single aggregate images were taken from two different

15 ml/min cultures. The individual stills that were used to construct the montage did not provide the resolution needed to differentiate between viable and non-viable cells as presented by haematoxylin nucleic acid staining.

Protein albumin synthesis shown in Figure 44, was maintained at a much higher rate per day than pervious cultures. The topmost rate of synthesis was recorded on the second day of the culture with a value of 28.615 µg/million cells/day. Protein production increased from day 1 to day 2 by 54% but decreased by 61% from day 2 to day 3. However production did, largely, remain constant until the last day where production abruptly plummeted by 72%. When compared to the control, the experimental culture bested it by 48% and 46% on day 1 and 2 respectively. It was not until the third day that synthesis in the control exceed that of the experimental condition. Furthermore, when evaluated using a paired t-test ($p > 0.05$), there was no significant difference in protein synthesis up to day 6. Significance was exhibited when the last day, from both groups, was factored into the analysis, which saw a 96% difference in secretion (4.68 vs. 114.01 µg/million cells/day).

Figure 45 shows urea secretion rates over the duration of the seven day culture. The highest point of ureagenesis was on day 1 with a value of 13.406 µg/million cells/day. Ureagenesis remained in the double digits for more than half the length of the experiment. Values dipped into single digit level on day 5 with a rate of 8.22 µg/million cells/day, which was a -29% change from the previous day. Similar to albumin, urea production reached its lowest level on the last day of the culture at 3.52 µg/million cells/day, which was a 51% drop from the previous day. When compared to the control the experimental condition outpaced it for the first two days with percent differences of 35% and 31% respectively. On the last day of the culture, which was the worst showing for the reactor but the best for the control, there was a production difference of 13.4 µg/million cells/day which translated to a 79% difference.

When evaluated using a paired t-test ($p > 0.05$), there was no significant difference in ureagenesis between both groups.

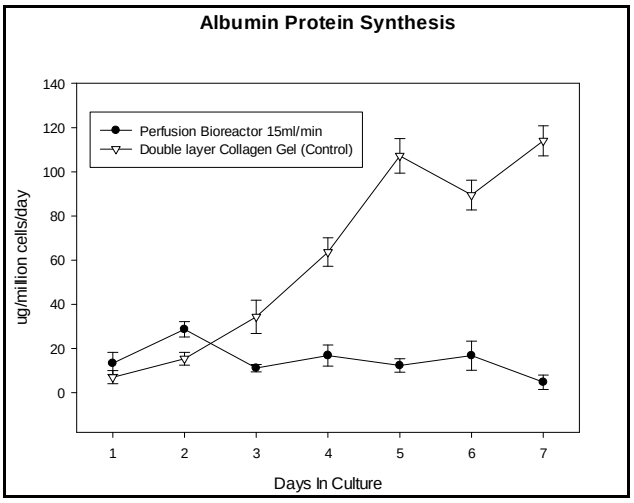

Figure. 44: Rate of albumin synthesis produced by hepatoctyes cultured at 15 ml/min vs. double layer collagen gel control. Error bars represent standard deviation of 2 repeated measurements.

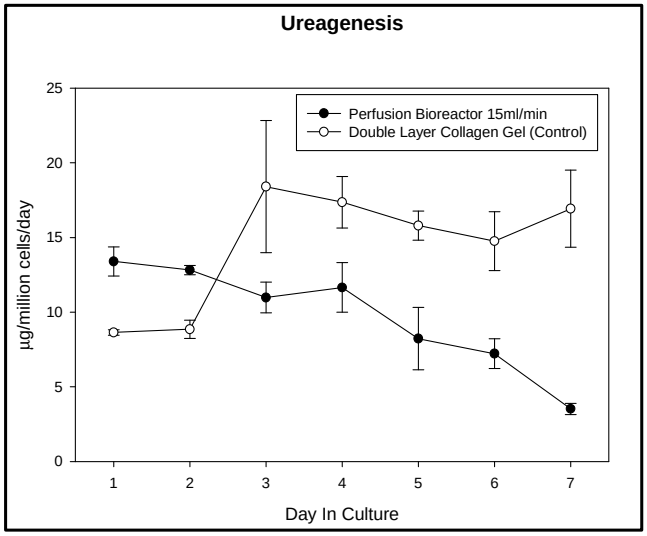

Figure. 45: Rate of Ureagenesis produced by hepatocytes cultured at 15 ml/min vs. double layer collagen gel control. Error bars represent standard deviation of 2 repeated measurements.

Figure 46 is a montage cross section that represents a segment of the scaffold. The majority of hepatocytes within the section are in aggregate form. Unlike previous cultures hepatocyte aggregation is very evident in all regions of the scaffold. However most of the cell masses are concentrated around the central port and, adjacent or in very close proximity to the oxygen tubing. Both of which are considered high oxygen tension regions of the scaffold. The size of the hepatocyte clusters appear to be larger in these areas and decreased in size downstream of the oxygen tubing. In addition to size, the geometry of each cluster, towards the inlet, appeared to be more irregular. The aggregates tend to be more ellipsoidal as they transition past the tubing to the scaffold periphery. Figure 47 A, B, C and D show that viability, as detected by visible nuclear staining, is well dispersed throughout the aggregate interior which would suggest that these cells were not deprived of oxygen and/or essential nutrients. This makes sense as these cells are located in high oxygen tension area. However aggregates in images 47 E and F, which are located towards the scaffold perimeter, also display comparable cell viability indicating good mass transport from inlet to outlet.

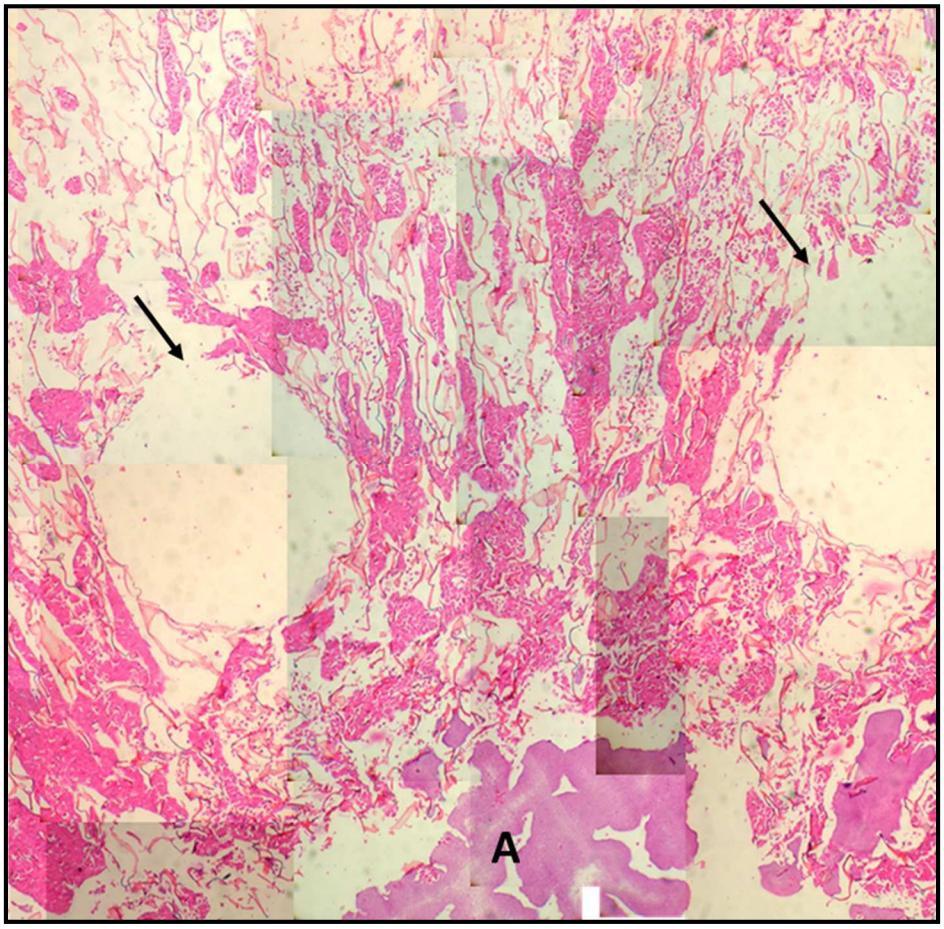

Figure 46: Histological montage (H&E stain) of scaffold cross-section from 15 ml/min bioreactor culture with direct and convective oxygenation. Arrows are pointing to embedded semi gas permeable tubing for direct oxygenation. A is positioned in the central port inlet.

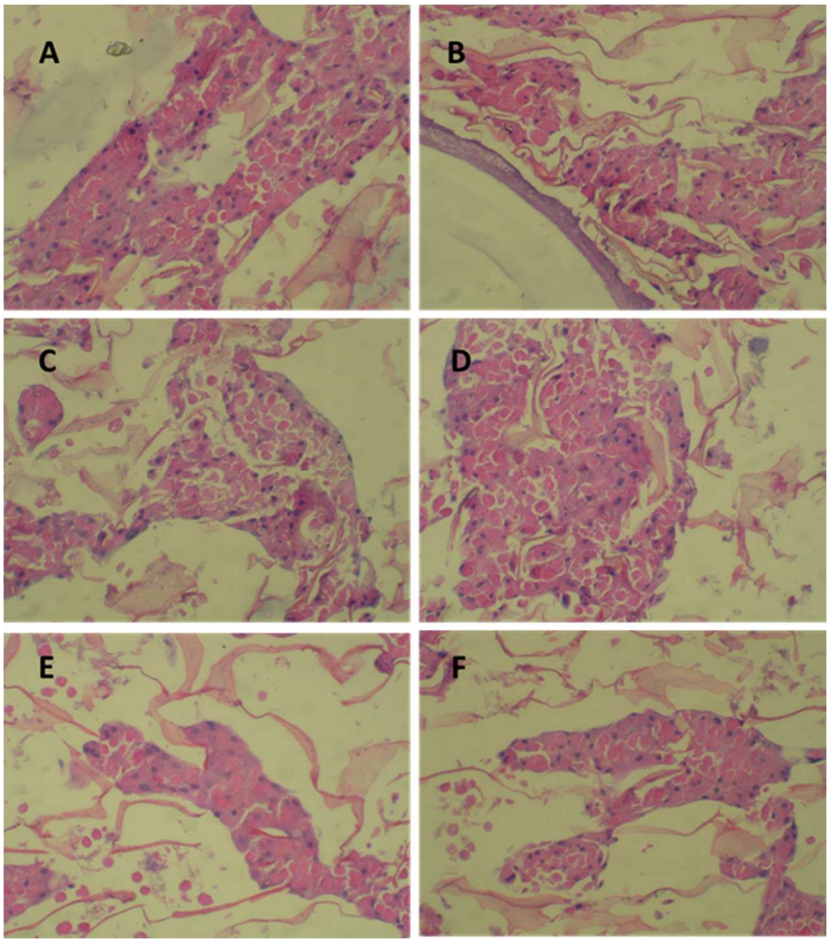

Figure 47: Enlarged images of cell aggregates from 15 ml/min flow rate bioreactor culture. A and B are aggregates located adjacent to the oxygen tubing. C and D are located in close proximity to the central port fluid inlet. E and F are positioned near the scaffold perimeter.

5.3.4 Effects of Direct Oxygenation and Convective Transport at 20 ml/min

The main objective of this trial was to observe how the perfusion rate of 20 ml/min impacts oxygen and nutrient transport, and hydrodynamic forces, which influences hepatic phenotypic behavior, morphology and death. The scaffolds used in both experiments were both seeded with 100 million hepatocytes and cultured for a duration of 7 days. The scaffolds were seeded and cultured at a flow rate of 20ml/min. In both cases the cell seeding process did not exceed 15 minutes. Cells were seeded and cultured in a 90% air/10% CO2 atmosphere. It should be noted that cultures at 20 and 25 ml/min were run simultaneously

from the same batch of isolated cells, and replicated with another isolated batch of cells on a different day.

The production of albumin per day is presented in Figure 48. Protein, in general, was secreted at very depressed levels each day of the experiment. The hepatocytes generated the most albumin (6.67 ug/million cells/day) on the first day of the experiment. On the second day of the culture expression rates decreased by 40%%. However levels seemed to stabilize at 4.2 ± .13 µg/million cells/day, with very little fluctuation over the next 3 days before dropping by 38% on day 5. It should be noted that production from day 5 to 7 also remained steady at an average of 2.5 ± 0.33 µg/million cells/day and a mean percent change of 19%. When compared to the control the experimental group secreted much less protein. The gap in synthesis continued to widen as the culture advanced. At the conclusion of the culture the control generated 100 µg (98%) more than the experimental group.

Figure 49 illustrates the amount of urea produced per day over the seven day culture period. Hepatocyte secretion was maximum on day 1 (4.8 µg/million cells/day) with very little variation over the first six days of the experimental period. The highest positive and lowest negative change was seen from day 1 to 2 (+Δ1.2 µg) and day 6 to 7 (-Δ 2.2 µg), respectively. Production was lowest on the last day of the culture with a value of 1.97 µg/million cells/day, which also showed greatest day-to-day slide of 52%. Contrasted to the experimental group, the control continuously generated more urea per day except for day 2. When averaged, there was little difference in the amount of urea produced on the first two days (4.2 µg – bioreactor vs. 4.5 µg – control). However on day 7 the gap in production was substantial at 16 µg/million cells/day or 89%.

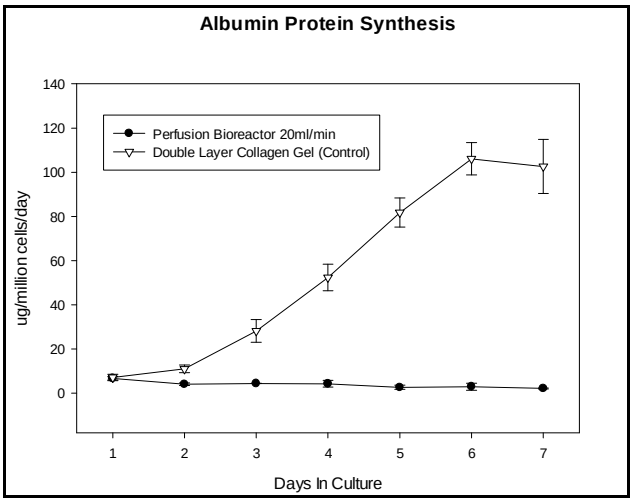

Figure 48: Rate of albumin synthesis produced by hepatoctyes cultured at 20 ml/min vs. double layer collagen gel control. Secretions rates for control were significantly higher when compared to perfusion bioreactor model. Error bars represent standard deviation of 2 repeated measurements.

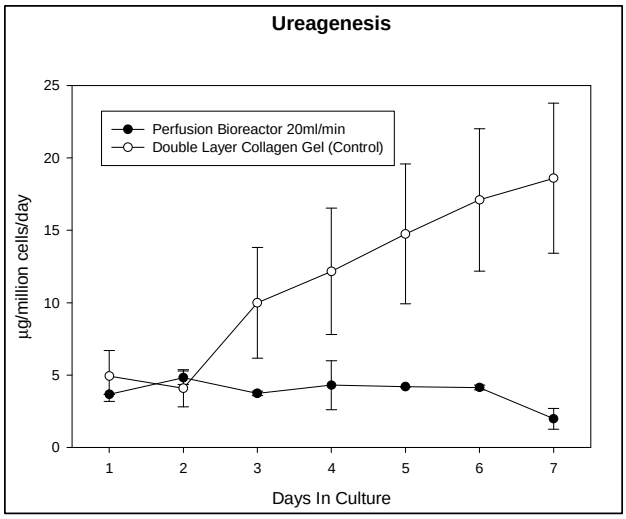

Figure 49: Rate of Ureagenesis produced by hepatocytes cultured at 20 ml/min vs. double layer collagen gel control. Secretion rates for control significantly outpaced those exhibited by the perfusion culture. Error bars represent standard deviation of 2 repeated measurements.

Figure 50 is a reconstructed montage cross section of the hepatocyte seeded and cultured scaffold at 20 ml/min. Under these conditions the cells were able to aggregate over the seven day period. Unlike the previous condition it seems that the distribution of the aggregates is more diffuse in nature which could be a function of the increased flow rate

pushing or repositioning cells within the micro-environment. This could also explain why more aggregates, in comparison to the previous condition, are noticeable towards the fluid outlet regions of the scaffold and not in the high flow rate fluid inlet area. Another explanation could be that high shear forces at the inlet caused cells to die thereby disrupting the aggregation process. However it is obvious that the bulk aggregate population is positioned between the oxygen tubing and not contiguous to the tubing. This is logical as this area has the greatest pore interconnectivity and is in the fluid path of least resistance from inlet to outlet. Because shear stress may be higher directly adjacent to the tubing, fluid displacement and a reduced flow area could also account for the high concentration of aggregates between the oxygen tubing.

In general the aggregates all look as if to have taken on the same shape, albeit varying in size. Figures 51 A, B, C and D indicate that the clusters contain a mixture of viable and dead hepatocytes. Although intact nucleic acid is present, when taking the biochemical output into account, it is clear that the viable cells are not functioning at full capacity. This could be due to shear stress imposed on the cells from the higher inlet flow rate.

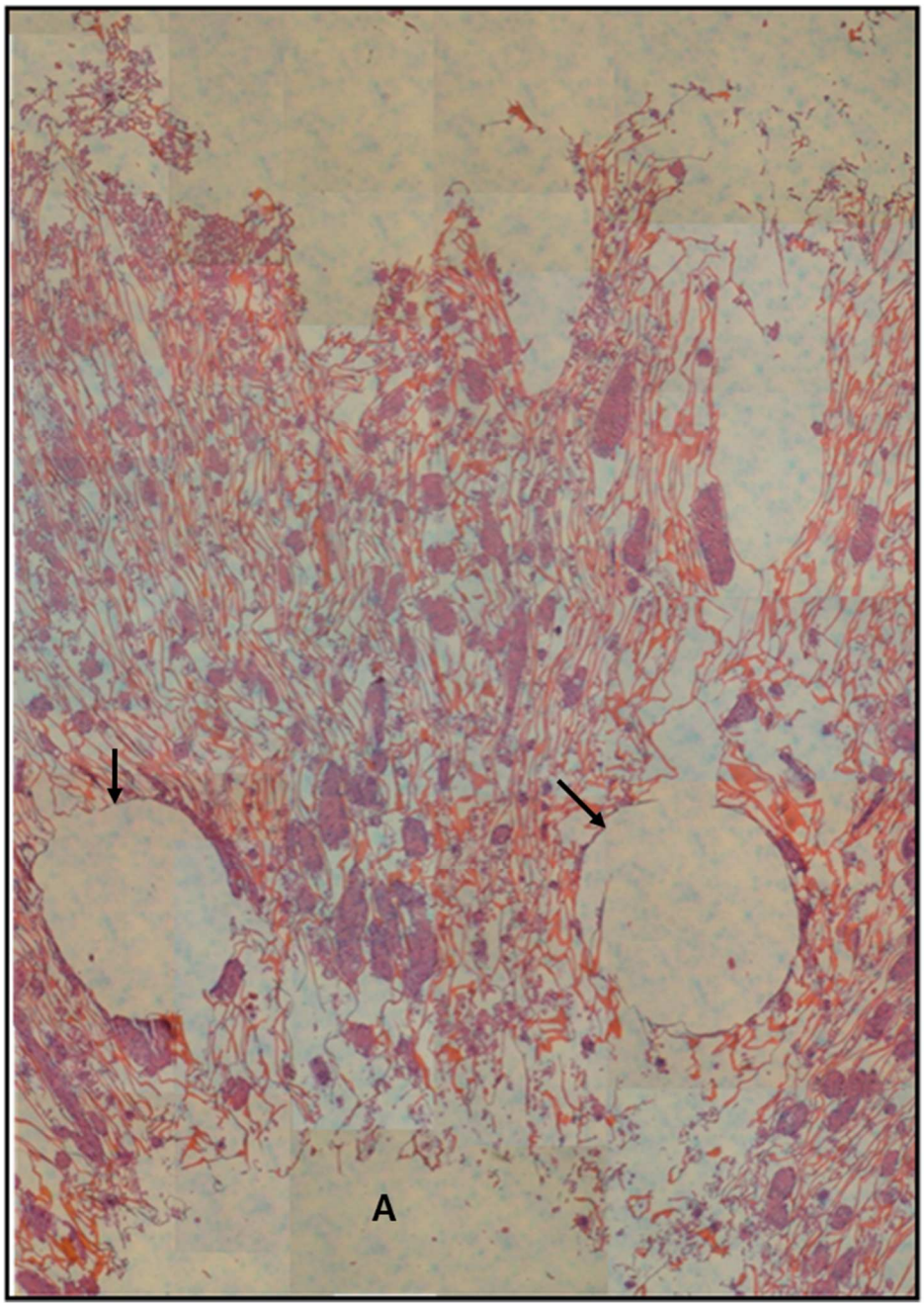

Figure 50: Histological montage (H&E stain) of 20 ml/min bioreactor culture with direct and convective oxygenation. Arrows are pointing to embedded semi gas permeable tubing for direct oxygenation. A is positioned in the central port inlet**.**

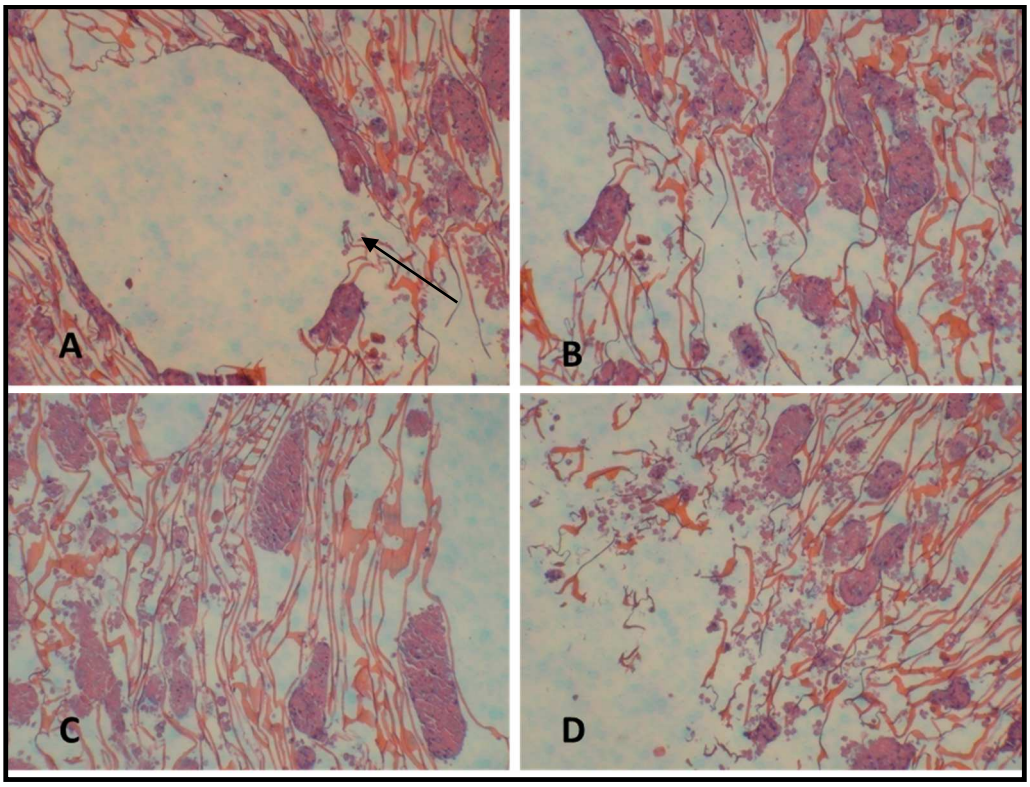

Figure 51: Enlarged images of aggregates cultured at 20 ml/min. A) arrow is pointing to area where semi-permeable oxygenation tubing was embedded. B) aggregates in area between oxygenation tubing. C) aggregates towards the scaffold border. D) aggregates adjacent to the central port fluid inlet.

5.3.5 Effects of Direct Oxygenation and Convective Transport at 25 ml/min

The main objective of this effort was to discern what impact, if any, does the flow rate of 25 ml/min have on hepatocyte functionality, spheroid formation and shape, and death. In this round of experiments scaffolds, in both trials, were seeded with 100 million hepatocytes and cultured for a duration of 7 days. The scaffolds were seeded at a flow rate of 20 ml/min until the desired number of cells were entrapped. The flow rate was subsequently switched to 25 ml/min for the duration of the culture period. In both cases the cell seeding process did not exceed 15 minutes. Cells were seeded and cultured in a 90% air/10% CO_2 atmosphere. It should be noted that cultures at 20 and 25 ml/min were run simultaneously from the same batch of isolated cells, and replicated with another isolated batch of cells on a different day.

The rate of albumin generated per day is presented in Figure 52. From the onset of the culture it was obvious that cell functionality was compromised. Protein expression reached its pinnacle on the first two days of culture with an average value of 4.43 ± 0.16 µg/million cells/day. Subsequent to this point synthesis fell sharply and output decreased 47% by day 3. Although there was a slight increase in production on day 4 and 5, by the end of the experiment, albumin secretion plummeted to 1.49 µg/million cells/day which equated to a 66% drop from the highest levels seen on day 1 and 2. When the results from the control group were compared to the experimental study, it's very obvious that the control group generated considerably more albumin on a per day basis. The gap in synthesis continued to widen as the culture advanced. At the conclusion of the culture the control generated 99% more protein than the experimental group.

Figure 53 shows the comparative rates of urea excretion by hepatocytes in the perfusion and control groups throughout the seven day study. Urea secretion from beginning to end was paltry. Rates on day 1 and 2 were relatively flat but increased 31% to reach its maximum value of 4.26 µg/million cells/day by day 3. Urea dropped by 17% by day 4 and remained rather constant (± .30) for the rest of the culture. Contrasted to the experimental group, the control performed much better per day. By the conclusion of the culture, the bioreactor culture was producing 15 µg/million cells/day or 62% less urea than the control group.

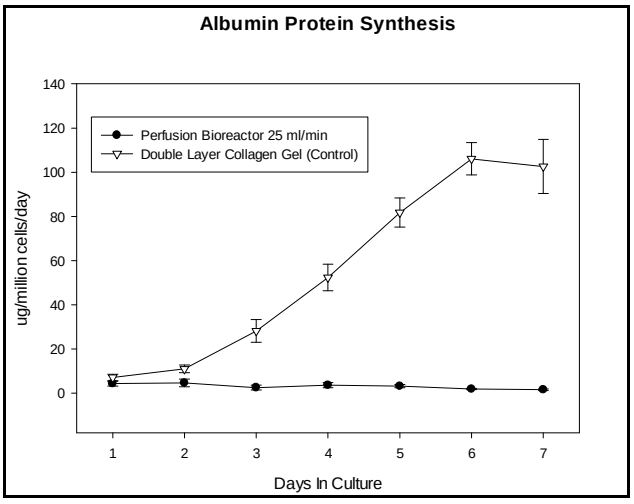

Figure 52: Rate of albumin synthesis produced by hepatoctyes cultured at 25 ml/min vs. double layer collagen gel control. Error bars represent standard deviation of 2 repeated measurements.

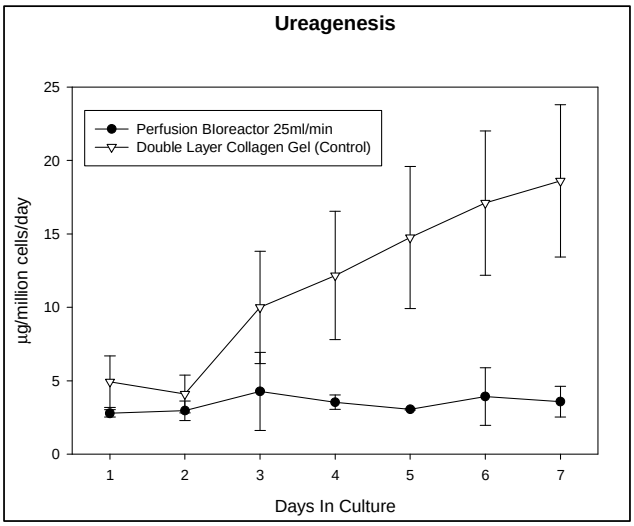

Figure 53: Rate of Ureagenesis produced by hepatocytes cultured at 25 ml/min vs. double layer collagen gel control. Error bars represent standard deviation of 2 repeated measurements.

Figure 54 is mosaic cross section of the hepatocyte embedded scaffold that was seeded and cultured at 25 ml/min. The overwhelming majority of hepatocytes were not able to form multi-cellular masses in this experimental setting. However spheroid formation is very noticeable in certain areas. Under the perfusion rate of 20 ml/min cell aggregation was mainly confined to the section between the oxygenation tubing as this was the assumed region

where the fluid trajectory was unburdened by the tubing. This image does deviate from this notion in that clustering is more prevalent around the inlet and adjacent to the oxygen tubing. It is also conceivable that the increased flow rate adversely affected the cell's ability to aggregate by adhesion molecule (E-cadherin or Integrin alpha 1) disruption. Although spheroid formation was negligible in the central body of the scaffold, the cells ability to interact seems to heighten towards the construct's border. This intensity of cell-to-cell interaction, at the margins, was not noticed in previous experiments. The shear stress in this area probably did not exceed the threshold for cell damage which permitted cells to aggregate and remain functional.

Of the hepatocytes that were able to form larger cell masses, the viability profile shown in Figure 55, in general, is very comparable to the previous cultures as these cells were randomly positioned and more than likely functioning at diminished capacities. In some masses it was observed that viable cells seem to be positioned one to two cell layers inward from the boundary. More than likely the cells at the aggregate border apoptosed due to the hydrodynamic force imposed on them. Regarding morphology, the aggregates in the front third of the scaffold, appear to be analogous to each other. The smaller cell clusters at the fluid egress also share the same shape.

Figure 54: Histological montage (H&E stain) of hepatocyte seeded scaffold cultured at 25 ml/mi. Arrows are pointing to embedded semi gas permeable tubing for direct oxygenation. A is positioned in the central port inlet.

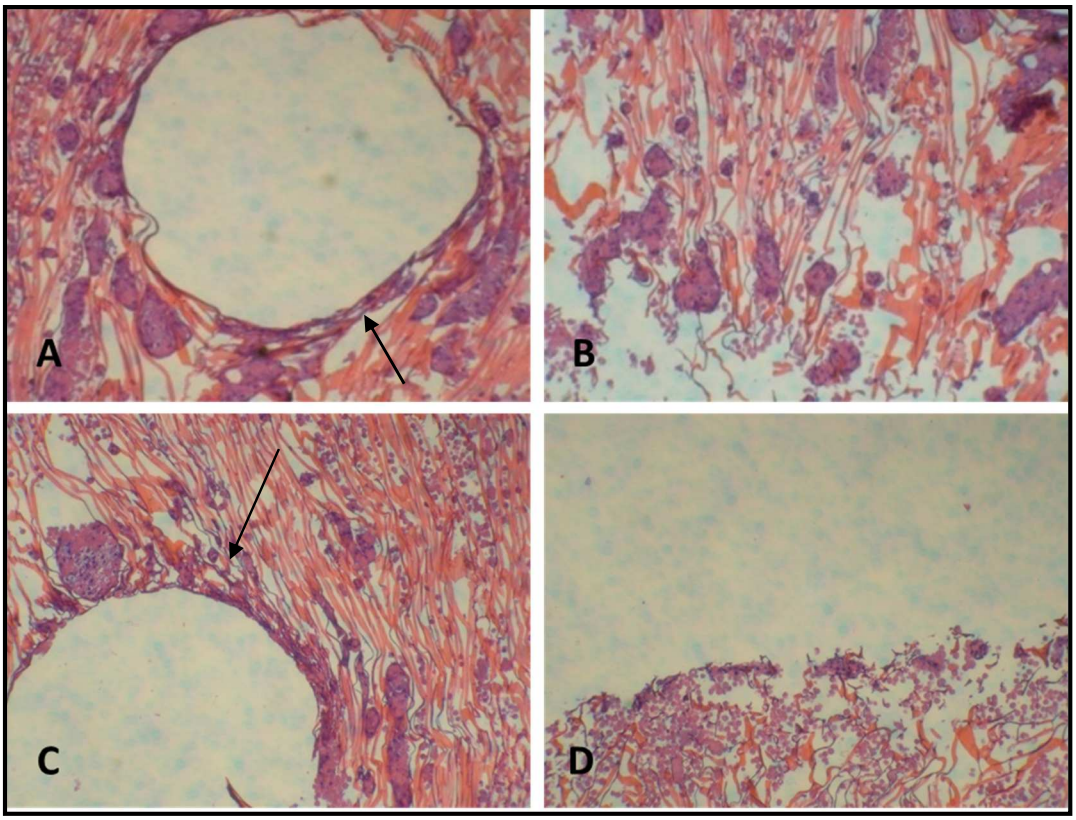

Figure 55: Enlarged images of aggregates cultured at 25 ml/min. A & C) arrows are pointing to areas where semi-permeable oxygenation tubing was embedded. B) hepatocyte spheroids adjacent to central port inlet. D) hepatocyte aggregates at scaffold border.

In addition to measuring against a control, results from all six experimental conditions were plotted together and compared versus each day in culture. Figures 56 and 57, show the compared results for albumin synthesis and ureagenesis versus each day in culture. When compared, the experimental condition of 15 ml/min, over the seven day timeframe, induced better albumin and urea secretion rates. Day 1 and day 2 expressed the best results for urea and albumin respectively. For both functional metrics 10 ml/min induced the second highest production rates followed by 5ml/min. On the day of peak functionality, albumin secretion at 15ml/min outpaced production at 10 ml/min by 68% and 87% under 5 ml/min. The contrast was not as stark for ureagenesis. The percent difference on day 1 between 15 and 10 ml/min was 24% and 59% between 15 and 5 ml/min. From both graphs it is evident that there is a causal relation between mass transport and flow rate. As the flow rate

increased from static to 15 ml/min so did the efficacy of mass transfer which is supported by higher protein and urea output. However because hepatocytes are shear averse the assumption that increased fluid velocity translates to better mass transport efficiency ergo enhanced liver-specific functionality is not sustainable. The inflection point where fluid flow became detrimental to hepatocyte phenotypic expression, most likely due to shear stress, was at 20 ml/min. At this rate and higher, biochemical yield was in general lower than the other dynamic cultures. Lastly, Figure 58 also shows somewhat of a relationship between flow rate and aggregate area. This relationship, to a lesser degree, does extend to the number of cell aggregates. When the montage images for all experimental conditions are equated it can be suggested that as flow rates increase, more cells masses are present. Though the appearance of more aggregates does seem to subside at 25 ml/min.

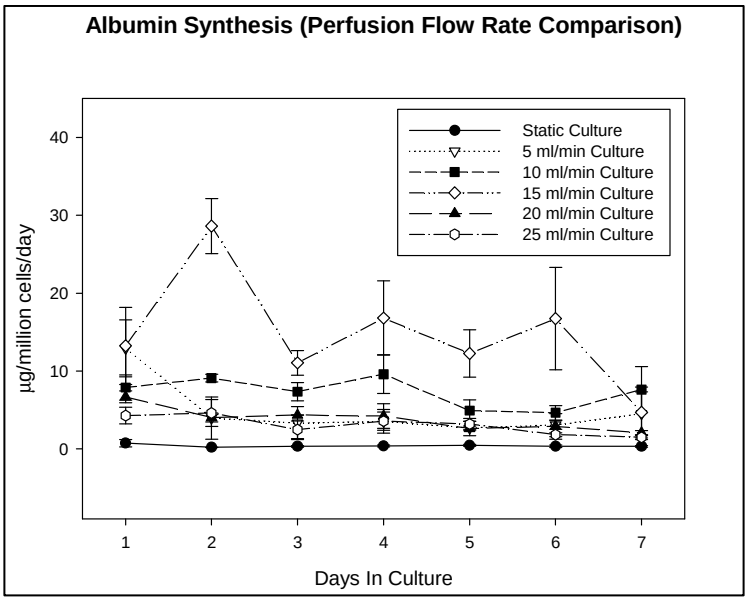

Figure 56: Albumin synthesis rates from each culture condition compared over the seven day culture period.

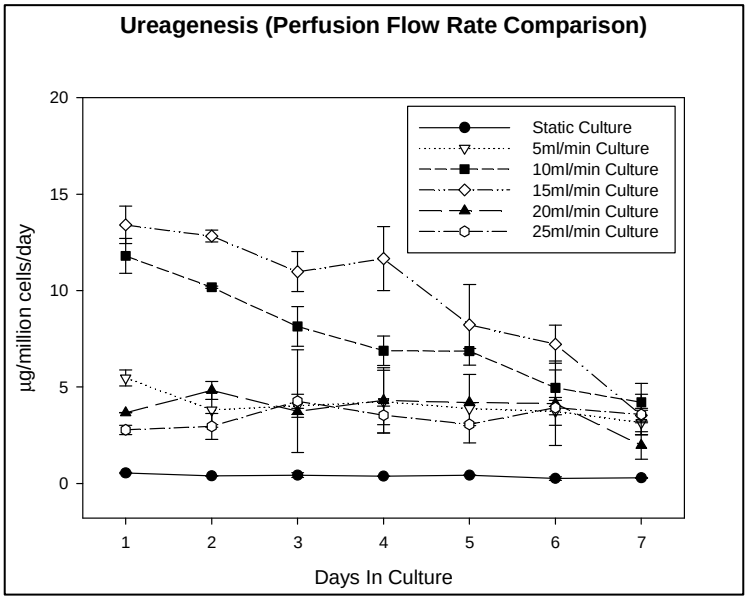

Figure 57: Ureagenesis rates from each culture condition compared over the seven day culture period.

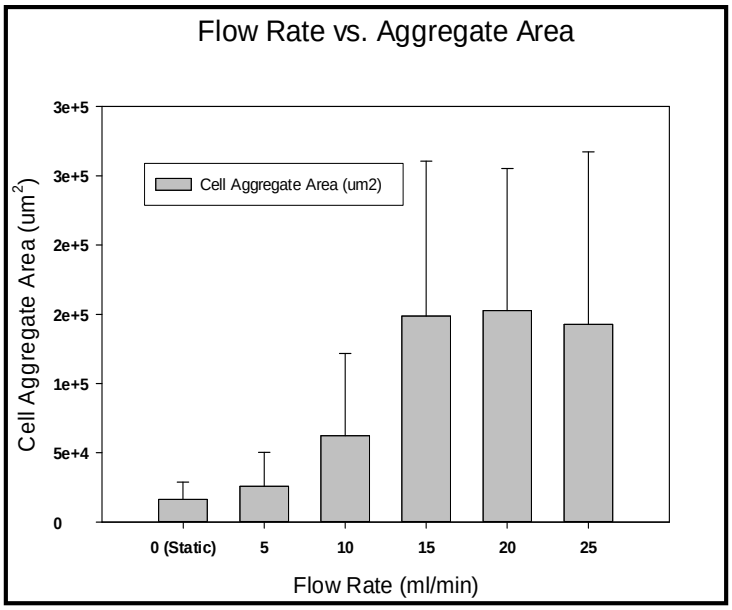

Figure 58: Flow rate culture conditions vs. hepatocyte aggregate area. Chart shows correlation between flow rate and hepatocyte area. Phase contrast microscopy images from replicates under each culture condition were used to generate area calculations.

	Static	5ml/min	10ml/min	15ml/min	20ml/min	25ml/min
Static	N/A	+	+	+	+	+
5ml/min	+	N/A	-	+	-	-
10ml/min	+	-	N/A	+	+	+
15ml/min	+	+	+	N/A	+	+
20ml/min	+	-	+	+	N/A	-
25ml/min	+	-	+	+	-	N/A

Table 5: paired t-test (equal variance) results that establish significance or insignificance between the effects of varying flow rates on albumin protein synthesis. Plus (+) denotes that there was a significant difference between the two populations. Minus (-) sign denotes that there was no significant difference between the two sample populations.

	Static	5ml/min	10ml/min	15ml/min	20ml/min	25ml/min
Static	N/A	+	+	+	+	+
5ml/min	+	N/A	+	+	-	-
10ml/min	+	+	N/A	-	+	+
15ml/min	+	+	-	N/A	+	+
20ml/min	+	-	+	+	N/A	-
25ml/min	+	-	+	+	-	N/A

Table 6: paired t-test (equal variance) results that establish significance or insignificance between the effects of varying flow rates on urea secretion. Plus (+) denotes that there was a significant difference between the two populations. Minus (-) sign denotes that there was no significant difference between the two sample populations.

A paired t-test (equal variance, $p>.05$) was performed on all samples from each experimental trial. From Table 5 the amount of albumin generated at 15 ml/min was statistically significant from every other group. The same can be said for urea except when compared to 10 ml/min where there was no statistical significance (Table 6). There was also no statistical significance between the 10 and 5 ml/min groups for albumin synthesis. Surprisingly there was no statistical difference between the data generated at 5 ml/min and, 20 ml/min and 25 ml/min for urea and albumin. This demonstrates how low flow (inefficient mass transfer) and excessive flow (damaging shear forces) can influence similar functional outcomes.

5.4 Discussion

Previous studies in this body of work demonstrated the iterative optimization of the current bioreactor perfusion system and the computational fluid dynamic simulations used to optimize inlet mass flow rates based on the oxygen uptake kinetics and hydrodynamic stress profiles with the scaffold micro-environment. In this study the flow rates utilized in the CFD simulations from the previous chapter were empirically evaluated to understand how shear

stress and mass transfer, via increased flow rates, affect cell morphology and spheroid formation, and liver-specific hepatocyte function with the scaffold micro-environment.

Dynamic cultures, regardless of the cell type, species, or dimension of the system (2D or 3D) tend to outperform their static counterparts. Every bioreactor culture condition in this study, irrespective of inlet flow rate, was continuously bested by its static control. However when these conditions are equated inter-experimentally, increased fluid flow, to a certain magnitude, did translate to better metabolic performance and, enhanced aggregate formation and area. This is likely due to better mass transport of oxygen and essential nutrients to hepatocytes, and the continuous removal of waste bi-products from the system. Moreover a similar perfusion study pointed out that increased fluid velocity, to a certain degree, produced a larger biochemical response (vs. static) because mechanical stress prompted the polymerization of actin fibers within the hepatic cytoskeleton, and subsequent cell aggregate-to-scaffold adherence [253]. These finding do suggest that within this experimental setup mechanical stress and mass transfer, both of which are facilitated by perfusion, do play a roles in fostering a micro-environment that is more conducive to spontaneous spheroid formation and enhanced cellular vitality. All of which are consistent with other hepatic perfusion bioreactor studies.

As the flow rate increased from static up to 15 ml/min there was a marketed surge in the number and area of hepatocyte clusters. The previous paragraph gave insight as why this happen mechanically. However from a gene expression perspective Hughes-Fulford and Chang [254] found that a number of beneficial genes are activated by intense cell-to-cell interactions. H*nf*4a (aka *Nr2a1*), a liver-enriched transcription factor known to be essential in maintaining mature differentiated liver function, was significantly upregulated in hepatic 3D aggregate cultures. In fact, of the genes activated due to hepatocyte aggregation more than 50% contained *HnF4a* binding sites. It concluded that aggregation is necessary for

maintaining *Hnf4a* expression and that it is a major transcriptional effector or master regulator of physiological hepatocyte function and phenotype.

The flow rate at which the benefits of efficient mass transport, facilitated through increase fluid flow, exceeded the threshold for compromised cell function, possibly through heightened shear stress, was observed at 20 ml/min. As experiments transitioned to higher flow rates (20 and 25 ml/min) it was quite evident that the hepatocyte's ability, over the duration of the culture, to establish cell-to-cell diminished. The lack of these interactions for anchorage dependent cells leads to depressed metabolic activity. The first mechanism that induces this form of cell death occurs when E-cadherin expression is perturbed or absent. E-cadherins are Ca^{2+}-dependent, cell-to-cell adhesion molecules that that have been implicated as a sources of cell death in epithelial cells when abrogated [255]. A study conducted by Nyberg et al. showed that E-cadherin inhibition produced maximal cell death, induced heightened levels of DNA fragmentation and suppressed spheroid formation. The study also concluded E-cadherins are responsible for protecting hepatocytes from caspase-independent apoptosis. Another study involving Nyberg showed that E-cadherins are present along the basolateral membrane between rat hepatocyte spheroids and their reduced interactions on the hepatic surface maybe responsible for increased cell loss [256]. These results lend more credence to the results presented in this study as the final hepatocyte orientation, post seeding, is random.

β-1 integrins are part of a family of adhesion molecules that contain numerous cell receptors that help govern cell-to-ECM interactions and trigger cell-survival signaling cascades during cell–ECM contact. It has been shown in epithelial cell cultures that caspases are activated during apoptosis in the absence of β1-integrin mediated signaling events [257]. From a histological examination it is evident that hepatocytes, in this study, are in contact with their ECM environment which would suggest that the upregulation of β-1 integrin expression

via cell-to-ECM interaction occurred or was feasible. However high shear forces imposed on the cells at the 20 and 25 ml/min conditions most like caused the cells to die either before or after the hepatocytes were able to establish contact with chitosan/collagen ECM. If cell death occurred after ECM attachment this could suggest that the death mechanisms caused by shear stress take precedence over those that lead to cell survival through β-1 integrin expression.

It is necessary to also mention how the direct application of shear stress up-regulates the expression of certain genes and proteins that can mediate cell death through pro-apoptotic pathways. Plasminogen activator inhibitor 1 (PAI-1) is involved in a number of biological processes such as cell migration, angiogenesis and ECM degradation. It was demonstrated that hepatocytes, when exposed to shear stresses up to 40 dyne/cm2, exhibited marketed increases in PAI-1 mRNA expression and PAI-1 protein release through the cooperative interactions between the transcription factors Sp1 and Ets-1 [258]. ECM accumulation is the hallmark of hepatic fibrosis. It has been shown that the overexpression of PAI-1 induces ECM accumulation and mitochondria-mediated apoptosis through TGF-B1 molecular mediators - Smad3/4 and p38 [259] . Both observations taken together might describe or provide an alternate explanation as to how excessive hydrodynamic forces, either debilitate hepatic functionality or encourage apoptotic cell death.

5.5 Conclusion and Future Work

The hepatocyte's ability to synthesize albumin protein and modify ammonia into urea are two major hallmarks of in-vivo function. Both of which were used to gauge the overall performance of this system. The results introduced in this chapter demonstrated that isolated primary hepatocytes can re-aggregate under mechanical stress and maintain cell vitality for the duration of the designated culture period. The data presented in this body of work also reveals how shear stress and mass transfer, both functions of fluid flow within the scaffold

micro-environment, can be tuned to foster optimum cellular output within this system. Because of the work conducted in this chapter and the understanding of oxygen uptake kinetics provided in the previous chapter, the flow rate 15ml/min at the central port inlet will be used for the remaining bioreactor experiments.

Efficient mass transfer of oxygen and essential nutrients, and the cell's ability to spontaneously aggregate are two major factors that influence the maintenance of mature hepatocyte differentiation. Thus improving both aspects would lend to the performance and viability of the scaffold-bioreactor complex utilized in this study. In the following chapter scaffold dimensions are reduced to determine if decreasing the cell number-to-scaffold void volume ratio can promote better metabolic activity. It is hypothesized that by doing this hepatocyte spheroids will be closer in proximity to an oxygen source (i.e. oxygen tubing or media), the time needed to aggregate will be mitigated while the number of aggregates will increase and the mass transfer distance to cells masses located at the scaffold periphery will be attenuated.

CHAPTER SIX: EVALUATION OF HOW THE REDUCTION IN SCAFFOLD DIMENSIONS AND INCREASED CELLULAR COMPACTNESS INFLUENCE LIVER PHENOTYPIC EXPRESSION AND AGGREGATE FORMATION

6.1 Introduction

Hepatocyte spheroid formation, in vitro, helps to mimic the in vivo morphology and ultrastructure by reestablishing necessary intercellular communication channels. The beneficial role of spheroids in recapitulating in vivo-like polarity and, maintaining viability and overall differentiated functionality has been well documented [260-262] especially when compared to hepatocytes cultured as monolayers. One of the challenges for perfusion-based seeding of single cell suspensions in bulk scaffolds is controlling the overall size and dimensions of the eventual hepatocyte aggregates. To some degree this can be controlled by the size and direction of the pore structure within the construct's interior. However just as important is creating a micro-environment that facilitates enhanced flow-mediated spheroid formation of these single cells suspensions during the seeding process.

The holy grail of tissue engineering scaffolds is to generate a construct that can fully integrate into and mimic the native tissue microenvironment, and facilitate fast functional regeneration of the defected tissue space. Much effort has been spent on understanding the how pore size [263-265], porosity [181, 265], scale of pore interconnectivity [266, 267] influence graft integration, mechanical stability and overall functionality of the scaffold's cellular inhabitants. However reciprocal energies have not been given to ascertaining how geometry, or more germane to this case, the geometrical size with increased cell density can modulate native cellular responses. Rumpler et. al demonstrated how geometrical features and scaffold size strongly influenced local growth rates of tissue formed by osteoblasts [268].

Troken et. al. reported the positive effects, via von Kossa staining, that increased hMSC-derived chondrogenic and osteogenic cells packing had on mineral deposition in in-vitro cultures [269]. Similarly with hepatocytes, higher density seeded scaffolds tend to induce more favorable cellular responses. Dvir-Ginzberg et. al. [270] showed the positive relationship between increased cell packing densities within alginate scaffolds and liver specific functionality. Essentially as hepatocyte densities increased viability, metabolic functionality and *P*-450 activity not only increased but were maintained at high levels for the duration of the culture periods. Furthermore in-vivo characteristics were more prominent with increased cellular compactness.

In the previous chapter it was noticed that the overwhelming majority of cellular clusters in the 15ml/min culture were localized between the central inlet-port and oxygen tubing. The aim of this chapter was to evaluate the effect that reducing the scaffold diameter/thickness and the mass transfer distance (i.e from central inlet to scaffold perimeter) has on cell aggregation, viability and overall functionality. The working hypothesis for this experiment was that increasing the cell packing density by decreasing the scaffold volume will increase the hepatocytes' ability to form more multi-cellular clusters thereby facilitating better cell-specific functionality byway of enhanced cell-to-cell and cell-to-ECM interactions. Because heightened aggregation can pose mass transfer limitations [193, 271], minimizing the gap between cells and, the main and adjunctive oxygen sources (central port inlet and oxygenation tubing respectively), will help overcome these limitations and aid in supporting hepatic respiration. Porous chitosan scaffolds at 14% and 30% of the original thickness were generated, seeded with hepatocytes, cultured in perfusion for the duration of seven days and assessed for their beneficial contribution to hepatocyte phenotypic expression.

6.2 Materials and Methods

6.2.1 Sources of Materials and Reagents

Medium molecular weight chitosan and glacial acetic acid were purchased from Sigma Aldrich (St. Louis, MO).

6.2.2 Scaffold Fabrication

Scaffold fabrication technique used in making the scaffolds for the experiments conducted in this chapter are consistent with those used in previous chapters. The scaffold diameters were decreased by 14% (1.29 cm) and 30% (1.05 cm). The height of the scaffold remained constant at 2.5 cm (Figure 59).

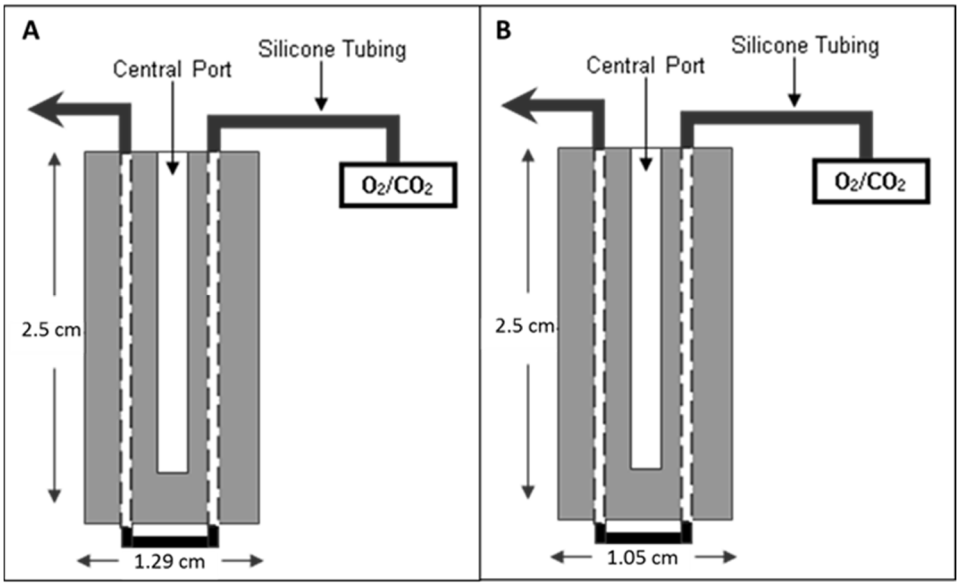

Figure 59: Schematic of 14% and 30% reduced diameter chitosan scaffolds with Silicone Tubing

6.2.3 Hepatocyte Isolation

The technique, type of rats and reagents used to isolate and purify the hepatocytes used in these experiments were consistent with those from chapter 3. Briefly, the hepatocytes were isolated from Fisher rats by a modified two-step collagenase perfusion technique.

6.2.4 Culture Conditions

The medium makeup (i.e components and concentrations) used for the experiments conducted in this chapter were similar to those used in chapter 3. However in this chapter hepatocytes were seeded and culture with a flow rate of 15 ml/min. All cultures were maintained in an atmosphere of 90% air/10% CO_2 which preserved the pH at ~7.2.

Albumin protein synthesis and ureagenesis assays were performed to assess efficacy of the bioreactor studies. The volume of medium in the bioreactor system and concentration of cells seeded in each scaffold were factored into both calculations. Similar to chapter 3 two double layer collagen sandwich culture systems were run in parallel with each bioreactor and utilized as controls. The protocols for cell concentration, volume of medium used and top collagen layer integration were consistent with those used in chapter 3.

The medium was extracted and replenished daily for both culture systems. All samples were stored at 4℃ until analysis were perf ormed. Hepatocyte morphology and viability were ascertained by Hematoxylin and Eosin Y staining.

6.2.5 Metabolic Output Measurements

Enzyme Linked Immunoassay (ELISA) for Albumin

The protocol, reagents and instrumentation used to perform the ELISA assays for these experiments were consistent to those from chapter 3.

Urea Assay

The protocol, reagents and instrumentation used to perform the urea colorimetric assays for these experiments were consistent to those from chapter 3.

6.2.6 Histological Analysis

The protocol, reagents and instrumentation used to perform the histological analysis for these experiments were consistent to those from chapter 3

6.2.7 Statistical Analysis

The biochemical functional output of the hepatocytes were calculated from duplicate runs. The rates per day were averaged across duplicate runs and values are reported as mean ± standard deviation.

6.3 Results

6.3.1 Effects of 14% Reduction in Scaffold Diameter

The focus of this effort was to recognize what effect or impact that reducing the scaffold's diameter by 14% (1.29 cm) had on spheroid formation which subsequently modulates hepato-cellular functionality and overall viability. In this round of experiments scaffolds were seeded with 87.5 and 90 million hepatocytes and cultured for a duration of 7 days. Based on the shear stress data presented in the previous two chapters the scaffolds were seeded at a flow rate of 15 ml/min for no more than 15 minutes. The time limit of 15 minutes was used in order to maintain continuity with previous experiments and to better compare data from chapter 5. Cells were seeded and cultured in a 90% air/10% CO_2 atmosphere. It should be noted that cultures with scaffold reductions of 14% and 30% were run simultaneously from the same batch of isolated cells, and replicated with another batch of isolated cells on a different day.

The rate of albumin secretion per day is exhibited in Figure 60. Protein expression under this culture condition reached its maximum level on day one with a value of 8.41 µg/million cells/day. From this point to on the secretion rates continued to drop with the final output of 1.84 µg/million cells/day on day 7. This represented a 78% decrease in functionality when compared to day one of the culture. When the results from the control group were compared to the experimental study, it's very obvious that it generated considerably more albumin on a per day basis. However it should be noted that the experimental group did outpace the control by .17 µg/million cells/day or 2% on day 1. From day 2 to 7 the margin

between the two groups increased and reached a peak difference of 112 µg/million cells/day or 98% at the conclusion of the experiment.

Figure 61 shows the comparative rates of urea excretion by hepatocytes in the perfusion and control groups throughout the seven day study. Similar to albumin, urea secretion on the first day of the culture reached its maximum value (5.476 µg/million cells/day) and exceeded that of the control group by .62mg/million cells/day or 11%. The amount of ammonia conversion from day 2 to 4 was relatively flat in that only a 10% decrease in phenotypic function was identified. Urea rates did exhibit downward shifts from day 5 forward with the final value of 1.655 µg/million cells/day on day 7. When contrasted to the experimental group, the control performed much better per day, except on day 1. By the conclusion of the culture, the bioreactor culture was producing 18.92 µg/million cells/day or 92% less urea than the control group.

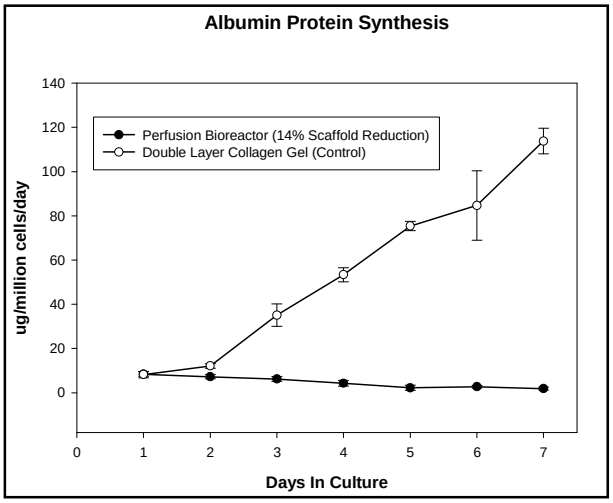

Figure 60: Rate of albumin synthesis produced by hepatoctyes cultured in scaffold with 14% reduced diameter vs. double layer collagen gel control. Error bars represent standard deviation of 2 repeated measurements.

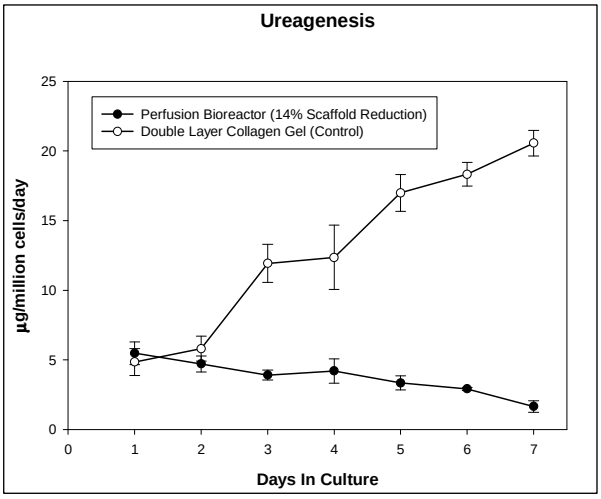

Figure 61: Rate of ureagenesis produced by hepatoctyes cultured in scaffold with 14% reduced diameter vs. double layer collagen gel control. Error bars represent standard deviation of 2 repeated measurements.

Figure 62 is a mosaic cross section of the hepatocyte seeded scaffold whose diameter was decreased from 1.5 cm to 1.29 cm, constituting a 14% reduction. Based on the montage it is clear that the majority of the pore space is occupied by hepatocytes. Spheroid formation was minimal and confined to areas adjacent to the oxygen tubing and central port inlet. There was also marginal aggregation in certain regions between the oxygenation tubing and by the fringes of the construct. Of the hepatocytes that were able to aggregate their morphology was very thin in width and lengthy, and did not resemble the irregular geometry of the previous 15 ml/min culture. The viability profile displayed in Figure 63 A, B, C and D showed that there is minimal cells that survived the experimental culture period. Based on the metabolic data in the aforementioned paragraphs it is evident that those that did survive were functioning in a very depressed state.

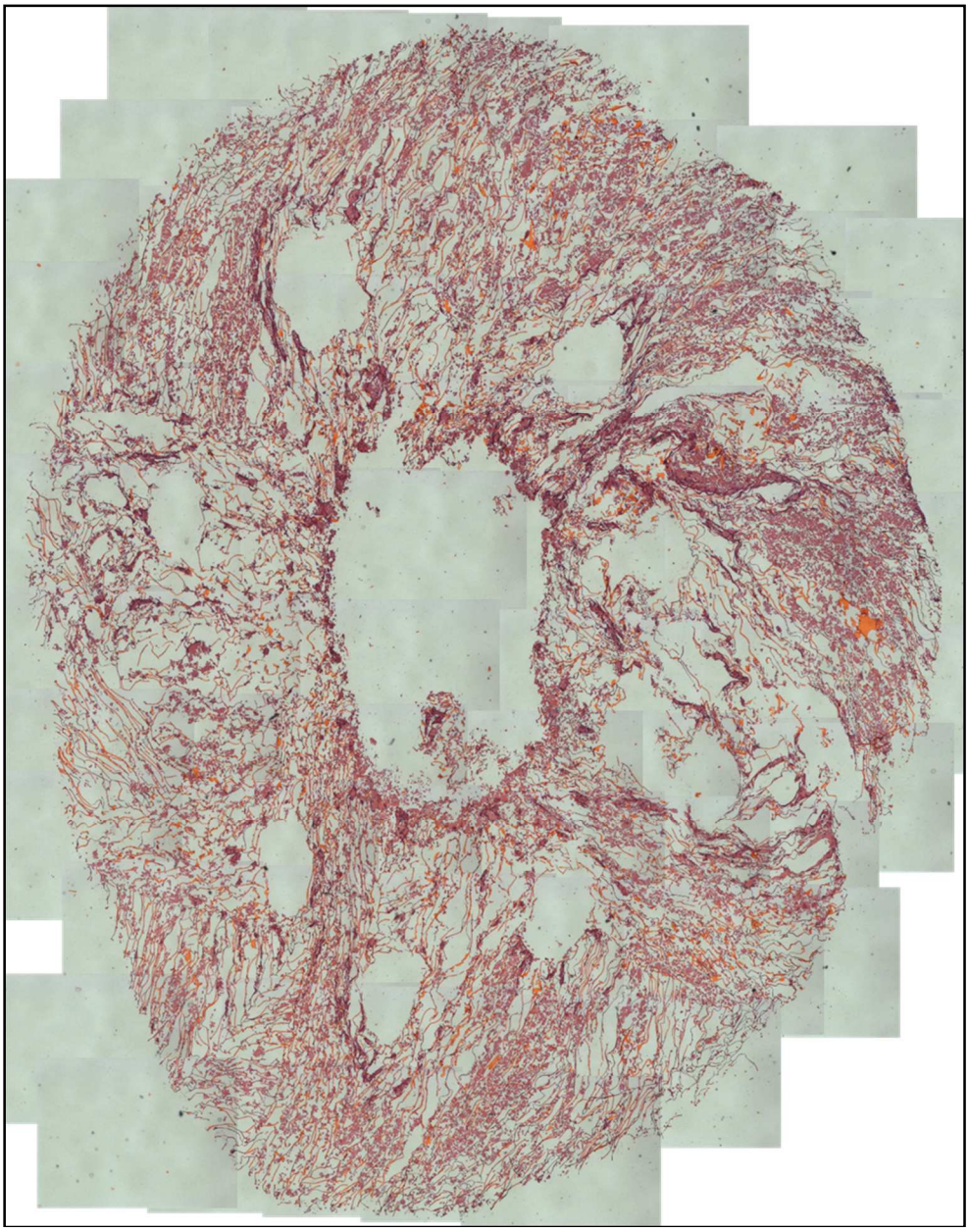

Figure 62: Histological montage (H&E stain) of hepatocyte seeded scaffold with a 14% reduction in the diameter.

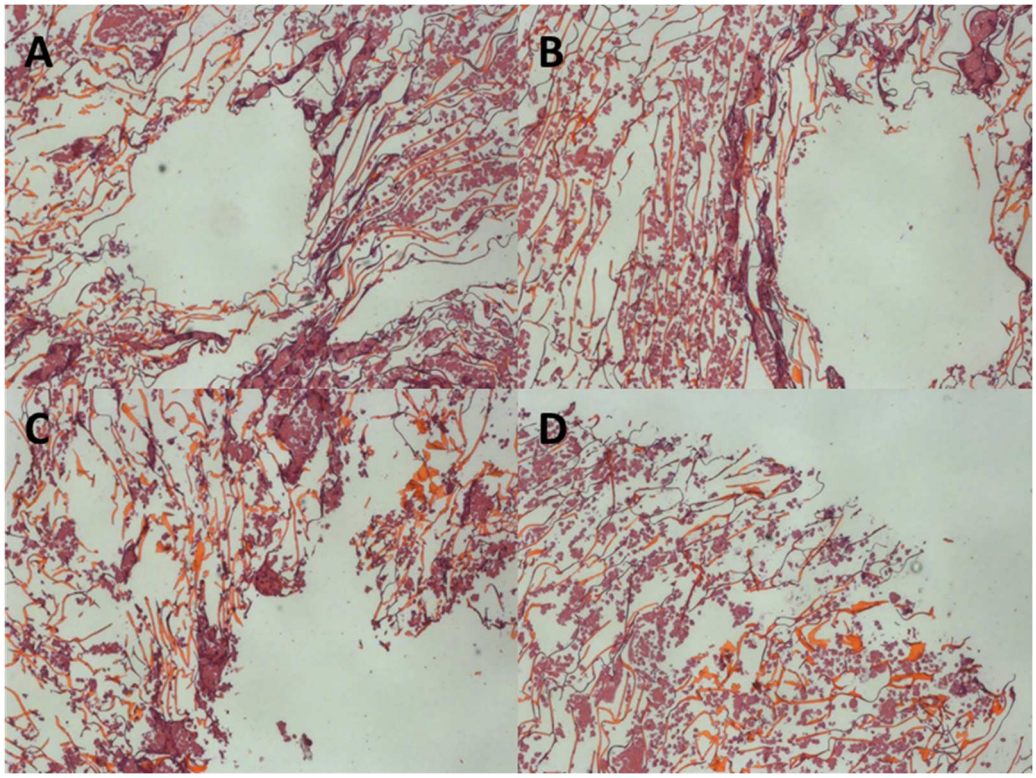

Figure 63: Enlarged images of single cells and aggregates cultured in the scaffold with a 14% reduced diameter. A & B) displaying hepatocytes and clusters adjacent to oxygenation tubes. C) hepatocytes and spheroids adjacent to central port inlet. D) hepatocytes and aggregates at scaffold border.

6.3.2 Effects of 30% Reduction in Scaffold Diameter

In this experiment the diameter of the scaffold was reduced by 30% (height did not change) to understand how decreasing the total mass transport distance (from central port to outlet) and increasing cell density within the construct would affects cells' ability to form mult-cellular aggregates, function and remain viable for the duration of the culture period. The scaffolds used in both experiments were seeded with 83 million and 81 million hepatocytes, respectively and cultured for a duration of 7 days. The scaffolds were seeded at 15 ml/min and maintained at this flow rate for the length of the culture. It should be noted that cultures with scaffold reductions of 14% and 30% were run simultaneously from the same batch of isolated cells, and replicated with another batch of cells isolated on a different day.

Protein albumin synthesis shown in Figure 64, was maintained at a much higher rate per day than all cultures presented in previous chapters. The topmost rate of synthesis was recorded on the second day of the culture with a value of 32.63 µg/million cells/day. The greatest increase in protein production (35%) was observed from day 1 to day 2. Secretion rates, in general, remained constant until the last day where production dropped by 27% to 22.19 µg/million cells/day. When compared the control the experimental culture secreted 61% and 63% more protein on day 1 and 2 respectively. It was not until the third day that synthesis in the control exceed that of the experimental condition. When evaluated using a paired t-test ($p > 0.05$), there was no significant difference in protein synthesis between both groups.

Figure 65 shows urea secretion rates over the duration of the seven day culture. Overall ureagenesis was maintained for the duration of the culture although there was a continuous decrease in rates as the culture progressed. However it should be noted that levels, on a day-to-day basis, did remaining higher than any previous experimental culture presented in this body of work. Days 1 and 2 both exhibited very similar rates of urea production, 18.189 and 18.334 µg/million cells/day respectively, and were the highest points of production for the span of the culture. Ureagenesis remained in the double digits for 5 out of 7 days. Values dipped into single digit level on day 6 with a rate of 6.81 µg/million cells/day, which was a -44% change from the previous day. The lowest level of 5.830 µg/million cells/day was observed on the last day of the culture which only represented a -14% from the previous day. When compared to the control the experimental condition outpaced it for the first four days with percent differences of 73%, 68%, 19% and 12%. On the last day of the culture, which was the worst showing for the reactor but the best for the control, there was a production difference of 14.74 µg/million cells/day which translated to a 71% difference.

When evaluated using a paired t-test ($p > 0.05$), there was no significant difference in ureagenesis between both groups.

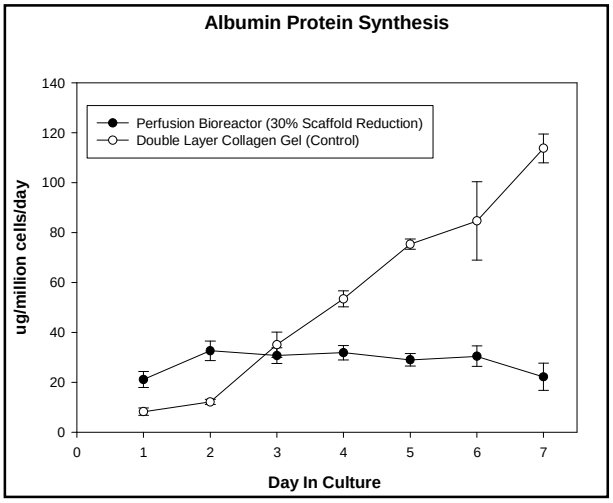

Figure 64: Rate of albumin synthesis produced by hepatoctyes cultured in scaffold with 30% reduced diameter vs. double layer collagen gel control. Error bars represent standard deviation of 2 repeated measurements.

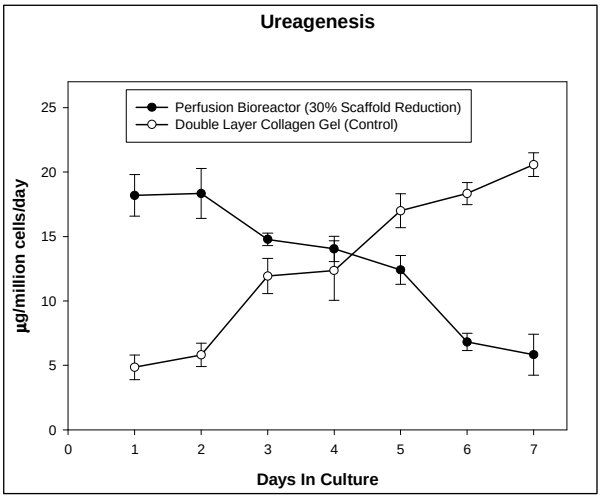

Figure 65: Rate of ureagenesis produced by hepatoctyes cultured in scaffold with 30% reduced diameter vs. double layer collagen gel control. Error bars represent standard deviation of 2 repeated measurements.

Figure 66 is a montage that represents a complete cross section of the scaffold diameter. The majority of hepatocytes within the section are, for the most part, were able to form and sustain multi-cellular masses. Hepatic aggregation is very pronounced in all regions of the scaffold with great evidence of such in regions near the central port, oxygenation tubing, midsections between the tubes and at the scaffold periphery. Because the majority of the scaffold's interior was either adjacent or in close proximity to the central port and gas permeable tubing, the bulk of the construct can be classified as a high oxygen tension region. The size of the hepatocyte aggregates, in general, appear to be larger in and around the central port and decrease downstream of this area. However aggregates of comparable size can be observed around the construct's periphery (Figure 67 C). The geometry of the aggregates in the midsections follows no distinct pattern although those near the oxygen tubing tend to mold themselves to the contours of the impregnated tubing. Figure 67 A, B, C and D show that viable cells are well dispersed throughout the aggregate interior which would suggest that these cells were not deprived of oxygen and/or essential nutrients. It should be noted that all viable cells, as detected by intact nucleic acid, are in aggregates. Viability among single cell hepatocytes was not evident. Aggregates located at the scaffold perimeter (Figure 67 D), also displayed viable cells which would indicate that these cells too were not deprived of nutrients or appropriate oxygen tensions. However there are peripheral segments of the scaffold where cell numbers are low or non-existent. It's assumed that larger spheroids before this area blocked fluid flow to these parts thus causing uneven flow distribution and diminishing the chances for aggregation and survival.

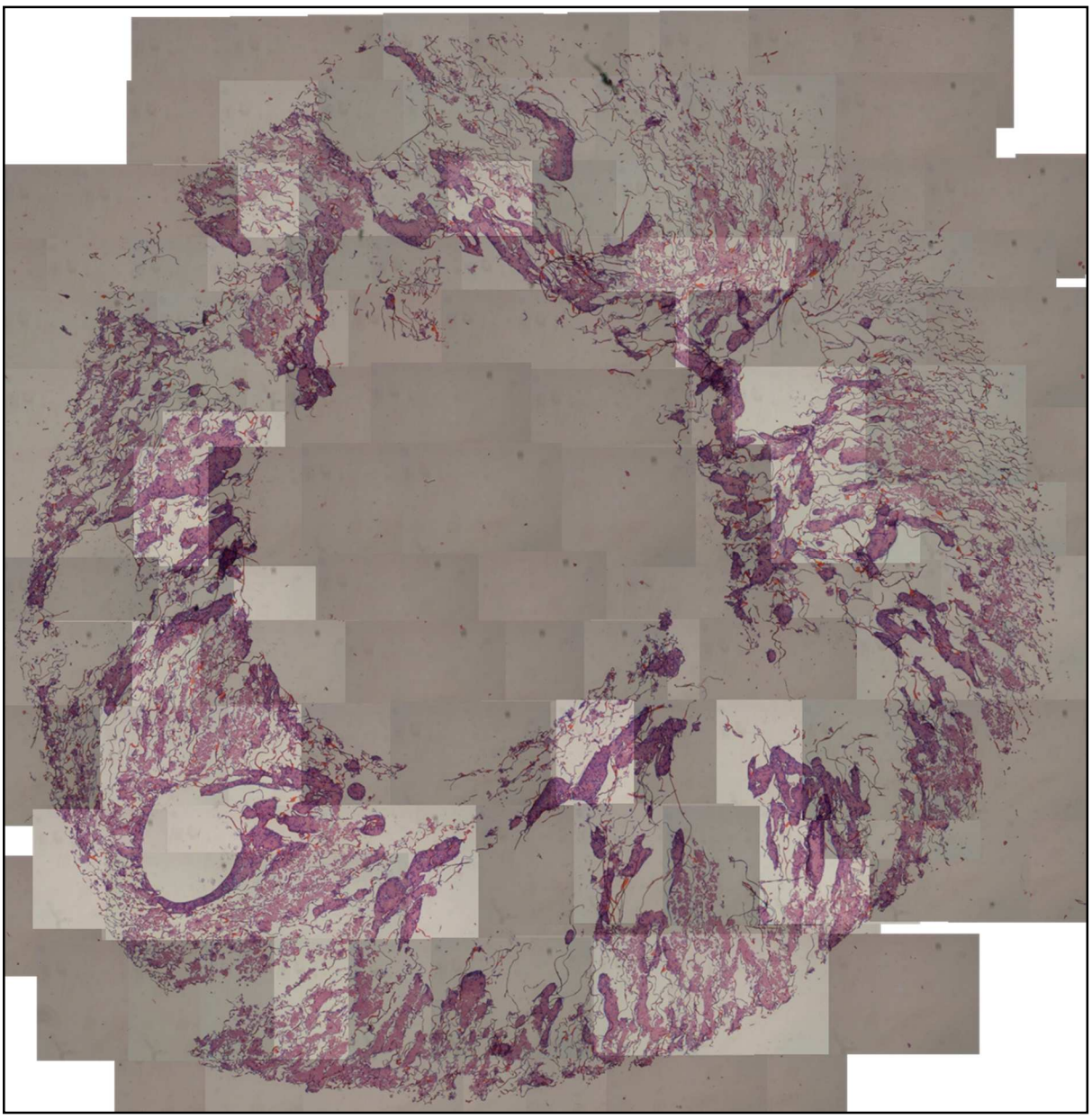

Figure 66: Histological montage (H&E stain) of hepatocyte seeded scaffold with a 30% reduction in the diameter.

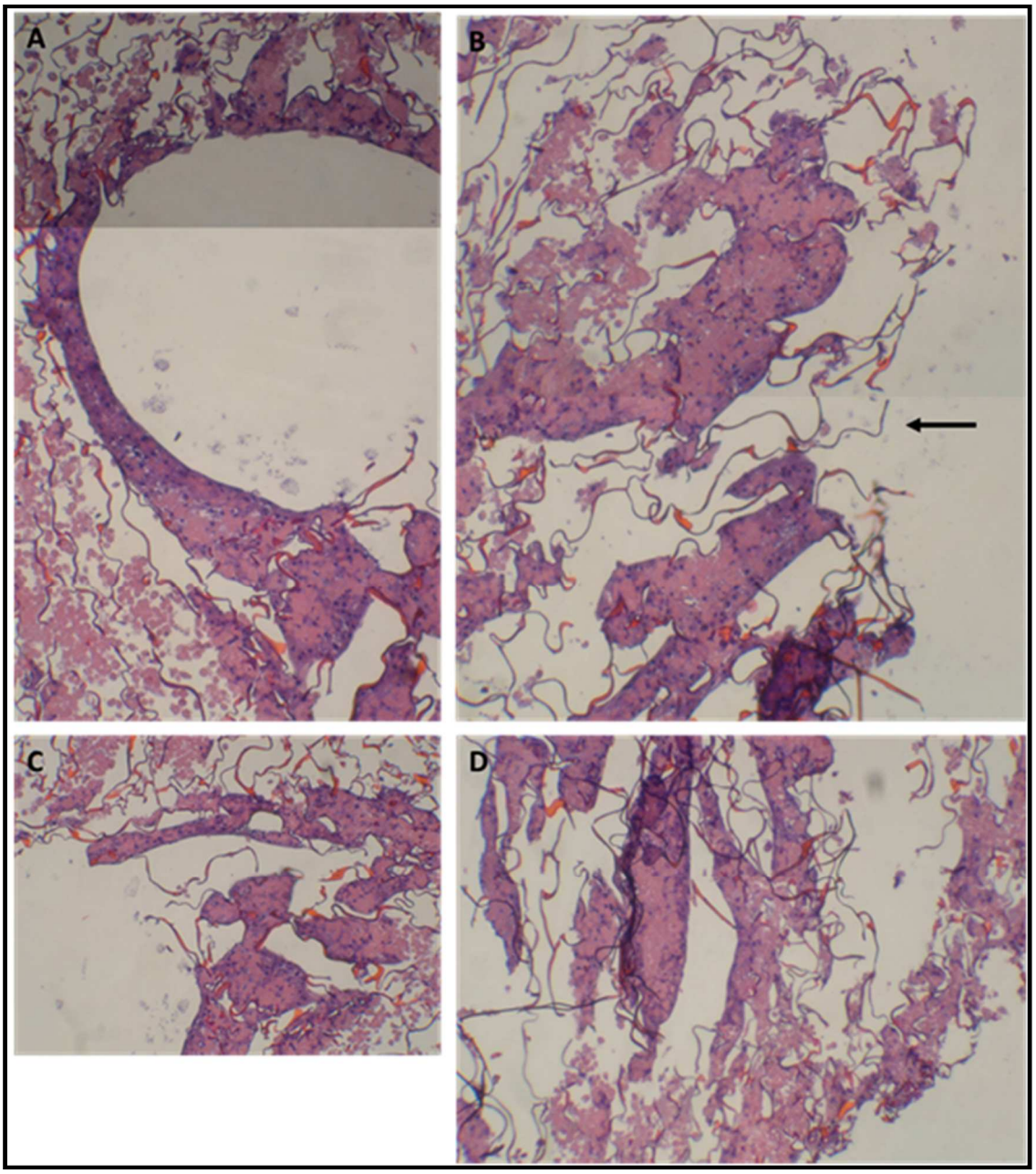

Figure 67: Enlarged images of aggregates cultured in scaffold with 30% reduced diameter. A & C) displaying hepatocyte clusters adjacent to semi-permeable oxygenation tubes. B) hepatocyte spheroids adjacent to central port inlet. D) hepatocyte aggregates at scaffold border.

To understand the scale of functionality from these experimental conditions the results were plotted together with the best results from the previous chapter (flow rate of 15 ml/min) and compared versus each day in culture. Figures 68 and 69, show the compared results for

albumin synthesis and ureagenesis versus each day in culture. When compared, the scaffold that had its diameter reduced by 30% had the greatest positive influence over hepatocyte-specific function as it facilitated better albumin and urea production over the seven day culture period. The 1.5 cm scaffold culture induced the second highest production rates followed by the culture that had the 1.29 cm scaffold diameter. Peak albumin production by the 1.05 cm scaffold culture was exhibited on day 2 which exceeded the other two conditions on their best days of secretion by 12.3% (1.5 cm – day 2) and 74.2% (1.29 cm – day 1). As the cultures progressed the gap in protein production widened even further. Because the decline in secretion rates by the 30% reduced diameter culture was not as drastic, at day 7 there was 92% gap in production when compared to the 1.29 cm scaffold culture and 79% with the 1.5 cm scaffold culture. Regarding ammonia conversion all three conditions followed similar trends in that rates were highest and consistent on day 1 and 2. However as the cultures continued, declines in transformation were exhibited on a daily basis in all three conditions. The percent difference on day 1 between the 1.05 cm and the 1.5 cm scaffolds was 26.2%, and 70% between the 1.5 cm and 1.29 cm scaffolds. On day 6 the 1.05 cm and 1.5 cm scaffold cultures demonstrated very similar ureagenesis rates as there was only a 6% difference in favor of the latter. On day 7 the 1.5 cm scaffold had a sharper drop in production than the 1.05 cm (51.2% vs. 14%), which overall represented a 40% difference in final secretions rates. If the 1.29 cm scaffold is included the percent difference in urea production is -53% when compared to the 1.5cm scaffold and -72% with the 1.05 cm scaffold. When comparing biochemical production from the 1.5 cm and 1.05 cm scaffolds it can be concluded empirically that, if the culture flow rate remains constant, distance and mass transport do share an association. However based on functional performance and IHC scaffold cross sections this conclusion cannot be applied to the 1.29 cm scaffold culture. However what might explain the difference in aggregate formation, viability and general functionality is the

flow rate during seeding. It is thought that the seeding flow rate of 15 ml/min in the scaffold of 1.29 cm was not sufficient to induce the primary stages of aggregation. Essentially at the scaffold diameter of 1.29 cm maybe 20 ml/min or more is initially needed to put the cells in close enough proximity to each other so that the culture flow rate of 15 ml/min would suffice to cause cell-to-cell contact. There is no conclusive data to support such a claim however it does provide a framework that, with more analysis, could support the experimental conclusions.

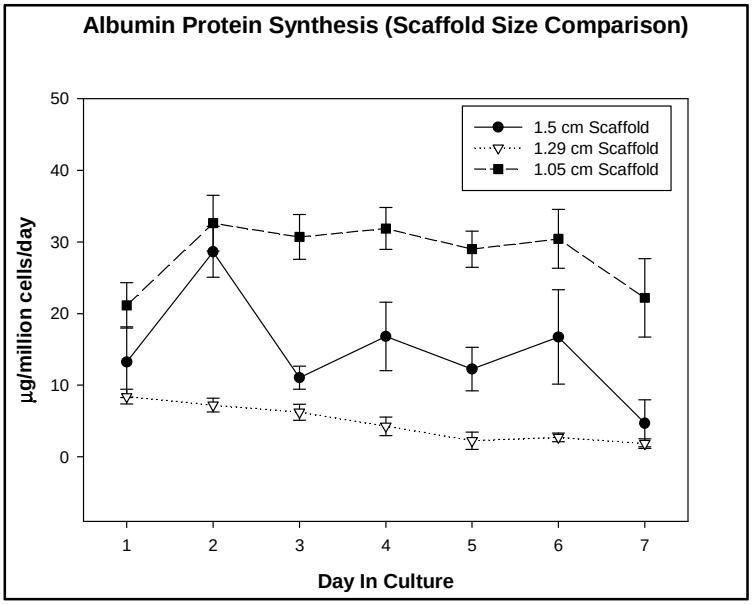

Figure 68: Albumin synthesis rates from each culture condition compared over the seven day culture period.

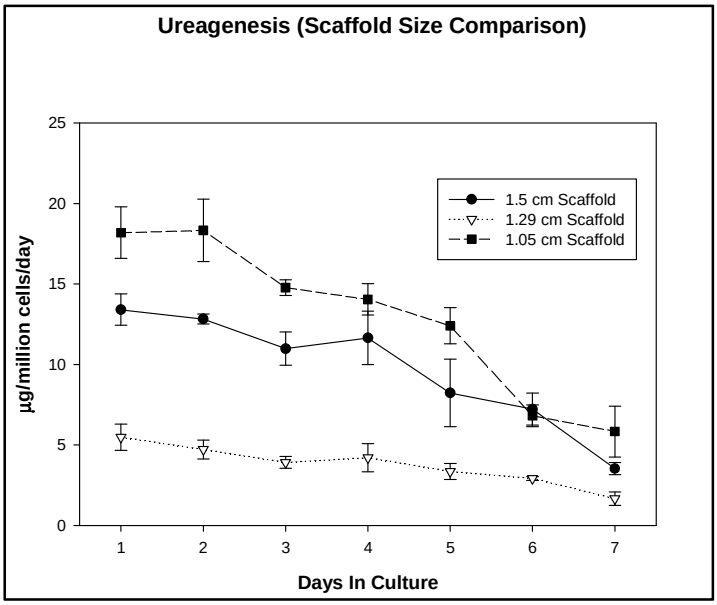

Figure 69: Urea secretion rates from each culture condition compared over the seven day culture period.

6.4 Discussion

For acellular or cell infused tissue engineered constructs one of the major impediments is achieving medically relevant cell densities that leads to proper functional integration into the damaged host tissue space. These densities facilitate the critical cell-to-cell and cell-to-ECM interactions that aids in mimicking a physiological architecture and intricacies of the native tissue. These interactions allow for biological functions such as protein harboring and secretion [272] and the dynamic interplay of ions, metabolites and reactive oxygen species [273] that modulate second messenger mediated signaling cascades. Innate functionality stemming from this types of high density cell seeding, prior to in vivo integration, is also challenged by mass transport limitations in vitro, and that spatial distribution of the cellular constituents may lead to inconsistencies in metabolite, cytotoxic by-product, and oxygen and nutrient gradients.

The main scope of this study was to increase the cell packing density of the scaffold constructs, condense the cell-to-oxygen source distance and assess the concomitant effect

that both have on metabolic functionality, morphology and viability. The experimental condition which decreased the scaffold diameter from 1.5 cm to 1.05 cm increased the cell packing density by ~14% by reducing the scaffold volume by 30% but only reducing the amount of seeded cells by 16%. The impact of this experimental condition clearly paid dividends in that it promoted a markedly increase in protein production and ureagenesis when compared to previous cultures. This increase in metabolic production was supported by increased colonization and cell viability throughout scaffold interior. Variations in seeding densities were used by Xu et al. [274] to examine their effects on hepato-specific function. They determined that by increasing the cell density from 1 x 10^5/ml to 5 x 10^6/ml in BAL reactors diazepam degradation, urea synthesis, incorporation of [^{3}H]-leucine into protein, and p53 gene expression were enhanced. Zhang et. al hypothesized that the level liver specific functionality seen in their high density cultures were maintained by, but not limited to, tight junction and desmosome formation by way of contiguous hepatocyte interaction [275]. Numerous viable cells were exhibited in multiple hepatocyte colonies. In addition to enhanced cell and extracellular matrix interactions brought about cell packing, it's feasible to correlate this level of viability and subsequent functionality to more efficient and effective mass transfer. Although there is no empirical data to support this but it is suspected that aggregate size hindered nutrient exchange thus causing the intermixed non-viable cells to die of necrotic medicated factors. Necrosis could also explain why dead cells within these multi-cellular masses are clustered together versus individually dispersed. Saito et. al. demonstrated that hepatocytes, when stimulated by an appropriate death cell (necrotic) stimuli, will undergo necrosis but more importantly will transfer similar death signals, via gap junction intracellular communication, to attached hepatocytes in a synchronic fashion [276]. Similar findings were also seen in glia cells that were susceptible to cell death via oxidative stress, metabolic inhibition or calcium overload. These cells, when connected to less

vulnerable cells through gap junctions, propagated and amplified the signals that induced cell injury. The level of cell injury leading to death was in direct proportion to the number and density of gap junctions formed with uncompromised cells [277].

The experimental condition which decreased the scaffold diameter from 1.5 cm to 1.29 cm increased the cell packing density by ~5% by reducing the scaffold volume by 14% but only reducing the amount of seeded cells by 9%. The impact of this experimental condition proved to be very detrimental to the culture's viability and hepatocellular expression. Contrary to the previous condition and the prevailing condition from chapter 5 (15 ml/min flow rate), this culture exhibited insignificant levels of aggregation which is tantamount to cellular activity. Because of this suppressed metabolic activity ensued at every 24 hr time point. This reduced scaffold dimension, although larger than the 1.05 cm construct, was expected to yield similar if not better results than the 1.5 cm scaffold from chapter 5. It is not clear as to why such nominal levels of functionality were exhibited however it is suspected that the seeding flow rate of 15 ml/min at the scaffold diameter of 1.29 cm was insufficient to induce flow mediated or forced aggregation.

6.5 Conclusion and Future Work

In this chapter, the effects of increased cell density, via reduced scaffold volume (30%), was shown to have be beneficial effects on hepatocyte specific functionality, morphology and viability. The results presented in this chapter also showed that decreasing the mass transfer distance between the hepatocytes and, the oxygen and nutrient sources also enhanced the overall longevity of cell health. Because of the information elucidated in this chapter, the understanding of oxygen uptake kinetics provided by the CFD simulations and the validated experiments, going forward future experiments should include reduced scaffold dimensions with high density seeding under seeding and experimental flow rates of 15 ml/min.

Regarding future work, in order to truly understand and optimize the fluid dynamic profile within the construct's micro-environment computational simulations encompassing 100% of the scaffold geometry should be modeled to include the complete fluid trajectory from the central port inlet to the scaffold outlet. The scaffold geometry should be simulated with porous media boundary constraints. This will allow the scaffold to be simulated as a complete porous structure with user specified levels of porosity. The porosity applied to the mesh geometry should be adjusted to account for the percent porosity of the actual 3D scaffold as well as the reduced void volume from the entrapped cells. This will aid in understanding the true pore inlet velocity, back pressure characteristics and the amount of nutrient and oxygen containing fluid that is actually moving in and through the scaffold. These parameters, once obtained, should be plugged into the CFD model in chapter 4. This will give a more accurate understanding of the shear stress imposed on the hepatocytes and the oxygen consumption kinetics and concentrations with respect to the length of the scaffold. Coupling this with the appropriate parametric inputs for mesh deformation we can also estimate which flows rates would provide the best cellular distribution during the seeding process, while minimizing shear effects and possible cellular washout in culture. Lastly experimental data detailing nutrient uptake and, protein and metabolite secretion can and should be incorporated into the model. Coupled together it is hypothesized that such a model would provide a more accurate and detailed prediction of the microenvironment's functional state and aid in future experimental designs.

With respect to the experimental workflow it is my belief that the mechanical properties of the scaffold should be in-line with that of the liver and the effects of these properties on cell health and signal transduction should be properly characterized. Additionally more studies should be conducted to ascertain how phenotypic expression is altered by the current scaffold configuration but tuned with ECM proteins and concentrations resembling that of the native

tissue. Lastly studies should be conducted to determine the feasibility of targeted seeding and culturing of periportal, mid-zonal/transition, and pericentral zone hepatocytes which would replicate a functional liver lobule within the current scaffold setup. Because oxygen tensions differ in each zone, additional gas permeable tubing should be incorporated into scaffold to carry zone specific oxygen tensions which will aid in creating the oxygen gradients seen in vivo. Once the effects of these efforts are understood co-cultures with sinusoidal endothelial cells would be the next logical step.

REFERENCES

1. Farmer, D.G., et al., *Liver transplantation for fulminant hepatic failure: experience with more than 200 patients over a 17-year period.* Ann Surg, 2003. **237**(5): p. 666-75; discussion 675-6.
2. Khan, S.A., et al., *Acute liver failure: a review.* Clin Liver Dis, 2006. **10**(2): p. 239-58, vii-viii.
3. Wolf, H.K. and G.K. Michalopoulos, *Hepatocyte regeneration in acute fulminant and nonfulminant hepatitis: a study of proliferating cell nuclear antigen expression.* Hepatology, 1992. **15**(4): p. 707-13.
4. Palmes, D., S. Skawran, and H.U. Spiegel, *Acute liver failure: from bench to bedside.* Transplant Proc, 2005. **37**(3): p. 1628-31.
5. Pless, G. and I.M. Sauer, *Bioartificial liver: current status.* Transplant Proc, 2005. **37**(9): p. 3893-5.
6. Keeffe, E.B., *[Acute liver failure].* Rev Gastroenterol Mex, 2005. **70**(1): p. 56-62.
7. Dhawan, A. and G. Mieli-Vergani, *Acute liver failure in neonates.* Early Hum Dev, 2005. **81**(12): p. 1005-10.
8. Schiodt, F.V., et al., *Etiology and outcome for 295 patients with acute liver failure in the United States.* Liver Transpl Surg, 1999. **5**(1): p. 29-34.
9. Pinelli, D., et al., *Transplantation for acute liver failure in children.* Transplant Proc, 2005. **37**(2): p. 1146-8.
10. Stieber, A.C., et al., *Orthotopic liver transplantation for fulminant and subacute hepatic failure.* Gastroenterol Clin North Am, 1988. **17**(1): p. 157-65.
11. Cole, C.R., et al., *Outcome after pediatric liver transplantation impact of living donor transplantation on cost.* J Pediatr, 2004. **144**(6): p. 729-35.

12. United Network for Organ Sharing. In: UNOS, R., Va, and the Division of Transplantation, Office of Special Programs, Health Resources and Services Administration, US Department of Health and Human Services, Rockville, Md; 2002.

13. Kasahara, M., et al., *Monosegmental living donor liver transplantation.* Transplant Proc, 2003. **35**(4): p. 1425-6.

14. Boraschi, P. and F. Donati, *Complications of orthotopic liver transplantation: imaging findings.* Abdom Imaging, 2004. **29**(2): p. 189-202.

15. Whitington, P.F., et al., *Liver transplantation in children.* J Pediatr Gastroenterol Nutr, 2002. **35 Suppl 1**: p. S44-50.

16. Tacke, F., T. Luedde, and C. Trautwein, *Inflammatory pathways in liver homeostasis and liver injury.* Clin Rev Allergy Immunol, 2009. **36**(1): p. 4-12.

17. Galun, E. and J.H. Axelrod, *The role of cytokines in liver failure and regeneration: potential new molecular therapies.* Biochim Biophys Acta, 2002. **1592**(3): p. 345-58.

18. Jungermann, K. and T. Kietzmann, *Zonation of parenchymal and nonparenchymal metabolism in liver.* Annu Rev Nutr, 1996. **16**: p. 179-203.

19. Ferri, D., et al., *Ultrastructural zonal heterogeneity of hepatocytes and mitochondria within the hepatic acinus during liver regeneration after partial hepatectomy.* Biol Cell, 2005. **97**(4): p. 277-88.

20. Martinez-Hernandez, A., *The hepatic extracellular matrix. I. Electron immunohistochemical studies in normal rat liver.* Lab Invest, 1984. **51**(1): p. 57-74.

21. Bedossa, P. and V. Paradis, *Liver extracellular matrix in health and disease.* J Pathol, 2003. **200**(4): p. 504-15.

22. Dziadek, M., Thomas, T., *Extracellular Matrix*, in *Molecular and Cell Biology of the Liver*, A.V. LeBautoun, Editor. 1993, CRC Press: Boca Raton. p. 369-403.

23. Fujita, M., et al., *Extracellular matrix regulation of cell-cell communication and tissue-specific gene expression in primary liver cultures.* Prog Clin Biol Res, 1986. **226**: p. 333-60.

24. Badylak, S.F., D.O. Freytes, and T.W. Gilbert, *Extracellular matrix as a biological scaffold material: Structure and function.* Acta Biomater, 2009. **5**(1): p. 1-13.

25. Williams, G.M. and M.J. Iatropoulos, *Alteration of liver cell function and proliferation: differentiation between adaptation and toxicity.* Toxicol Pathol, 2002. **30**(1): p. 41-53.

26. Somasundaram, R. and D. Schuppan, *Type I, II, III, IV, V, and VI collagens serve as extracellular ligands for the isoforms of platelet-derived growth factor (AA, BB, and AB).* J Biol Chem, 1996. **271**(43): p. 26884-91.

27. Arthur, M.J., *Matrix degradation in the liver.* Semin Liver Dis, 1990. **10**(1): p. 47-55.

28. Kim, T.H., et al., *Extracellular matrix remodeling at the early stages of liver regeneration in the rat.* Hepatology, 1997. **26**(4): p. 896-904.

29. Sell, S., *The hepatocyte: heterogeneity and plasticity of liver cells.* Int J Biochem Cell Biol, 2003. **35**(3): p. 267-71.

30. Malarkey, D.E., et al., *New insights into functional aspects of liver morphology.* Toxicol Pathol, 2005. **33**(1): p. 27-34.

31. MacSween, R.B., A; Portmann, B; Ishak, K; Scheuer, P; Anthony, P, *Pathology of the Liver*. 4th ed. 2002: Churchill Livingstone. 982.

32. Hubbard, A.L., D.A. Wall, and A. Ma, *Isolation of rat hepatocyte plasma membranes. I. Presence of the three major domains.* J Cell Biol, 1983. **96**(1): p. 217-29.

33. Feldmann, G., *The cytoskeleton of the hepatocyte. Structure and functions.* J Hepatol, 1989. **8**(3): p. 380-6.

34. SW, F., *Cytoskeleton: Intermediate Filaments*. 3rd ed. The Liver: Biology and Pathobiology, ed. B.J. Arias IM, Fausto N, Jakoby WB, Schacher DA, Shafritz DA. 1994, New York: Raven Press Ltd.

35. Jungermann, K., *Metabolic zonation of liver parenchyma.* Semin Liver Dis, 1988. **8**(4): p. 329-41.

36. Vinken, M., et al., *Involvement of cell junctions in hepatocyte culture functionality.* Crit Rev Toxicol, 2006. **36**(4): p. 299-318.

37. Saez, J.C., et al., *Hepatocyte gap junctions are permeable to the second messenger, inositol 1,4,5-trisphosphate, and to calcium ions.* Proc Natl Acad Sci U S A, 1989. **86**(8): p. 2708-12.

38. Anderson, J.M. and C.M. Van Itallie, *Physiology and function of the tight junction.* Cold Spring Harb Perspect Biol, 2009. **1**(2): p. a002584.

39. Sawada, N., et al., *Tight junctions and human diseases.* Med Electron Microsc, 2003. **36**(3): p. 147-56.

40. Lee, N.P. and J.M. Luk, *Hepatic tight junctions: from viral entry to cancer metastasis.* World J Gastroenterol, 2010. **16**(3): p. 289-95.

41. Massimi, M. and L.C. Devirgiliis, *Adhesion to the extracellular matrix is positively regulated by retinoic acid in HepG2 cells.* Liver Int, 2007. **27**(1): p. 128-36.

42. Kim, T.H., et al., *Differential expression and distribution of focal adhesion and cell adhesion molecules in rat hepatocyte differentiation.* Exp Cell Res, 1998. **244**(1): p. 93-104.

43. Hansen, L.K., J. Wilhelm, and J.T. Fassett, *Regulation of hepatocyte cell cycle progression and differentiation by type I collagen structure.* Curr Top Dev Biol, 2006. **72**: p. 205-36.

44. Cornillon, J., L. Campos, and D. Guyotat, *[Focal adhesion kinase (FAK), a multifunctional protein].* Med Sci (Paris), 2003. **19**(6-7): p. 743-52.

45. Boudreau, N.J. and P.L. Jones, *Extracellular matrix and integrin signalling: the shape of things to come.* Biochem J, 1999. **339 (Pt 3)**: p. 481-8.

46. Hoshiba, T., et al., *Primary hepatocyte survival on non-integrin-recognizable matrices without the activation of Akt signaling.* Biomaterials, 2007. **28**(6): p. 1093-104.

47. Kulig, K.M. and J.P. Vacanti, *Hepatic tissue engineering.* Transpl Immunol, 2004. **12**(3-4): p. 303-10.

48. Nahmias, Y., F. Berthiaume, and M.L. Yarmush, *Integration of technologies for hepatic tissue engineering.* Adv Biochem Eng Biotechnol, 2007. **103**: p. 309-29.

49. Jungermann, K. and T. Kietzmann, *Oxygen: modulator of metabolic zonation and disease of the liver.* Hepatology, 2000. **31**(2): p. 255-60.

50. Eguchi, A., A. Wree, and A.E. Feldstein, *Biomarkers of liver cell death.* J Hepatol, 2014. **60**(5): p. 1063-74.

51. Malhi, H., G.J. Gores, and J.J. Lemasters, *Apoptosis and necrosis in the liver: a tale of two deaths?* Hepatology, 2006. **43**(2 Suppl 1): p. S31-44.

52. Kheloufi, M., et al., *Liver autophagy in anorexia nervosa and acute liver injury.* Biomed Res Int, 2014. **2014**: p. 701064.

53. Lauterio, A., et al., *Current status and perspectives in split liver transplantation.* World J Gastroenterol, 2015. **21**(39): p. 11003-15.

54. Park, J.I., K.H. Kim, and S.G. Lee, *Laparoscopic living donor hepatectomy: a review of current status.* J Hepatobiliary Pancreat Sci, 2015. **22**(11): p. 779-88.

55. Matsubara, S., et al., *Continuous removal of middle molecules by hemofiltration in patients with acute liver failure.* Crit Care Med, 1990. **18**(12): p. 1331-8.

56. Mito M, N.Y., Kjellstrand C, Ivanovich P, eds., *Hepatic Assist: Present and Future*. Progress in Artificial Organs (1985). 1986, Cleveland: ISAO Press.

57. Sadamori, H., et al., *High-flow-rate haemodiafiltration as a brain-support therapy proceeding to liver transplantation for hyperacute fulminant hepatic failure.* Eur J Gastroenterol Hepatol, 2002. **14**(4): p. 435-9.

58. Davison AM, C.J., Grunfeld JP, Kerr DNS, Ritz E, Winerals CG, eds., *Oxford Textbook of Clinical Nephrology*. 2nd ed. Vol. 2. 1998, New York: Oxford University Press Inc. . 1403-1417.

59. Mullin, E.J., M.S. Metcalfe, and G.J. Maddern, *Artificial liver support: potential to retard regeneration?* Arch Surg, 2004. **139**(6): p. 670-7.

60. Court, F.G., et al., *Bioartificial liver support devices: historical perspectives.* ANZ J Surg, 2003. **73**(9): p. 739-48.

61. Filip, K., et al., *Bilirubin and bile acids removal by haemoperfusion through synthetic resin "Persorb".* Czech Med, 1990. **13**(1): p. 34-7.

62. Stange, J., et al., *The molecular adsorbents recycling system as a liver support system based on albumin dialysis: a summary of preclinical investigations, prospective, randomized, controlled clinical trial, and clinical experience from 19 centers.* Artif Organs, 2002. **26**(2): p. 103-10.

63. Dixit, V. and T.M. Chang, *In vitro and clinical studies of the removal of cortisol, thyroxine, insulin, and thyroid-stimulating hormone by coated charcoal haemoperfusion.* Life Support Syst, 1984. **2**(4): p. 238-44.

64. Kokot, F., J. Pietrek, and M. Seredynski, *Influence of hemoperfusion on the concentration of beta-methyldigoxin and hormones in plasma.* Kidney Int, 1979. **15**(4): p. 404-10.

65. Winchester, J.F., et al., *Solute, amino acid, and hormone changes with coated charcoal hemoperfusion in uremia.* Kidney Int, 1978. **14**(1): p. 74-81.

66. Kondrup, J., et al., *High volume plasma exchange in fulminant hepatic failure.* Int J Artif Organs, 1992. **15**(11): p. 669-76.

67. Stange, J., et al., *Liver support by extracorporeal blood purification: a clinical observation.* Liver Transpl, 2000. **6**(5): p. 603-13.

68. Buturovic-Ponikvar, J., A.M. Pernat, and R. Ponikvar, *Citrate anticoagulation during plasma exchange in a patient with thrombotic thrombocytopenic purpura: short heparin-free hemodialysis helps to attenuate citrate load.* Ther Apher Dial, 2005. **9**(3): p. 258-61.

69. Iwai, H., et al., *Removal of endotoxin and cytokines by plasma exchange in patients with acute hepatic failure.* Crit Care Med, 1998. **26**(5): p. 873-6.

70. Maiwall, R., et al., *Liver dialysis in acute-on-chronic liver failure: current and future perspectives.* Hepatol Int, 2014. **8 Suppl 2**: p. 505-13.

71. Horslen, S.P., et al., *Extracorporeal liver perfusion using human and pig livers for acute liver failure.* Transplantation, 2000. **70**(10): p. 1472-8.

72. Levy, M.F., et al., *Liver allotransplantation after extracorporeal hepatic support with transgenic (hCD55/hCD59) porcine livers: clinical results and lack of pig-to-human transmission of the porcine endogenous retrovirus.* Transplantation, 2000. **69**(2): p. 272-80.

73. Luo, Y., et al., *HDAF transgenic pig livers are protected from hyperacute rejection during ex vivo perfusion with human blood.* Xenotransplantation, 2002. **9**(1): p. 36-44.

74. Matsushita, T., et al., *Suppressed complement activation in human decay accelerating factor transgenic porcine liver cross-circulated with nonhuman primates.* Transplantation, 2003. **75**(11): p. 1807-12.

75. Nishitai, R., et al., *Absence of PERV infection in baboons after transgenic porcine liver perfusion.* J Surg Res, 2005. **124**(1): p. 45-51.

76. Muraca, M., et al., *Intraportal hepatocyte transplantation in the pig: hemodynamic and histopathological study.* Transplantation, 2002. **73**(6): p. 890-6.

77. Yu, C.H., et al., *Portal hemodynamic changes after hepatocyte transplantation in acute hepatic failure.* J Biomed Sci, 2004. **11**(6): p. 756-63.

78. Jirtle, R.L. and G. Michalopoulos, *Effects of partial hepatectomy on transplanted hepatocytes.* Cancer Res, 1982. **42**(8): p. 3000-4.

79. Elcin, Y.M., et al., *Xenotransplantation of fetal porcine hepatocytes in rats using a tissue engineering approach.* Artif Organs, 1999. **23**(2): p. 146-52.

80. Ohashi, K., et al., *Liver tissue engineering at extrahepatic sites in mice as a potential new therapy for genetic liver diseases.* Hepatology, 2005. **41**(1): p. 132-40.

81. Fox, I.J. and J.R. Chowdhury, *Hepatocyte transplantation.* Am J Transplant, 2004. **4 Suppl 6**: p. 7-13.

82. Chan, C., et al., *Hepatic tissue engineering for adjunct and temporary liver support: critical technologies.* Liver Transpl, 2004. **10**(11): p. 1331-42.

83. Kawashita, Y., et al., *Liver repopulation: a new concept of hepatocyte transplantation.* Surg Today, 2005. **35**(9): p. 705-10.

84. Laconi, E. and S. Laconi, *Principles of hepatocyte repopulation.* Semin Cell Dev Biol, 2002. **13**(6): p. 433-8.

85. Baccarani, U., et al., *Human hepatocyte transplantation for acute liver failure: state of the art and analysis of cell sources.* Transplant Proc, 2005. **37**(6): p. 2702-4.

86. Selden, C. and H. Hodgson, *Cellular therapies for liver replacement.* Transpl Immunol, 2004. **12**(3-4): p. 273-88.

87. Marongiu, F., et al., *Liver repopulation and carcinogenesis: two sides of the same coin?* Am J Pathol, 2008. **172**(4): p. 857-64.

88. Patzer, I.J., et al., *Bioartificial liver assist devices in support of patients with liver failure.* Hepatobiliary Pancreat Dis Int, 2002. **1**(1): p. 18-25.

89. Lee, S.Y., H.J. Kim, and D. Choi, *Cell sources, liver support systems and liver tissue engineering: alternatives to liver transplantation.* Int J Stem Cells, 2015. **8**(1): p. 36-47.

90. Morsiani, E., et al., *Biologic liver support: optimal cell source and mass.* Int J Artif Organs, 2002. **25**(10): p. 985-93.

91. Fu, T., et al., *Apoptosis occurs in isolated and banked primary mouse hepatocytes.* Cell Transplant, 2001. **10**(1): p. 59-66.

92. Tilles, A.W., et al., *Bioengineering of liver assist devices.* J Hepatobiliary Pancreat Surg, 2002. **9**(6): p. 686-96.

93. van de Kerkhove, M.P., et al., *Clinical application of bioartificial liver support systems.* Ann Surg, 2004. **240**(2): p. 216-30.

94. McKenzie, T.J., J.B. Lillegard, and S.L. Nyberg, *Artificial and bioartificial liver support.* Semin Liver Dis, 2008. **28**(2): p. 210-7.

95. Kobayashi, N., et al., *Insertion of a suicide gene into an immortalized human hepatocyte cell line.* Cell Transplant, 2001. **10**(4-5): p. 373-6.

96. Christ, B. and W.E. Fleig, *[Hepatocyte transplantation].* Med Klin (Munich), 2005. **100**(10): p. 650-5.

97. Wigg, A.J. and R.T. Padbury, *Liver support systems: promise and reality.* J Gastroenterol Hepatol, 2005. **20**(12): p. 1807-16.

98. Naruse, K., *Artificial liver support: future aspects.* J Artif Organs, 2005. **8**(2): p. 71-6.

99. Jauregui, H.O., *Hepatocyte cell lines as the biological component of liver support.* Artif Organs, 2001. **25**(7): p. 509-12.

100. Griffith, L.G. and G. Naughton, *Tissue engineering--current challenges and expanding opportunities.* Science, 2002. **295**(5557): p. 1009-14.

101. Vogel, V. and G. Baneyx, *The tissue engineeting puzzle: a molecular perspective.* Annu Rev Biomed Eng, 2003. **5**: p. 441-63.

102. Rubin, K., et al., *Substrate adhesion of rat hepatocytes: mechanism of attachment to collagen substrates.* Cell, 1981. **24**(2): p. 463-70.

103. Edward L. LeCluyse, P.L.B., Andrew Parkinson, *Strategies for restoration and maintenance of normal hepatic structure and function in long-term cultures of rat hepatocytes.* Advanced Drug Delivery Reviews, 1996. **22**: p. 133-186.

104. Lindblad, W.J., et al., *Hepatocellular phenotype in vitro is influenced by biophysical features of the collagenous substratum.* Hepatology, 1991. **13**(2): p. 282-8.

105. Rogiers, V. and A. Vercruysse, *Rat hepatocyte cultures and co-cultures in biotransformation studies of xenobiotics.* Toxicology, 1993. **82**(1-3): p. 193-208.

106. Buscher, H.-P., Griedrich,H., Thom,H., Schneider, S., Gerok, W., Kurz, G., *Hepatocyte primary cultures represent a cholestatic state. Meeting of the Eur. Assoc. for the Study of the Liver. abstract no. 51.* 1985.

107. Gebhardt, R., *Use of isolated and cultured hepatocytes in studies of bile formation.* Research in Isolated and Cultured Hepatocytes, ed. C.G.-G. A. Guillouzo. 1986, London: John Libbey. 353-376.

108. Bissell, D.M. and P.S. Guzelian, *Phenotypic stability of adult rat hepatocytes in primary monolayer culture.* Ann N Y Acad Sci, 1980. **349**: p. 85-98.

109. Guguen-Guillouzo, C. and A. Guillouzo, *Modulation of functional activities in cultured rat hepatocytes.* Mol Cell Biochem, 1983. **53-54**(1-2): p. 35-56.

110. Goulet, F., C. Normand, and O. Morin, *Cellular interactions promote tissue-specific function, biomatrix deposition and junctional communication of primary cultured hepatocytes.* Hepatology, 1988. **8**(5): p. 1010-8.

111. Sirica, A.E., et al., *Fetal phenotypic expression by adult rat hepatocytes on collagen gel/nylon meshes.* Proc Natl Acad Sci U S A, 1979. **76**(1): p. 283-7.

112. Ben-Ze'ev, A., et al., *Cell-cell and cell-matrix interactions differentially regulate the expression of hepatic and cytoskeletal genes in primary cultures of rat hepatocytes.* Proc Natl Acad Sci U S A, 1988. **85**(7): p. 2161-5.

113. Etienne, P.L., et al., *Transient expression of c-fos and constant expression of c-myc in freshly isolated and cultured normal adult rat hepatocytes.* Oncogene Res, 1988. **3**(3): p. 255-62.

114. Hong, J.T. and H.P. Glauert, *Effect of extracellular matrix on the expression of peroxisome proliferation associated genes in cultured rat hepatocytes.* Toxicol In Vitro, 2000. **14**(2): p. 177-84.

115. Dunn, J.C., R.G. Tompkins, and M.L. Yarmush, *Long-term in vitro function of adult hepatocytes in a collagen sandwich configuration.* Biotechnol Prog, 1991. **7**(3): p. 237-45.

116. Moghe, P.V., et al., *Culture matrix configuration and composition in the maintenance of hepatocyte polarity and function.* Biomaterials, 1996. **17**(3): p. 373-85.

117. Talamini, M.A., B. Kappus, and A. Hubbard, *Repolarization of hepatocytes in culture.* Hepatology, 1997. **25**(1): p. 167-72.

118. Liu, X., et al., *Biliary excretion in primary rat hepatocytes cultured in a collagen-sandwich configuration.* Am J Physiol, 1999. **277**(1 Pt 1): p. G12-21.

119. LeCluyse, E.L., K.L. Audus, and J.H. Hochman, *Formation of extensive canalicular networks by rat hepatocytes cultured in collagen-sandwich configuration.* Am J Physiol, 1994. **266**(6 Pt 1): p. C1764-74.

120. Gomez-Lechon, M.J., et al., *Long-term expression of differentiated functions in hepatocytes cultured in three-dimensional collagen matrix.* J Cell Physiol, 1998. **177**(4): p. 553-62.

121. Saad, B., H. Schawalder, and P. Maier, *Crude liver membrane fractions as substrate preserve liver-specific functions in long-term, serum-free rat hepatocyte cultures.* In Vitro Cell Dev Biol, 1993. **29A**(1): p. 32-40.

122. Saad, B., et al., *Crude liver membrane fractions and extracellular matrix components as substrata regulate differentially the preservation and inducibility of cytochrome P-450 isoenzymes in cultured rat hepatocytes.* Eur J Biochem, 1993. **213**(2): p. 805-14.

123. Tomonaga, T., et al., *Signaling pathway other than phosphatidylinositol turnover is responsible for constant expression of c-myc gene in primary cultures of rat hepatocytes.* Biochem Mol Biol Int, 1994. **33**(3): p. 429-37.

124. Lin, P., et al., *Assessing porcine liver-derived biomatrix for hepatic tissue engineering.* Tissue Eng, 2004. **10**(7-8): p. 1046-53.

125. Santhosh, A., S. Mathew, and P.R. Sudhakaran, *Modulation of biochemical activity of hepatocytes in culture by matrix substratum.* Indian J Biochem Biophys, 1998. **35**(4): p. 200-7.

126. Otsu, K., et al., *Differential regulation of liver-specific and ubiquitously-expressed genes in primary rat hepatocytes by the extracellular matrix.* Cell Physiol Biochem, 2001. **11**(1): p. 33-40.

127. Salehi-Nik, N., et al., *Engineering parameters in bioreactor's design: a critical aspect in tissue engineering.* Biomed Res Int, 2013. **2013**: p. 762132.

128. Catapano, G., Gerlach, J.C., *Bioreactors for Liver Tissue Engineering*, in *Topics in Tissue Engineering*, R.R. N. Ashammakhi, E. Chiellini Editor. 2007, Biomaterials and Tissue Engineering Group: Online. p. 1 - 42.

129. Kim, S.S., et al., *Survival and function of hepatocytes on a novel three-dimensional synthetic biodegradable polymer scaffold with an intrinsic network of channels.* Ann Surg, 1998. **228**(1): p. 8-13.

130. Park, T.G., *Perfusion culture of hepatocytes within galactose-derivatized biodegradable poly(lactide-co-glycolide) scaffolds prepared by gas foaming of effervescent salts.* J Biomed Mater Res, 2002. **59**(1): p. 127-35.

131. Fiegel, H.C., et al., *Influence of flow conditions and matrix coatings on growth and differentiation of three-dimensionally cultured rat hepatocytes.* Tissue Eng, 2004. **10**(1-2): p. 165-74.

132. Torok, E., et al., *Optimization of hepatocyte spheroid formation for hepatic tissue engineering on three-dimensional biodegradable polymer within a flow bioreactor prior to implantation.* Cells Tissues Organs, 2001. **169**(1): p. 34-41.

133. Pollok, J.M., et al., *Formation of spheroidal aggregates of hepatocytes on biodegradable polymers under continuous-flow bioreactor conditions.* Eur J Pediatr Surg, 1998. **8**(4): p. 195-9.

134. Torok, E., et al., *Hepatic tissue engineering on 3-dimensional biodegradable polymers within a pulsatile flow bioreactor.* Dig Surg, 2001. **18**(3): p. 196-203.

135. Torok, E., et al., *Morphological and functional analysis of rat hepatocyte spheroids generated on poly(L-lactic acid) polymer in a pulsatile flow bioreactor.* Tissue Eng, 2006. **12**(7): p. 1881-90.

136. Kim, S.S., et al., *Dynamic seeding and in vitro culture of hepatocytes in a flow perfusion system.* Tissue Eng, 2000. **6**(1): p. 39-44.

137. Kaihara, S., et al., *Survival and function of rat hepatocytes cocultured with nonparenchymal cells or sinusoidal endothelial cells on biodegradable polymers under flow conditions.* J Pediatr Surg, 2000. **35**(9): p. 1287-90.

138. Kurosawa, H., et al., *Polyurethane membrane as an efficient immobilization carrier for high-density culture of rat hepatocytes in the fixed-bed reactor.* Biotechnol Bioeng, 2000. **70**(2): p. 160-6.

139. Saavedra, Y.G., et al., *Polyvinylalcohol three-dimensional matrices for improved long-term dynamic culture of hepatocytes.* J Biomed Mater Res A, 2003. **66**(3): p. 562-70.

140. Chen, J.P., et al., *Loofa sponge as a scaffold for the culture of human hepatocyte cell line.* Biotechnol Prog, 2003. **19**(2): p. 522-7.

141. Chen, J.P. and C.T. Lin, *Dynamic seeding and perfusion culture of hepatocytes with galactosylated vegetable sponge in packed-bed bioreactor.* J Biosci Bioeng, 2006. **102**(1): p. 41-5.

142. Yinghui, Z., Jianchun, L., Yandao, G., Nanming, Z., Xiufang, Z. , *Feasibility of Using Chitosan in Nerve Repair.* TSINGHUA SCIENCE AND TECHNOLOGY, 2000. **5**(4): p. 432-435.

143. Kas, H.S., *Chitosan: properties, preparations and application to microparticulate systems.* J Microencapsul, 1997. **14**(6): p. 689-711.

144. Hirano, S., H. Tsuchida, and N. Nagao, *N-acetylation in chitosan and the rate of its enzymic hydrolysis.* Biomaterials, 1989. **10**(8): p. 574-6.

145. Muzzarelli, R.A.A., *Chitin and enzymes in the human body.* Advances in Chitin Science, 1996. **1**: p. 448 - 461.

146. Xia, W., Muzzarelli, R.A.A., *Depolymerization of chitosan and its derivatives.* Wuxi Qinggong Daxue Xuebao, 1996. **15**(1): p. 1 - 5.

147. Nakajima, M., et al., *Chitin is an effective material for sutures.* Jpn J Surg, 1986. **16**(6): p. 418-24.

148. Madihally, S.V. and H.W. Matthew, *Porous chitosan scaffolds for tissue engineering.* Biomaterials, 1999. **20**(12): p. 1133-42.

149. Muzzarelli, R., et al., *Biological activity of chitosan: ultrastructural study.* Biomaterials, 1988. **9**(3): p. 247-52.

150. Anbar, M., *Nitric oxide: a synchronizing chemical messenger.* Experientia, 1995. **51**(6): p. 545-50.

151. Pan, Y., et al., *Bioadhesive polysaccharide in protein delivery system: chitosan nanoparticles improve the intestinal absorption of insulin in vivo.* Int J Pharm, 2002. **249**(1-2): p. 139-47.

152. Usami, Y., et al., *Migration of canine neutrophils to chitin and chitosan.* J Vet Med Sci, 1994. **56**(6): p. 1215-6.

153. Di Martino, A., M. Sittinger, and M.V. Risbud, *Chitosan: a versatile biopolymer for orthopaedic tissue-engineering.* Biomaterials, 2005. **26**(30): p. 5983-90.

154. Sandford, P., Steinnes, A., *Biomedical Applications of High-Purity Chitosan: Physical, Chemical and Bioactive Properties*. Vol. S. 430 - 444.

155. Raimondi, M.T., et al., *Mechanobiology of engineered cartilage cultured under a quantified fluid-dynamic environment.* Biomech Model Mechanobiol, 2002. **1**(1): p. 69-82.

156. Raimondi, M.T., et al., *The effect of media perfusion on three-dimensional cultures of human chondrocytes: integration of experimental and computational approaches.* Biorheology, 2004. **41**(3-4): p. 401-10.

157. Boschetti, F., et al., *Prediction of the micro-fluid dynamic environment imposed to three-dimensional engineered cell systems in bioreactors.* J Biomech, 2006. **39**(3): p. 418-25.

158. Van Cleynenbreugel, T., et al., *Micro-CT-based screening of biomechanical and structural properties of bone tissue engineering scaffolds.* Med Biol Eng Comput, 2006. **44**(7): p. 517-25.

159. Jones, A.C., et al., *Analysis of 3D bone ingrowth into polymer scaffolds via micro-computed tomography imaging.* Biomaterials, 2004. **25**(20): p. 4947-54.

160. Jones, A.C., et al., *Investigation of microstructural features in regenerating bone using micro computed tomography.* J Mater Sci Mater Med, 2004. **15**(4): p. 529-32.

161. Cartmell, S., et al., *Quantitative microcomputed tomography analysis of mineralization within three-dimensional scaffolds in vitro.* J Biomed Mater Res A, 2004. **69**(1): p. 97-104.

162. Lin, A.S., et al., *Microarchitectural and mechanical characterization of oriented porous polymer scaffolds.* Biomaterials, 2003. **24**(3): p. 481-9.

163. Porter, B., et al., *3-D computational modeling of media flow through scaffolds in a perfusion bioreactor.* J Biomech, 2005. **38**(3): p. 543-9.

164. Cioffi, M., et al., *Modeling evaluation of the fluid-dynamic microenvironment in tissue-engineered constructs: a micro-CT based model.* Biotechnol Bioeng, 2006. **93**(3): p. 500-10.

165. Singh, H., et al., *Flow modelling within a scaffold under the influence of uni-axial and bi-axial bioreactor rotation.* J Biotechnol, 2005. **119**(2): p. 181-96.

166. Williams, K.A., S. Saini, and T.M. Wick, *Computational fluid dynamics modeling of steady-state momentum and mass transport in a bioreactor for cartilage tissue engineering.* Biotechnol Prog, 2002. **18**(5): p. 951-63.

167. Xiao, W., et al., *The importance of physiological oxygen concentrations in the sandwich cultures of rat hepatocytes on gas-permeable membranes.* Biotechnol Prog, 2014. **30**(6): p. 1401-10.

168. Semenza, G.L., *Regulation of mammalian O2 homeostasis by hypoxia-inducible factor 1.* Annu Rev Cell Dev Biol, 1999. **15**: p. 551-78.

169. Kim, J.S., et al., *Role of the mitochondrial permeability transition in apoptotic and necrotic death after ischemia/reperfusion injury to hepatocytes.* Curr Mol Med, 2003. **3**(6): p. 527-35.

170. Smith, M.K. and D.J. Mooney, *Hypoxia leads to necrotic hepatocyte death.* J Biomed Mater Res A, 2007. **80**(3): p. 520-9.

171. Hansmann, J., et al., *Bioreactors in tissue engineering - principles, applications and commercial constraints.* Biotechnol J, 2013. **8**(3): p. 298-307.

172. Berthiaume, F., T.J. Maguire, and M.L. Yarmush, *Tissue engineering and regenerative medicine: history, progress, and challenges.* Annu Rev Chem Biomol Eng, 2011. **2**: p. 403-30.

173. S. Partap, N.A.P., F.J. O'Brien, *Bioreactors in Tissue Engineering*. Tissue Engineering, ed. D. Eberlie. 2010: InTech.

174. Bueno, E.M., et al., *Increased rate of chondrocyte aggregation in a wavy-walled bioreactor.* Biotechnol Bioeng, 2004. **88**(6): p. 767-77.

175. El Haj, A.J., et al., *Controlling cell biomechanics in orthopaedic tissue engineering and repair.* Pathol Biol (Paris), 2005. **53**(10): p. 581-9.

176. Pancrazio, J.J., F. Wang, and C.A. Kelley, *Enabling tools for tissue engineering.* Biosens Bioelectron, 2007. **22**(12): p. 2803-11.

177. Y.I. Yang, D.L.S., H. I. Kim, M. H. Cho, S. J. Lee, *Continuous perfusion culture for generation of functional tissue-engineered soft tissues.* Current Applied Physics, 2007. **7**(1): p. 80 - 84.

178. Loh, Q.L. and C. Choong, *Three-dimensional scaffolds for tissue engineering applications: role of porosity and pore size.* Tissue Eng Part B Rev, 2013. **19**(6): p. 485-502.

179. Hollister, S.J., *Porous scaffold design for tissue engineering.* Nat Mater, 2005. **4**(7): p. 518-24.

180. Causa, F., P.A. Netti, and L. Ambrosio, *A multi-functional scaffold for tissue regeneration: the need to engineer a tissue analogue.* Biomaterials, 2007. **28**(34): p. 5093-9.

181. Karageorgiou, V. and D. Kaplan, *Porosity of 3D biomaterial scaffolds and osteogenesis.* Biomaterials, 2005. **26**(27): p. 5474-91.

182. Salerno, A., Di Maio, E., Iannace, S., Netti, P., *Tailoring the pore structure of PCL scaffolds for tissue engineering prepared via gas foaming of multi-phase blends.* J. Porous Mater, 2012. **19**.

183. Shi, G. and R.N. Coger, *Use of perfluorocarbons to enhance the performance of perfused three-dimensional hepatic cultures.* Biotechnol Prog, 2013. **29**(3): p. 718-26.

184. Chen, G. and A.F. Palmer, *Hemoglobin regulates the metabolic, synthetic, detoxification, and biotransformation functions of hepatoma cells cultured in a hollow fiber bioreactor.* Tissue Eng Part A, 2010. **16**(10): p. 3231-40.

185. Matsui, H., Osada T, Moroshita Y, Sekijima M, Fujii T, Takeuchi S, Sakai Y, *Rapid and enhanced repolarization in sandwich-cultured hepatocytes on an oxygen-permeable membrane.* Biochem Eng J, 2010. **52**: p. 255-262.

186. Gleeson, D., N.D. Smith, and J.L. Boyer, *Bicarbonate-dependent and -independent intracellular pH regulatory mechanisms in rat hepatocytes. Evidence for Na+-HCO3-cotransport.* J Clin Invest, 1989. **84**(1): p. 312-21.

187. Berezhkovskiy, L.M., S. Wong, and J.S. Halladay, *On the maintenance of hepatocyte intracellular pH 7.0 in the in-vitro metabolic stability assay.* J Pharmacokinet Pharmacodyn, 2013. **40**(6): p. 683-9.

188. Gregory J. Gores, A.-L.N., Thomas L. Dawson, Brian Herman, John J. Lemaster, *Relationship between Extracellular pH, Intracellular pH, and Cell Injury During "Chemical Hypoxia".* in *Integration of Mitochondrial Function*, C.R.H. J.J. Lemaster, R.G. Thurman, H.V. Westerhoff, Editor. 1988, Plenum Press: New York. p. 421 - 428.

189. Fraczek, J., et al., *Primary hepatocyte cultures for pharmaco-toxicological studies: at the busy crossroad of various anti-dedifferentiation strategies.* Arch Toxicol, 2013. **87**(4): p. 577-610.

190. Beigel, J., et al., *Genomics and proteomics analysis of cultured primary rat hepatocytes.* Toxicol In Vitro, 2008. **22**(1): p. 171-81.

191. Park, J., et al., *Radial flow hepatocyte bioreactor using stacked microfabricated grooved substrates.* Biotechnol Bioeng, 2008. **99**(2): p. 455-67.

192. Tilles, A.W., et al., *Effects of oxygenation and flow on the viability and function of rat hepatocytes cocultured in a microchannel flat-plate bioreactor.* Biotechnol Bioeng, 2001. **73**(5): p. 379-89.

193. Glicklis, R., J.C. Merchuk, and S. Cohen, *Modeling mass transfer in hepatocyte spheroids via cell viability, spheroid size, and hepatocellular functions.* Biotechnol Bioeng, 2004. **86**(6): p. 672-80.

194. Vinken, M., et al., *Modifications in connexin expression in liver development and cancer.* Cell Commun Adhes, 2012. **19**(3-4): p. 55-62.

195. Maes, M., et al., *Connexin and pannexin (hemi)channels in the liver.* Front Physiol, 2014. **4**: p. 405.

196. Pinkse, G.G., et al., *Hepatocyte survival depends on beta1-integrin-mediated attachment of hepatocytes to hepatic extracellular matrix.* Liver Int, 2004. **24**(3): p. 218-26.

197. Pinkse, G.G., et al., *RGD peptides confer survival to hepatocytes via the beta1-integrin-ILK-pAkt pathway.* J Hepatol, 2005. **42**(1): p. 87-93.

198. Folkman, J. and M. Hochberg, *Self-regulation of growth in three dimensions.* J Exp Med, 1973. **138**(4): p. 745-53.

199. Kinasiewicz, A., et al., *Impact of oxygenation of bioartificial liver using perfluorocarbon emulsion perftoran on metabolism of human hepatoma C3A cells.* Artif Cells Blood Substit Immobil Biotechnol, 2008. **36**(6): p. 525-34.

200. Naruto, H., et al., *Feasibility of direct oxygenation of primary-cultured rat hepatocytes using polyethylene glycol-decorated liposome-encapsulated hemoglobin (LEH).* J Biosci Bioeng, 2007. **104**(4): p. 343-6.

201. Alayash, A.I., *Oxygen therapeutics: can we tame haemoglobin?* Nat Rev Drug Discov, 2004. **3**(2): p. 152-9.

202. Patrachari, A.R., J.T. Podichetty, and S.V. Madihally, *Application of computational fluid dynamics in tissue engineering.* J Biosci Bioeng, 2012. **114**(2): p. 123-32.

203. Bloch, R. and A. Talalla, *A mathematical model of cerebrospinal fluid dynamics.* J Neurol Sci, 1976. **27**(4): p. 485-98.

204. Isaacs, K.K., R.B. Schlesinger, and T.B. Martonen, *Three-dimensional computational fluid dynamics simulations of particle deposition in the tracheobronchial tree.* J Aerosol Med, 2006. **19**(3): p. 344-52.

205. Ho, C.Y., et al., *Numerical analysis of airflow alteration in central airways following tracheobronchial stent placement.* Exp Hematol Oncol, 2012. **1**(1): p. 23.

206. Ghaffari, S., R.L. Leask, and E.A. Jones, *Simultaneous imaging of blood flow dynamics and vascular remodelling during development.* Development, 2015.

207. Wu, J. and S.C. Shadden, *Coupled Simulation of Hemodynamics and Vascular Growth and Remodeling in a Subject-Specific Geometry.* Ann Biomed Eng, 2015. **43**(7): p. 1543-54.

208. Berg, P., et al., *The Computational Fluid Dynamics Rupture Challenge 2013-Phase II: Variability of Hemodynamic Simulations in Two Intracranial Aneurysms.* J Biomech Eng, 2015. **137**(12).

209. Cebral, J.R., et al., *Wall Mechanical Properties and Hemodynamics of Unruptured Intracranial Aneurysms.* AJNR Am J Neuroradiol, 2015. **36**(9): p. 1695-703.

210. Good, B.C., S. Deutsch, and K.B. Manning, *Hemodynamics in a Pediatric Ascending Aorta Using a Viscoelastic Pediatric Blood Model.* Ann Biomed Eng, 2015.

211. Podichetty, J.T. and S.V. Madihally, *Modeling of porous scaffold deformation induced by medium perfusion.* J Biomed Mater Res B Appl Biomater, 2014. **102**(4): p. 737-48.

212. Hossain, M.S., X.B. Chen, and D.J. Bergstrom, *Investigation of the in vitro culture process for skeletal-tissue-engineered constructs using computational fluid dynamics and experimental methods.* J Biomech Eng, 2012. **134**(12): p. 121003.

213. Adebiyi, A.A., M.E. Taslim, and K.D. Crawford, *The use of computational fluid dynamic models for the optimization of cell seeding processes.* Biomaterials, 2011. **32**(34): p. 8753-70.

214. Guyot, Y., et al., *A three-dimensional computational fluid dynamics model of shear stress distribution during neotissue growth in a perfusion bioreactor.* Biotechnol Bioeng, 2015. **112**(12): p. 2591-600.

215. Hsu, M.N., et al., *Computational fluid model incorporating liver metabolic activities in perfusion bioreactor.* Biotechnol Bioeng, 2014. **111**(5): p. 885-95.

216. Debbaut, C., et al., *Perfusion characteristics of the human hepatic microcirculation based on three-dimensional reconstructions and computational fluid dynamic analysis.* J Biomech Eng, 2012. **134**(1): p. 011003.

217. Mitchell, S. and P. Mendes, *A computational model of liver iron metabolism.* PLoS Comput Biol, 2013. **9**(11): p. e1003299.

218. Tsoukias, N.M., et al., *A computational model of oxygen delivery by hemoglobin-based oxygen carriers in three-dimensional microvascular networks.* J Theor Biol, 2007. **248**(4): p. 657-74.

219. Chen, G. and A.F. Palmer, *Hemoglobin-based oxygen carrier and convection enhanced oxygen transport in a hollow fiber bioreactor.* Biotechnol Bioeng, 2009. **102**(6): p. 1603-12.

220. Chen, G. and A.F. Palmer, *Mixtures of hemoglobin-based oxygen carriers and perfluorocarbons exhibit a synergistic effect in oxygenating hepatic hollow fiber bioreactors.* Biotechnol Bioeng, 2010. **105**(3): p. 534-42.

221. Podichetty, J.T., et al., *Multiple approaches to predicting oxygen and glucose consumptions by HepG2 cells on porous scaffolds in an axial-flow bioreactor.* Biotechnol Bioeng, 2015. **112**(2): p. 393-404.

222. Tan, G.D., et al., *A thin-walled polydimethylsiloxane bioreactor for high-density hepatocyte sandwich culture.* Biotechnol Bioeng, 2013. **110**(6): p. 1663-73.

223. Weise, F., et al., *Analysis and comparison of oxygen consumption of HepG2 cells in a monolayer and three-dimensional high density cell culture by use of a matrigrid(R).* Biotechnol Bioeng, 2013. **110**(9): p. 2504-12.

224. Mareels, G., et al., *Three-dimensional numerical modeling and computational fluid dynamics simulations to analyze and improve oxygen availability in the AMC bioartificial liver.* Ann Biomed Eng, 2006. **34**(11): p. 1729-44.

225. Peeters, G., et al., *A multilevel modeling framework to study hepatic perfusion characteristics in case of liver cirrhosis.* J Biomech Eng, 2015. **137**(5): p. 051007.

226. Mazzei, D., et al., *A low shear stress modular bioreactor for connected cell culture under high flow rates.* Biotechnol Bioeng, 2010. **106**(1): p. 127-37.

227. Buchwald, P., *A local glucose-and oxygen concentration-based insulin secretion model for pancreatic islets.* Theor Biol Med Model, 2011. **8**: p. 20.

228. Oller, A.R., et al., *Growth of mammalian cells at high oxygen concentrations.* J Cell Sci, 1989. **94 (Pt 1)**: p. 43-9.

229. Haselgrove, J.C., I.M. Shapiro, and S.F. Silverton, *Computer modeling of the oxygen supply and demand of cells of the avian growth cartilage.* Am J Physiol, 1993. **265**(2 Pt 1): p. C497-506.

230. Nyberg, S.L., et al., *Primary hepatocytes outperform Hep G2 cells as the source of biotransformation functions in a bioartificial liver.* Ann Surg, 1994. **220**(1): p. 59-67.

231. Frohlich, E.M., X. Zhang, and J.L. Charest, *The use of controlled surface topography and flow-induced shear stress to influence renal epithelial cell function.* Integr Biol (Camb), 2012. **4**(1): p. 75-83.

232. Macown, R.J., F.S. Veraitch, and N. Szita, *Robust, microfabricated culture devices with improved control over the soluble microenvironment for the culture of embryonic stem cells.* Biotechnol J, 2014. **9**(6): p. 805-13.

233. Hutmacher, D.W. and H. Singh, *Computational fluid dynamics for improved bioreactor design and 3D culture.* Trends Biotechnol, 2008. **26**(4): p. 166-72.

234. Provin, C., et al., *A method for the design of 3D scaffolds for high-density cell attachment and determination of optimum perfusion culture conditions.* J Biomech, 2008. **41**(7): p. 1436-49.

235. Lesman, A., Y. Blinder, and S. Levenberg, *Modeling of flow-induced shear stress applied on 3D cellular scaffolds: Implications for vascular tissue engineering.* Biotechnol Bioeng, 2010. **105**(3): p. 645-54.

236. Melchels, F.P., et al., *The influence of the scaffold design on the distribution of adhering cells after perfusion cell seeding.* Biomaterials, 2011. **32**(11): p. 2878-84.

237. Cioffi, M., et al., *Computational evaluation of oxygen and shear stress distributions in 3D perfusion culture systems: macro-scale and micro-structured models.* J Biomech, 2008. **41**(14): p. 2918-25.

238. Lawrence, B.J., M. Devarapalli, and S.V. Madihally, *Flow dynamics in bioreactors containing tissue engineering scaffolds.* Biotechnol Bioeng, 2009. **102**(3): p. 935-47.

239. Devarapalli, M., B.J. Lawrence, and S.V. Madihally, *Modeling nutrient consumptions in large flow-through bioreactors for tissue engineering.* Biotechnol Bioeng, 2009. **103**(5): p. 1003-15.

240. Dardik, A., et al., *Differential effects of orbital and laminar shear stress on endothelial cells.* J Vasc Surg, 2005. **41**(5): p. 869-80.

241. Yamamoto, K., et al., *Fluid shear stress activates Ca(2+) influx into human endothelial cells via P2X4 purinoceptors.* Circ Res, 2000. **87**(5): p. 385-91.

242. Conway, D.E., et al., *Fluid shear stress on endothelial cells modulates mechanical tension across VE-cadherin and PECAM-1.* Curr Biol, 2013. **23**(11): p. 1024-30.

243. Honda, M.J., et al., *Shear stress facilitates tissue-engineered odontogenesis.* Bone, 2006. **39**(1): p. 125-33.

244. Kamegaya, Y., et al., *Role of endothelin receptors in endothelin-1-induced morphological changes of hepatic sinusoidal endothelial fenestrae: morphometric evaluation with scanning electron microscopy.* Hepatol Res, 2002. **22**(2): p. 89-101.

245. Rudich, N., et al., *Focal liver necrosis appears early after partial hepatectomy and is dependent on T cells and antigen delivery from the gut.* Liver Int, 2009. **29**(8): p. 1273-84.

246. Kan, P., et al., *Effects of shear stress on metabolic function of the co-culture system of hepatocyte/nonparenchymal cells for a bioartificial liver.* ASAIO J, 1998. **44**(5): p. M441-4.

247. Esch, M.B., et al., *Multi-cellular 3D human primary liver cell culture elevates metabolic activity under fluidic flow.* Lab Chip, 2015. **15**(10): p. 2269-77.

248. Xia, L., et al., *Laminar-flow immediate-overlay hepatocyte sandwich perfusion system for drug hepatotoxicity testing.* Biomaterials, 2009. **30**(30): p. 5927-36.

249. Torii, T., M. Miyazawa, and I. Koyama, *Effect of continuous application of shear stress on liver tissue: continuous application of appropriate shear stress has advantage in protection of liver tissue.* Transplant Proc, 2005. **37**(10): p. 4575-8.

250. Hegde, M., et al., *Dynamic interplay of flow and collagen stabilizes primary hepatocytes culture in a microfluidic platform.* Lab Chip, 2014. **14**(12): p. 2033-9.

251. Tanaka Y, Y.M., Okano T, Kitamori T, Sato K, *Evaluation of effects of shear stress on hepatocytes by a microchip-based system.* Measurement Science and Technology, 2006. **17**(12): p. 3167-3170.

252. Mufti, N.A. and M.L. Shuler, *Induction of cytochrome P-450IA1 activity in response to sublethal stresses in microcarrier-attached Hep G2 cells.* Biotechnol Prog, 1995. **11**(6): p. 659-63.

253. Miyazawa, M., et al., *Hepatocyte dynamics in a three-dimensional rotating bioreactor.* J Gastroenterol Hepatol, 2007. **22**(11): p. 1959-64.

254. Chang, T.T. and M. Hughes-Fulford, *Molecular mechanisms underlying the enhanced functions of three-dimensional hepatocyte aggregates.* Biomaterials, 2014. **35**(7): p. 2162-71.

255. Kang, H.G., et al., *E-cadherin cell-cell adhesion in ewing tumor cells mediates suppression of anoikis through activation of the ErbB4 tyrosine kinase.* Cancer Res, 2007. **67**(7): p. 3094-105.

256. Brophy, C.M., et al., *Rat hepatocyte spheroids formed by rocked technique maintain differentiated hepatocyte gene expression and function.* Hepatology, 2009. **49**(2): p. 578-86.

257. Boudreau, N., et al., *Suppression of ICE and apoptosis in mammary epithelial cells by extracellular matrix.* Science, 1995. **267**(5199): p. 891-3.

258. Nakatsuka, H., et al., *Shear stress induces hepatocyte PAI-1 gene expression through cooperative Sp1/Ets-1 activation of transcription.* Am J Physiol Gastrointest Liver Physiol, 2006. **291**(1): p. G26-34.

259. Park, J.H., M.K. Lee, and J. Yoon, *Gamma-linolenic acid inhibits hepatic PAI-1 expression by inhibiting p38 MAPK-dependent activator protein and mitochondria-mediated apoptosis pathway.* Apoptosis, 2015. **20**(3): p. 336-47.

260. Kang, I.K., et al., *Co-culture of hepatocytes and fibroblasts by micropatterned immobilization of beta-galactose derivatives.* Biomaterials, 2004. **25**(18): p. 4225-32.

261. Abu-Absi, S.F., et al., *Structural polarity and functional bile canaliculi in rat hepatocyte spheroids.* Exp Cell Res, 2002. **274**(1): p. 56-67.

262. Lillegard, J.B., et al., *Normal atmospheric oxygen tension and the use of antioxidants improve hepatocyte spheroid viability and function.* J Cell Physiol, 2011. **226**(11): p. 2987-96.

263. Joly, P., et al., *Geometry-driven cell organization determines tissue growths in scaffold pores: consequences for fibronectin organization.* PLoS One, 2013. **8**(9): p. e73545.

264. Ma, T., et al., *Effects of pore size in 3-D fibrous matrix on human trophoblast tissue development.* Biotechnol Bioeng, 2000. **70**(6): p. 606-18.

265. Mandal, B.B. and S.C. Kundu, *Cell proliferation and migration in silk fibroin 3D scaffolds.* Biomaterials, 2009. **30**(15): p. 2956-65.

266. Aydin, H.M., et al., *Improving pore interconnectivity in polymeric scaffolds for tissue engineering.* J Tissue Eng Regen Med, 2009. **3**(6): p. 470-6.

267. Brahatheeswaran Dhandayuthapani, Y.Y., Toru Maekawa, and D. Sakthi Kumar, *Polymeric Scaffolds in Tissue Engineering Application: A Review.* International Journal of Polymer Science, 2011. **2011**: p. 19.

268. Rumpler, M., et al., *The effect of geometry on three-dimensional tissue growth.* J R Soc Interface, 2008. **5**(27): p. 1173-80.

269. Troken, A., et al., *Tissue engineering of the synovial joint: the role of cell density.* Proc Inst Mech Eng H, 2007. **221**(5): p. 429-40.

270. Dvir-Ginzberg, M., et al., *Liver tissue engineering within alginate scaffolds: effects of cell-seeding density on hepatocyte viability, morphology, and function.* Tissue Eng, 2003. **9**(4): p. 757-66.

271. Curcio, E., et al., *Mass transfer and metabolic reactions in hepatocyte spheroids cultured in rotating wall gas-permeable membrane system.* Biomaterials, 2007. **28**(36): p. 5487-97.

272. Palakkan, A.A., et al., *Polarisation and functional characterisation of hepatocytes derived from human embryonic and mesenchymal stem cells.* Biomed Rep, 2015. **3**(5): p. 626-636.

273. Maurel, M. and J. Rosenbaum, *Closing the gap on drug-induced liver injury.* Hepatology, 2012. **56**(2): p. 781-3.

274. Qingxiang Xu, X.S., Yudong Qiu, Heyuan Zhang and Yitao Ding, *The Optimal Hepatocyte Density for a Hollow-Fiber Bioartificial Liver.* Annals of Clinical & Laboratory Science, 2003. **34**(1): p. 87-93.

275. Zhang, M.Y., et al., *Microfluidic environment for high density hepatocyte culture.* Biomed Microdevices, 2008. **10**(1): p. 117-21.

276. Saito, C., K. Shinzawa, and Y. Tsujimoto, *Synchronized necrotic death of attached hepatocytes mediated via gap junctions.* Sci Rep, 2014. **4**: p. 5169.

277. Lin, J.H., et al., *Gap-junction-mediated propagation and amplification of cell injury.* Nat Neurosci, 1998. **1**(6): p. 494-500.

ABSTRACT

OXYGEN TRANSPORT, SHEAR STRESS, AND METABOLISM IN PERFUSED HEPATOCYTE-SEEDED SCAFFOLDS WITH RADIAL PORE ARCHITECTURE: EXPERIMENTAL AND COMPUTATIONAL ANALYSES

by

CHIJIOKE ANAELE MBANU

May 2016

Advisor: Dr. Howard W.T. Matthew

Major: Biomedical Engineering

Degree: Doctor of Philosophy

Several modalities have been proposed as treatments or temporary stop-gap for patients suffering from liver failure until a suitable organ is available. However there is still an urgent need for an off-the-shelf device that can accommodate clinically relevant cell numbers, be cultured at physiological oxygen tensions and, can be fully integrated into and heal the injured hepatic space. In this study we investigated the effects that convective and direct oxygenation had on hepatocyte functionality, morphology and viability while cultured in bulk 3D chitosan scaffolds and perfusion bioreactor systems. Cylindrical chitosan scaffolds with radial directed pore structures were fabricated by a thermal gradient directed from the center to the periphery. Capillary-like direct oxygenation was facilitated by embedding gas permeable silicone tubing throughout the scaffold body. Three iterations of bioreactor design and optimization produced a perfusion system that could enable direct oxygenation, accommodate high density hepatocyte seeding ($8x10^{-7}$ to $1x10^{-8}$ cells), ensure adequate mass transfer and induce sustainable metabolic outputs for a least 7 days at a flow rate of 10

ml/min. A computational fluid dynamics model of the internal scaffold pore structure infused with spheroids that resembled hepatocyte aggregates was utilized to understand how varying flow rates (5, 10, 15, 20 and 25 ml/min) effected fluid flow profiles, shear stress imposed on the cells and oxygen consumption within the microenvironment. The results showed that the volumetric flow rate of 15 ml/min at the scaffold's central port inlet produced the best oxygen consumption profile with no damaging effects due to shear stress or eddies flow. The simulation was validated and showed good correlation to empirically derived data. Experimentally the flow rate of 15 ml/min induced the most favorable hepatic response out of the five experimental flow conditions and a static culture (only direct oxygenation). We also looked at how increasing cellular compactness, via reduced scaffold dimensions, would affect phenotypic expression and viability. It was discerned that increasing the cell packing density by 14% increased the rate of albumin and urea production by 79% and 40% respectively. In total the results show that the experimental measures conducted in this study enhanced hepatocyte metabolic performance, viability and morphological appearance.

AUTOBIOGRAPHICAL STATEMENT

EDUCATION

M. Sc., Biomedical Engineering, Wayne State University, (WSU), December 2003

B. Sc., Chemical Engineering, Purdue University, December 1999

CONFERENCE PRESENTATIONS

Chijioke A. Mbanu, Howard W.T. Matthew. "In Vitro Evaluation of Direct Oxygenation, Variable Flow-Rates and Computational Fluid Dynamic Predicted Shear Stress on Sustained Functionality of Hepatocyte-Seeded Scaffolds". Biomedical Engineering Society (BMES). October 2006 Annual Fall Meeting. Chicago, Illinois, USA

Chijioke A. Mbanu, Howard W.T. Matthew. "In Vitro Evaluation of Direct Oxygenation, Variable Flow-Rates and Computational Fluid Dynamic Predicted Shear Stress on Sustained Functionality of Hepatocyte-Seeded Scaffold". VII. Annual Graduate Research Symposium '07, October 2007. Detroit, Michigan, USA

Chijioke A. Mbanu, Howard W.T. Matthew. "Direct Oxygenation and Perfusion Enhance Viability and Function of Hepatocyte-Seeded Scaffolds". The Journal of the Federation of American Societies for Experimental Biology (FASEB). March 2008. Orlando, Florida, USA